Technical Note N-1199

REDUCTION OF STRESSES IN BURIED STRUCTURES

by

S. K. Takahashi and R. N. Murtha

December 1971

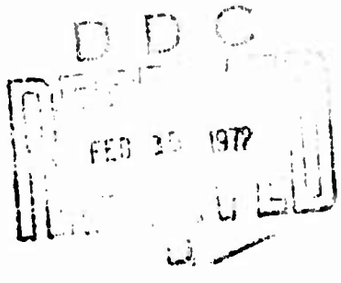

NAVAL CIVIL ENGINEERING LABORATORY
Port Hueneme, California 93043

100

Unclassified

Security Classification

DOCUMENT CONTROL DATA - R & D

(Security classification of title, body of abstract and indexing annotation must be entered when the overall report is classified)

1. ORIGINATING ACTIVITY (Corporate author)	2a. REPORT SECURITY CLASSIFICATION
Naval Civil Engineering Laboratory Port Hueneme, California 93043	Unclassified
	2b. GROUP

3. REPORT TITLE

REDUCTION OF STRESSES IN BURIED STRUCTURES

4. DESCRIPTIVE NOTES (Type of report and inclusive dates)

Final; September 1968 – February 1971

5. AUTHOR(S) (First name, middle initial, last name)

S. K. Takahashi and R. N. Murtha

6. REPORT DATE	7a. TOTAL NO. OF PAGES	7b. NO. OF REFS
December 1971	100	16

8a. CONTRACT OR GRANT NO.	9a. ORIGINATOR'S REPORT NUMBER(S)
b. PROJECT NO. 51-009	TN-1199
c.	9b. OTHER REPORT NO(S) (Any other numbers that may be assigned this report)
d.	

10. DISTRIBUTION STATEMENT

Approved for public release; distribution unlimited.

11. SUPPLEMENTARY NOTES	12. SPONSORING MILITARY ACTIVITY
	Office of Naval Research Arlington, Virginia 22217

13. ABSTRACT

Tests were performed in Event DIAL PACK on 1- and 3-foot diameter steel cylinders with hemispherical end caps to obtain information on the dynamic behavior of structures containing fluid (a) internally pressurized and (b) with backpacking. The four test structures were oriented with their longitudinal axes parallel to the surface and normal to a radius through ground zero. The data were used to compare the variation of the parameters of internal pressurization and backpacking and to check the results of a two-dimensional, nonlinear, large deformation computer code developed for this task. The 3-foot diameter models were designed according to the recently developed optimization equations by NCEL. The 3-foot diameter, 0.134-inch models were not damaged when subjected to a peak surface overpressure of 680 psi. The 1-foot diameter model buckled in several locations because of its shallow depth of burial. However, all the tanks were still operational after the blast. Strains, deflections, and accelerations were less for the internally pressurized capsule with backpacking than for the other two capsules with no backpacking. Peak interface pressure measured for the model with no backpacking and with internal pressure was about 44% of the peak surface overpressure. Finite element computer data gave conservative estimates. The NCEL optimization equations can be used, with proper discretion, to design a buried fuel container to survive blast loading.

DD FORM 1 NOV 68 1473 (PAGE 1)

S/N 0101-807-6801

Unclassified

Security Classification

REDUCTION OF STRESSES IN BURIED STRUCTURES

Technical Note N-1199

51-009

by

S. K. Takahashi and R. N. Murtha

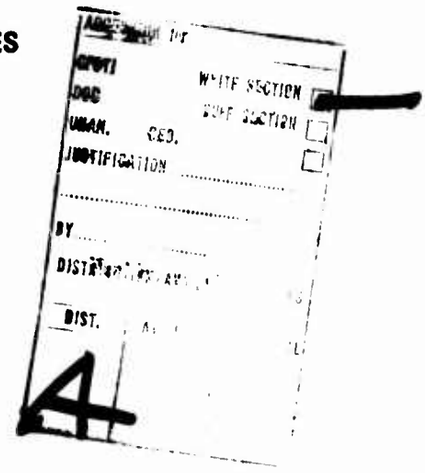

ABSTRACT

Tests were performed in Event DIAL PACK on 1- and 3-foot diameter steel cylinders with hemispherical end caps. The objective was to obtain information on the dynamic behavior of structures containing fluid, internally pressurized and with backpacking. The four test structures were oriented with their longitudinal axes parallel to the surface and normal to a radius through ground zero. The data obtained were used in comparing the variation of the parameters of internal pressurization and backpacking and also for checking the results of a two-dimensional, nonlinear, large deformation computer code developed for this task. The 3-foot diameter models were designed according to the recently developed optimization equations by NCEL.

The 3-foot-diameter models were not damaged despite the thinness of the wall when subjected to a peak surface overpressure of 680 psi. The 1-foot diameter model buckled in several locations because of its shallow depth of burial. However, all the tanks were still operational after the blast. Valuable information on the survivability of high-pressure hose connections to the buried structures was also obtained.

Strains, deflections and accelerations were less for the internally pressurized capsule with backpacking than for the other two capsules with no backpacking. Peak interface pressure measured for the model with no backpacking and with internal pressure was about 44 percent of the peak surface overpressure.

Finite element computer data gave conservative estimates because of its two-dimensional nature and because the diameter-to-length ratio was large; valuable information was obtained from the computer plots. The NCEL optimization equations can be used, with proper discretion, to design a buried fuel container to survive blast loading.

14 KEY WORDS	LINK A		LINK B		LINK C	
	ROLE	WT	ROLE	WT	ROLE	WT
Stresses						
Buried structures						
Fuel tanks						
Structural analysis						
Overpressure						
Blast effects						
Stress analysis						
Instrumentation						
Finite element analysis						
Optimization equations						

CONTENTS

FOREWORD

This report constitutes a portion of the Project Clarinet-Sanguine facilities research program. The facilities research program was sponsored by the Earth Sciences Division of the Office of Naval Research (ONR) who were charged by the Naval Electronic Systems Command (NAVELEX) with management of the research program for Project Sanguine.

General direction of the program was provided by Dr. T. P. Quinn and Mr. J. L. Warner of the Earth Sciences Division of ONR. Direction, particularly in program formulation, was also provided by Dr. B. Kruger and Mr. E. Pray of NAVELEX. Mr. J. R. Allgood served as NCEL project coordinator.

INTRODUCTION

Objective

The principal objective of Project LN311 was to obtain information that would permit establishing criteria for backpacking and internal pressurization as methods for reducing the stresses transmitted to buried structures.

Specific objectives were the following:

1. To obtain data for checking recently developed optimizing relations for the design of buried structures with backpacking.
2. To verify the results of laboratory experiments on fuel containers with internal pressurization.
3. To provide data for checking a nonlinear, large deformation, finite element computer program.

Background

This program is in support of Project Clarinet-Sanguine, which is a large communication system. The results are intended to serve as a check on theoretical developments and laboratory experiments that have been in progress for a number of years. D. A. Linger[1] and others have performed experiments on small-scale buried structures with backpacking, with generally favorable results. Subsequent to Linger's work, tests were performed on 6-foot-high vertical capsules or tanks (Figure 1a) with and without backpacking under Project LN311 of Operation Prairie Flat.[2] Those tests were primarily intended to provide a check on an arching equation; this equation determines the load transferred through the soil over a structure as a function of the ratio of the stiffness of the inclusion to the stiffness of the soil. Where backpacking is used, the inclusion consists of the structure and the backpacking. In Prairie Flat Project LN311, peak stresses, accelerations, and relative displacements were reduced by a factor of about 2 in the tanks with backpacking compared to the ones without backpacking. The arching equation was verified and subsequently was used in an optimization theory.[3] Calculations from the optimization theory led to the conclusion that the interface pressures and, thus, the induced stresses in a buried structure can be reduced by factors of up to 10 compared to the surface pressures.

A preliminary feasibility study has shown that large increases in the capacity of the structure to carry loads can also be achieved by internal pressurization.[4] Static and dynamic tests have been conducted on 12-inch-diameter, internally pressurized models in the laboratory.[5,6] Finite element computer analyses of the models have been made for comparison of experimental and analytical data to determine the influence of internal pressurization and other effects.[7,8] Tests on pressurized tanks (Reference 5) indicated:

1. More load is transferred to a pressurized tank than a non-pressurized tank.

2. Large tensile meridional strains occurred along the side of the horizontally buried tanks due to the action of the hemispherical end caps.

3. Buckling failure for pressurized tanks was delayed; internal pressurization increased the buckling load. Even though the models buckled, there was no loss of internal pressure.

To combine the effects of internal pressurization and backpacking on buried fuel containers and to check the results with the current version of linear and nonlinear computer programs, tests were planned to be conducted under Project LN311 in the 1970 500-ton DIAL PACK shot in Canada.* The DIAL PACK test scheme is illustrated in Figure 1b.

Theory

The design procedures utilizing the optimization (arching) equations[3] and a computer program for the selection of the thickness of a buried fuel container with internal pressurization are given in Reference 6. However, the program does not account for the stiffening of the model walls when internal pressure is introduced. In brief, the procedure is:

1. Determine the positive phase duration, t_d
2. Determine the natural period of the model, T_n
3. Calculate the dynamic amplification factor, **DF**
4. Calculate the pressure attenuation factor α_z:

$$\alpha_z = \frac{1}{1 + \frac{z}{L_w}} \qquad (1)$$

where z = depth below ground surface

L_w = depth factor

* Event DIAL PACK took place at the Defence Research Establishment Suffield, Ralston, Alberta, Canada at 11 a.m. MST on 23 July 1970.

5. Compute the arching factor, **A**, by estimating tank thickness, **t**:

$$\left(1 - \frac{A}{A_o}\right)^{1-A} = e^{-n\Phi} \tag{2}$$

where A_o, n = experimentally determined constants

$$\Phi = A_g\left(\frac{M_c}{p_v}\right)\delta$$

$$A_g = \frac{\text{(plan perimeter of tank)(depth of cover over crown)}}{\text{(plan area of tank)(mean diameter of tank)}}$$

M_c = confined compression (secant) modulus of soil

p_v = uniform pressure in free field at elevation of crown

δ = relative deflection between soil and tank

6. Compute the dead load pressure, p_{DL}, acting on the crown of the tank.

7. Calculate the total effective pressure, p_e, acting at the crown of the tank; neglect internal pressure.

$$p_e = (1 - A)(p_v + p_{DL})$$

8. Calculate the internal pressure, p_i:

$$p_i = \frac{p_e}{3} \tag{3}$$

9. Determine the critical yield pressure on the tank, p_y:

$$p_y = p_e - p_i \tag{4}$$

10. Determine the required tank thickness to resist p_y:

$$t = \frac{(p_e - p_i)D}{2.54 f_y} \tag{5}$$

where D = diameter of cylinder

f_y = yield stress of tank material

11. If the computed tank thickness is the same as that assumed in step 5, the tank is properly designed; if not, use new tank thickness and repeat from step 5.

12. Check for the critical buckling pressure of the tank (Reference 9):

$$p_{cr} = 0.621 \sqrt{\frac{E_s E_t}{(r/t)^3}} \tag{6}$$

where E_s = modulus of soil

E_t = modulus of cylinder material

r = radius of tank

t = thickness of tank

Large reductions in the pressure transmitted to buried structures are possible by proper placement of low modulus materials in the overburden. A buried inclusion may receive a greater or lesser load than that in the adjacent free-field, depending upon whether it is more or less stiff than the soil. Use of backpacking is merely a means for reducing the stiffness of the total inclusion consisting of the structure and the backpacking, so that most of the load will be carried by the soil.

From experiments and fundamental considerations, it has been deduced that the following are necessary in order for backpacking to be effective:

1. The ratio of depth of cover to diameter must be large enough to permit formation of a soil arch over the inclusion.

2. Unless it is inordinately thick, the backpacking must yield to transfer a large percentage of the applied load to the soil arch.

3. A certain minimum stress must exist under the soil arch to maintain its integrity.

4. If conditions 1 through 3 are met, the peak pressure on the structure will be the yield stress of the backpacking.

Allgood[3] has shown that the required thickness of the backpacking can be expressed as:

$$\frac{t_L}{H} = \frac{\epsilon_s}{\epsilon_{hL}} \left(\frac{\Phi_m}{A_g H} + 1 \right) \tag{7}$$

where t_L = thickness

H = height of inclusion

ϵ_s = average strain in free field over height of inclusion

ϵ_{hL} = hardening strain of backpacking

Φ_m = 4.0 for maximum arching of sand

This equation is based on the assumption that all of the strain in the inclusion is from deformation of the backpacking.

PROCEDURE

General Operations

Four capsule-shaped structures with hemispherical ends were designed utilizing the arching theory and checked with a finite element computer program. The fabricated models were then instrumented and made air tight before being shipped to the test site. They were horizontally buried with their axes of symmetry normal to the direction of propagation of the blast wave at a range of 180 feet from GZ as shown in Figure 2. The 180-foot range corresponded to a predicted peak overpressure of 600 psi.

Design of Models

The procedure for the design of a pressurized, buried fuel container has been discussed in an earlier section. The computer program utilizing the procedures has been used for the design of the 36-inch diameter capsules. The computer output data are presented in Table 1. The design procedure takes into account the effect of attenuation of the pressure in the soil media, the soil arching over the model, and the pressure in the model. For a predicted overpressure of 600 psi, the calculated thickness of the model was 0.115 inch; the calculated effective pressure at the crown on the model was 610 psi. However, from previous test data,[2] the attenuation factor at a depth of 36 inches was about one-third. Considering this information, and from simple calculations of thin spheres and cylinders as guidelines, the final thickness selected was 0.134 inch for the 36-inch-diameter capsules. The design of the 12-inch-diameter model is reported in Reference 5; the wall thickness was 0.024 inch. This small model was a back-up specimen for the dynamic tests conducted recently by NCEL at the Waterways Experiment Station (WES) and had not been tested previously. Other pertinent information of all the models is presented in Table 2.

Table 1. Computer Output From Design And Cost Optimization Program

Design Parameter	Value
Overpressure	600.00 psi
Water table level	22 ft
Dynamic amplification function for	
T (initial)	2.00254
T (total)	2.00205
Factor used	2.00254
Pressure amplification factor due to water table	1.00000
Deadload and water pressure	1.35 psi
Internal pressure	203.62 psi
Effective pressure at tank	610.87 psi
Critical pressure	407.25 psi
Alpha	0.83896
Arching factor	0.40501
Burial depth	3.00 ft
Tank diameter	3.00 ft
Length of tank	6.00 ft
Calculated tank thickness	0.11544 in.
Thickness used (commercial use)	0.25000 in.
Buoyancy effect—uplift force	0 lb
Volume of excavation	36 cu yd
Volume of special backfill	35 cu yd
Volume of ordinary backfill	0 cu yd
Volume of tank	35.34 cu ft 264 gals
Total cost of tank	$932.27

Table 2. Model Designation, Dimension, And Burial Characteristics

Designation	Hemisphere and Cylinder Diameter (in.)	Overall Length (in.)	Thickness (in.)	Backpacking		Internal Pressure (psi)	Depth of Crown (in.)	Model Material	Liquid[c]
				Type	Size (in.) L x W x t				
CP-1	36	72-1/4	0.134	none	NA	150	36	Cor-Ten	1/2 full
CP-2	36	72-1/4	0.134	1043-2[a]	84 x 48 x 3	150	36	Cor-Ten	1/2 full
CP-3	12	24	0.024	AM[b]	24 x 14 x 1	100	12	T-304	1/2 full
CN-1	36	72-1/4	0.134	none	NA	0	36	Cor-Ten	none

[a] CPR rigid polyurethane foam, 1040 Series

[b] Styrofoam

[c] Dow Corning 200 fluid, Bulletin 05-145

The design of the backpacking thickness was performed by using Equation 7 to give maximum arching. The information on the type of backpacking used is given in Table 2.

Preliminary Analysis of Models

A dynamic nonlinear finite element computer program[8] was used to gain insight into the stress magnitudes imposed on the capsules. The computer program is expected to yield higher values than did the experiment because the models tested had a small aspect ratio (length to diameter ratio of 2) and the hemispherical end caps restrained the cylinder walls. Since the buried capsules were not axisymmetrical about a vertical axis, a plane strain condition was assumed at the midsection.

In the analytical model, the cylinder was assumed to be infinitely long and the finite element grid was drawn as shown in Figure 3. The top surface (nodal points 347 to 361 inclusive) was loaded using the load function approximated by measurements recorded during Operation Prairie Flat in 1968[10] at a distance of 180 feet from ground zero (Figure 4). A 3-inch thick rectangular backpacking material was located 3 inches above the crown. Samples of the deflection contours at 6 and 18 msec are shown in Figure 5.

The plots of the stresses with respect to time are shown in Figure 6 for element 51 in the soil above the crown and in Figure 7 for element 4 in the shell at the springing. These are labeled "nonlinear, with B.P." The same finite element mesh was used and the problem rerun without the backpacking using the nonlinear, large deformation program and the linear elastic program. The results of the stress-time curves are also plotted in Figures 6 and 7 for comparison with the model with backpacking. The figures show that the analytical model with backpacking received the lowest stress, whereas the elastic run with no backpacking received the highest stress.

However, to properly model the horizontal capsule analytically by the finite element method, a three-dimensional computer program would be required since the structure is not axisymmetrical about the vertical axis. An elastic three-dimensional program (Structural Analysis Program, SAP) has recently been made available for static and dynamic analyses (Reference 11). The dynamic version of this program utilizes the incremental step-by-step procedure. A mesh for using SAP is presently being assembled for the buried fuel container and the results will be presented in a future report.

Fabrication of Models

Three of the capsules (**CP-1**, **CP-2**, and **CN-1**) were fabricated by Southwest Welding and Manufacturing Company of Alhambra, California (see Figures 8 and 9). They have an inside diameter of 36 inches and an overall length of 72-1/4 inches. The walls are 0.134 inch thick and were made of USS Cor-Ten steel. The yield strength and Young's modulus of elasticity for the 10-gage USS Cor-Ten steel are 61,000 psi and 29.3×10^6 psi. A post-shot view of model **CP-3** will be shown later.

Tensile stress-strain curves for the USS Cor-Ten steel and for the T-304 stainless steel are presented as Figures 10 and 11.

The models were fabricated in three sections: the two hemispherical end caps, and the cylinder. Instrumentation was mounted after one end cap was welded on to the cylinder. The instrumentation wires were passed through special connectors in the walls of the model and the opening was filled with liquid-type plastic steel made by Devcon Corporation of Danvers, Massachusetts. After the second end cap was welded to the other end of the cylinder, the model was air tested for leaks. It was important to detect any leaks at that time because the models were to be pressurized in the field just prior to the day of the shot.

Instrumentation

Forty-eight channels of electronic instrumentation were employed for the test as shown in Figure 12.

Pressure Gages. One Bytrex Model HFG-1000-SE pressure gage was used to measure the surface overpressure. One Bytrex Model HFG-500-SE gage was placed inside each of Models **CP-1** and **CP-2** to measure the internal gas pressure. One Sensotec Model M-7F pressure gage was mounted outside on top of Model **CP-1** to measure the pressure reaching the capsule.

Velocity Gages in Structure. Six Sparton Southwest Models 601-H (horizontal) and 601-V (vertical) gages were mounted on Models **CP-1**, **CP-2**, and **CN-1** to measure the velocity of the capsules from which the rigid body displacement and horizontal acceleration were calculated. Both models contained a pendulum suspended in a viscous oil. Model 601-V had a spring which compensated for the force of gravity on the pendulum.

Velocity Gages in Free-Field. Two free-field velocity gages were placed at depths of 3 and 6 feet to measure vertical velocities. These gages (the same model as those mounted on the structures) were mounted in aluminum canisters.

Accelerometers. Three Endevco Model 2261 (range of 2,500 g's) accelerometers were mounted in Models **CP-1**, **CP-2**, and **CN-1** to measure vertical acceleration. One Endevco Model 2264M1 (range of 4,500 g's) accelerometer was mounted in Model **CP-3**. All of the accelerometers were of the undamped piezo-resistive type.

Strain Gages. A total of 21 BLH Type FAE-50-12S6 strain gages were mounted inside and outside of Models **CP-1**, **CP-2**, and **CN-1** to measure the meridional and circumferential strain induced in the model walls. Seven Micro-Measurements Type EA-06-250-BG-120 strain gages were mounted in Model **CP-3**.

Deflection Gages. Three Bourns linear motion potentiometers, Type 108 (travel of 4 inches), were connected to the crown and invert of Models **CP-1**, **CP-2**, and **CN-1** to measure the relative movement. One Bourns linear deflection potentiometer, Type 108 (travel of 2.31 inches) was connected similarly in Model **CP-3**.

More detailed information on the transducers, signal conditioning, amplifying, and recording systems and procedures is presented in Appendix A.

Immediately after the blast the tapes were played back and data recorded on direct-write oscillographs for preliminary field reduction. This reduction consisted of applying calibrations to the oscillogram data and determining peak values of overpressure, velocity, acceleration, strain, and deflection. Upon returning to the Laboratory, a complete analysis of each data channel was made on a Control Data Corporation 6600 computer.

Preshot and postshot surveys provided data on the vertical displacement of the structures, and a visual examination of the models provided information on permanent deformations.

Pressurization Equipment

Nitrogen bottles served as the internal pressure source for the cylinders. A console consisting of a pressure regulator, low and high pressure gages, hose fittings and valves was used to reduce the high bottle pressure of the nitrogen to the desired tank pressure.

Backpacking Material

Two types of backpacking were used in this task. Model **CP-2** had a rigid urethane foam with a density of 2 lbs per cubic foot and a static compressive yield strength of 25 psi. The vendor was the CPR Division of the Upjohn Company in Torrance, California. The stress-strain curves for this backpacking were obtained from Reference 12 and are shown in Figure 13. The three stress-strain curves indicate that the material is quite strain rate sensitive. The dynamic yield stress of the material tested at a strain rate of 7.64 in./in./sec is about 40 psi. For higher strain rates, the yield stress may become higher.

Model **CP-3** utilized the SM Styro Foam backpacking which was made by Dow Chemical Service Center in Vernon, California. The stress-strain curve for this material is shown in Figure 14.

Placement of Models

All of the capsules were buried with a depth of cover over the crown of one diameter. **CN-1** was not internally pressurized and had no backpacking. **CP-1** was internally pressurized to 150 psi and had no backpacking. **CP-2** was also pressurized to 150 psi and had a 48 x 84 x 3-inch layer of rigid urethane foam (2 pcf) directly above it. **CP-3** was internally pressurized to 100 psi and had a 14 x 24 x 1-inch layer of styrofoam (2 pcf) placed directly above it. The three pressurized capsules were half filled with nonconducting Dow Corning 200 silicone fluid.

Undisturbed soil samples of the in-situ material at the bottom of the pits were taken by U. S. Army Corps of Engineers, Waterways Experiment Station (WES), personnel after excavation. WES later performed one-dimensional static and dynamic compression tests which were used as soil input data for computer and other analyses[13] (Appendix B).

Cook's Bayou sand was shipped from WES and used to backfill **CP-3**. This dry sand was "rained" from a height of 26 inches (Figure 15). No testing of this material was required because its properties are well documented in many of the Waterways Experiment Station reports.[14] Some of the properties are reproduced in Appendix B, Figures B-17, B-18, and B-19. Watching Hill sand near the Buffalo Trail was used to backfill the other three capsules. Moisture-density tests were performed by NCEL personnel as the backfilling operation progressed. Three bags of disturbed sand were shipped to WES for further one-dimensional static and dynamic compression tests; the results are presented in Appendix B.

The four capsules were buried in three pits as shown in Figure 2. The pit for **CP-1** and **CN-1** was 26 feet long, 8 feet wide, and 7 feet deep. The pit for **CP-2** was 12 feet long, 8 feet wide, and 7 feet deep. The pit for **CP-3** was 5 feet long, 3 feet wide, and 3-1/2 feet deep. The two large pits were then backfilled with Watching Hill sand to a depth of 5-1/2 feet. For proper seating, a bed was carved for each of these large capsules to a depth of 4-3/4 inches. The capsules were then carefully placed in position by a crane (Figure 16). Instrumentation and pressure lines were looped to safeguard against possible damage during the blast (Figure 17).

Backfill was then compacted up to the surface, except for **CP-2**. The sand was backfilled to 3 inches above the crown of **CP-2** and then the rigid urethane foam was placed at this level (Figure 18). Sand backfill was placed in 6-inch lifts and compacted with three passes of a vibrating Whacker.

The pit for **CP-3** was backfilled to a depth of about 1-3/4 feet. The silicone fluid filled capsule was then hand placed in a 2-5/8 inch deep carved bed at this depth. The "raining" process was continued to a height of 1 inch above the capsule crown; a styrofoam backpacking was placed at this level. Cook's Bayou sand was then placed up to the ground level.

The liquid and nitrogen lines for **CP-1** and **CP-2** were brought up to 1 foot from the surface. Five days before the shot, the liquid was added. The day before the shot, pressure was applied to all three capsules in three steps after the zero reading was taken; the loads applied internally were 50, 100, and 150 psi for **CP-1** and **CP-2** and 50, 75, and 100 psi for **CP-3**. After each increment the static strains were recorded and used to compare with theoretical strain values. Model **CN-1** was not pressurized. Once the pressures were raised to the desired levels of 150 and 100 psi for the 36-inch and 12-inch diameter models, respectively, the valves were closed to maintain the pressure. Four hours later, the pressures were checked and no leakage was found. On the day of the shot, the pressures were checked once more and there was no loss of pressure. The pressure valves in the hand holes were then protected with styrofoam backpacking and the hand holes were filled with Ottawa sand to distinguish the location from the regular backfill. Shortly after the blast, the hand holes were dug open and the internal pressures were relieved so that a zero reading could be recorded.

RESULTS

The day before the blast, static data were recorded for pressure, deflections, and strains for the internally pressurized models. The 36-inch diameter and 12-inch diameter models were pressurized to 150 and 100 psi, respectively. This information was necessary so that the effect of initial internal pressurization could be added algebraically to the dynamic value.

Computer plots for the channels of dynamic information recorded during the test are presented in Appendix C. Where the zero time for the computer plots is not the time of detonation of the TNT, the actual time after detonation is indicated within the parenthesis placed adjacent to the zero time. The reduced data for maximum values are summarized in Table 3. These maximum values are the actual responses by the models with the effects of internal pressurization taken into consideration. The deflection and strain gage locations were the same for the four models.

Upon excavating the soil to retrieve the models, it was found that the pressurized flexible hoses were not damaged from the blast; it seems that the loops adjacent to the models (Figure 17) helped to reduce the tension in the hoses during the differential displacement between the soil medium and the models.

General Ground Surface and Model Elevation Data

Prior to backfilling, horizontal and vertical controls were established for the tops of the models. The post-shot elevation of the models and the settlement of the ground surface are shown in Figure 19. The 36-inch-diameter capsules were lowered an average of 2.81 feet by the blast; the 12-inch diameter capsule was lowered about 2.52 feet. A view of the three undamaged 36-inch-diameter models after the test is shown in Figure 20.

Free-Field Response

Pressure cell PC1 was placed on the ground surface between **CN-1** and **CP-2**; the peak overpressure recorded was 680 psi at 16.3 msec after the blast; however, the pressure was nearly constant at about 350 psi for about 4 msec before decaying to zero (see Figure C-1). The positive phase duration was 10 msec.

The free-field velocity gages registered initial peak velocities of about -145 and -95 inches per second at 3 and 6 feet below the ground surface, respectively (Figures C-2 and C-3). The corresponding times of arrival were approximately 19 and 22 msec. Horizontal and vertical particle velocities versus distance measurements made by Project LN302 personnel are shown in Figures 21 and 22. No horizontal velocity measurement was recorded for Project LN311. However, values of the vertical velocity for the 3- and 6-foot depths are indicated in Figure 22.

[illegible] Summary of Maximum

Measurement	CP-1				CP-2			
	[illegible]	[illegible]	[illegible]	[illegible]	[illegible]	[illegible]	Subsequent Maximum or Minimum	[illegible]
Overpressure psi		+[illegible]				[illegible]	370	
Interface pressure psi		[illegible]						
Interface pressure psi	[illegible]	[illegible]	[illegible]		[illegible]	[illegible]	+1[illegible]	
Diameter Deformation in	[illegible]	[illegible]		[illegible]	[illegible]	[illegible]	-0.2 +0.19	
Strain 1 μin/in	[illegible]	[illegible]	[illegible]	[illegible]	+44	+[illegible]	-70 -480	
Strain 2 μin/in	[illegible]	[illegible]	[illegible]	[illegible]	[illegible]	+38[illegible]	+360	
Strain 3 μin/in	[illegible]	[illegible]	[illegible]	[illegible]	[illegible]	-25[illegible]	+1,280, -700	
Strain 4 μin/in	[illegible]	[illegible]		[illegible]	[illegible]	-26[illegible]	+1,200 -800	
Strain 5 μin/in	[illegible]	[illegible]	[illegible]		+24[illegible]		+[illegible]00	
Strain 6 μin/in	+2[illegible]	[illegible]			[illegible]	-4[illegible]	+360	
Strain 7 μin/in	[illegible]	[illegible]	[illegible]	[illegible]	[illegible]	[illegible]	-800 [b] +300	
Acceleration		[illegible]	[illegible]			[illegible]	-270	
Vert Velocity Integrated in/sec		[illegible]	[illegible]			[illegible]	[illegible]	
Hor Velocity in/sec		[illegible]	[illegible]			[illegible]	[illegible] +4[illegible]	
Vert Velocity in/sec		[illegible]	[illegible]			[illegible]	[illegible]	
Low Field Vert Velocity (3.5) in/sec		[illegible]	[illegible]					
Low Field Vert Velocity (6.5) in/sec		[illegible]	[illegible]					

[a] [illegible]

[b] Extrapolated

Preceding page blank

n Response for LN311 Test Modes

	CN-1				CP-3			
rmanent, ormation	Initial Reading	Initial Maximum or Maximum	Subsequent Maximum or Maximum			Initial Minimum or Maximum	Subsequent Maximum or Minimum	Permanent Deformation
	0	690	37			670	370	
	0							
	0							
	0	-0.430				+0.250		+0.047
+70	0	-250	+350 -190			-460	-670 +430	-300
+10	0	-850				-650	-1.360 +220	-430
-160	0	-770	+290			+1.700		
-130	0	-670				+1.750		
-50	0	-250	-500 +4			-240		
-30	0	-350						-50
-30	0	+440				+520		+900
		-400					-250 -1.250	

Model CP-1 Response

Model **CP-1** was internally pressurized to 150 psi and had no backpacking. The blast wave arrived at 180 feet from **GZ** at 16.3 msec after detonation; then in an additional 2.9 msec (or 19.2 msec after detonation), the shock wave traveled through the ground to the top of the model. The peak interface pressure recorded was about 300 psi (Figure C-1); this was about 56% less than the peak surface overpressure. The 150 psi air pressure inside the tank increased and decreased alternatively with the maximum and minimum values being 157 and 133 psi, respectively (Figure C-4). The maximum vertical diametral deformation recorded was about -0.76 inch. The deformation remained negative (or shortened) for about 11.5 msec and then extended to about +0.1 inch after the surface overpressure decayed to zero (Figure C-5).

Strain gages 1 and 2 located at the springing of the capsule both had initial maximum values of about -800 μin./in. Strain trace 1 returned to its initial static strain of +570 μin./in. in 8 msec (Figure C-6). Strain gages 3 and 4 had almost identical traces with maximum negative meridional strains of -1,150 and -790 μin./in., respectively at the crown (Figure C-7). Strain gages 5 and 6 were located at the springing of the hemispherical end caps to measure the vertical thrust and moments. For model **CP-1**, strain gage 5 short-circuited so no reading was obtained; strain gage 6 peaked to about -130 μin./in. and returned to the initial static value of +260 μin./in. in about 22 msec (Figure C-8). Strain gage 7 was located at the springing to measure the meridional strain. From previous tests[5] it was found that models with a length-to-diameter aspect ratio of 2 to 1 had high tensile strains induced at this location. The maximum value obtained from gage 7 was about +1,010 μin./in. and returned to the initial static strain value of +160 μin./in. in about 19.5 msec (Figure C-8).

Figures C-9 through C-11 are traces of the vertical acceleration, velocity and deflection from an accelerometer placed at the springing inside model **CP-1**; the velocity and deflection traces were obtained by integrating the acceleration data.

The horizontal and vertical velocity traces of model **CP-1** are shown in Figures C-12 and C-13.

Model CP-2 Response

Model **CP-2** was internally pressurized to 150 psi and had a 3-inch thick polyurethane foam backpacking placed 3 inches above the crown. The backpacking has reduced the blast energy transmitted to the model. Post-shot measurements of the backpacking thickness were taken and are presented in Figure 23; near the center of the backpacking, the thickness decreased from 3 inches to 1-1/2 inches for a strain of 50%. The horizontal movement of the backpacking with respect to the model is shown in Figure 24. The internal pressure decreased and increased 3 and 6 psi respectively during the shot (Figure C-14). The maximum diametral deformation was about -0.03 inch (Figure C-15); the gage was defective after the initial maximum deflection was reached. The blast reduced the strain for gage 1 from its initial static value of +440 μin./in. to +60 μin./in.; for gage 2 the strain was reduced from +710 μin./in. to +380 μin./in. (Figure C-16).

The presence of the backpacking above the crown and internal pressure inside the model caused the initial maximum response of strain trace 3 to rebound from -260 μin./in. to about +1,280 μin./in. Strain gage trace 4 behaved in a similar manner by rebounding from -250 μin./in. to +1,200 μin./in. The responses of these two curves are shown in Figure C-17.

Strain traces 5 and 6 behaved in a similar pattern. Strain trace 5 dipped down to zero strain and rebounded to +600 μin./in. while strain trace 6 also dipped to -40 μin./in. and rebounded to +460 μin./in. These curves are shown in Figure C-18.

Strain trace 7 increased from an initial static value of +50 μin./in. to +280 μin./in. However, unlike the result for model **CP-1**, in which the strains oscillated in the tensile range, the strain suddenly dipped to about -800 μin./in. The actual value is not known because the gain on the recorder was not set for this large negative value (Figure C-19).

The initial maximum and minimum vertical accelerations of model **CP-2** were +60 g and -280 g (Figure C-20).

The resulting values of the horizontal and vertical velocities of the model and the respective integrated values (deflections) are presented in Figures C-21 through C-24. The minimum and maximum values of the velocities were -120 and +45 in./sec for the horizontal direction and -85 and +40 in./sec for the vertical direction.

Model CN-1 Response

Model **CN-1** had no backpacking and was not internally pressurized; therefore, internal pressure was not measured. Diametral deformation measurements gave a peak value of about -0.43 inch which decayed to zero in about 25 msec (Figure C-25).

Strain trace 1 behaved differently from strain trace 2 in that the former oscillated about the zero value between -250 and +350 μin./in. for the first 10 msec, while the latter remained in the compression range; the maximum value for strain gage 2 was about -1,360 μin./in. (Figure C-26).

Strain traces 3 and 4 were quite similar for the first 10 msec and indicated that the crown had negligible meridional moment but did have a compressive meridional thrust (Figure C-27).

Strain traces 5 and 6 behaved similarly to strain traces 3 and 4 but were of a lower magnitude. The compressive meridional thrust continued for about 20 msec (Figure C-28).

Strain trace 7 for **CN-1** behaved similarly to strain trace 7 for **CP-1** and remained in tension for about 15 msec before dipping into the compressive range (Figure C-29).

A maximum negative acceleration value of -1,170 g was recorded (Figure C-30). The recording for the horizontal velocity was faulty and hence is not included in this report. The vertical velocity of the capsule first had a maximum value of -140 in./sec and then had a value of +40 in./sec on the rebound. This trace and the integrated deflection curve is shown in Figures C-31 and C-32.

Model CP-3 Response

This 12-inch diameter model (the others were 36 inches in diameter) was initially internally pressurized to 100 psi and had a 1-inch backpacking placed 1 inch above the crown. Measurement after the test showed that the thickness of the material was still about 1 inch indicating that the backpacking was ineffective. In Figure 23, the top elevations of the backpacking after the test are given; the edge of the backpacking away from the blast was about 3 inches below the edge nearest the blast. Additionally, in Figure 24, it is shown that the backpacking moved horizontally about 5 inches farther away from ground zero than the model. The vertical spacing between the backpacking and the crown of the model was about 4 to 5 inches after the shot; prior to the blast, the vertical distance was 1 inch. The above extreme displacement was caused by the overthrusting of the top soil layer.

Considering the effects of the internal pressure, the blast produced a maximum vertical diametral deformation of -0.25 inch (Figure C-33). A permanent deformation of +0.05 inch or an increase in the vertical diameter occurred because of the buckling of the cylindrical shell near the crown away from ground zero (Figure 25). Buckling also occurred along the intersection of the cylinder and the hemisphere. An unusual meridional buckling occurred on the hemisphere end cap above the springing line on the vertical plane of symmetry (Figure 23).

The respective initial static strains for gages 1 and 2 were +720 and +760 μin./in. The maximum subsequent strain traces of -670 and -1,060 μin./in. were recorded by gages 1 and 2 respectively (Figure C-34). For the previous models, strain traces 3 and 4 initially went into the compression range; however, for this model the strain traces started to go into the compression range but suddenly reversed their direction and went in the tensile direction to a maximum strain of about 1,700 μin./in. (Figure C-35) and remained at that magnitude. Strain 5 oscillated about its initial value of +310 μin./in. for the first 25 msec, while strain trace 6 went into the compression range with a maximum value of -1,750 μin./in. (Figure C-36).

As expected, strain gage 7 registered a tensile strain of about +2,200 μin./in. from an initial value of about +180 μin./in. (Figure C-37). The maximum vertical acceleration recorded was about -1,050 g (Figure C-38).

DISCUSSION

The purpose of this experiment was to determine the effectiveness of internal pressurization and backpacking. It was not possible to test all the desired configurations and combinations of internal pressurization and backpacking because of economical reasons.

Thirty-Six-Inch-Diameter Models

Experimental strain data obtained from the internal pressurization static test compared reasonably well with theoretical strains. The values for 150 psi are presented in Table 4 for **CP-1**, and **CP-2**. Equations 8 and 9 were used for obtaining the theoretical values:

$$f_\theta = \frac{p_i R}{t} \quad \text{(circumferential stress)} \tag{8}$$

$$f_m = \frac{p_i R}{2t} \quad \text{(meridional stress)} \tag{9}$$

The corresponding strains are

$$\epsilon_\theta = \frac{f_\theta}{E} - \frac{\nu f_m}{E} \quad \text{or} \quad f_\theta = \frac{E}{1 - \nu^2}\left(\epsilon_\theta + \nu \epsilon_m\right) \tag{10}$$

$$\epsilon_m = \frac{-\nu f_\theta}{E} + \frac{f_m}{E} \quad \text{or} \quad f_m = \frac{E}{1 - \nu^2}\left(\nu \epsilon_\theta + \epsilon_m\right) \tag{11}$$

where p_i = internal pressure

R = radius of cylinder

t = thickness of cylinder

E = Young's modulus of elasticity

ν = Poisson's ratio

m, θ = subscripts indicating meridional and circumferential directions respectively

Equations 10 and 11 were also used to calculate the dynamic thrust and moment at the springing line of the models. The assumption made was that the strain in the meridional direction at the springing was in pure tension with no bending. Strain gages S1, S2, and S7 as located in Figure 12 were used to calculate the values presented in Figures 26 and 27. The maximum/minimum values as well as the initial values are summarized in Table 5; they are the resultant (net) values of the static and dynamic combination. The thrust and moment values for model **CP-3** were not realistic since the strains were in the inelastic range and hence have not been included. Models **CP-1** and **CP-2** had initial static thrusts of +2,500 lb/in. of length from the initial internal pressure. **CN-1**, the cylinder without backpacking and without internal pressurization, had the greatest dynamic thrust of -3,100 lb/in. It was followed by **CP-1**

with -2,200 lb/in. and **CP-2** with +240 lb/in. (The large dip into the negative thrust region at t = 11 msec was because of a faulty gage reading. See Figure C-16, gage S1.) This indicates that backpacking with internal pressurization is very beneficial to the increased survivability of buried fuel containers. The 36-inch diameter models were internally pressurized to 150 psi which produces stresses equivalent to about one-third of the yield strength of the material. The largest dynamic strain from the blast was about -1,360 μin./in. (model **CN-1**) which indicated a stress near the proportional limit of 42,000 psi.

Table 4. Comparison of Experimental and Theoretical Strains for Internal Pressurization

Strain Gage No.	Strain (μin./in.)				
	Internal Pressure = 150 psi			Internal Pressure = 100 psi	
	Model **CP-1**	Model **CP-2**	Theory	Model **CP-3**	Theory
S1	570	440	590	720	732
S2	500	710	590	760	732
S3	140	110	138	240	172
S4	140	140	138	240	172
S5		290	243		301
S6	260	230	243	240	301
S7	160	50	138	180	172

Table 5. Summary of Circumferential Thrust and Moment

Model No.	Thrust			Moment		
	From Internal Pressure (lb/in.)	Maximum and/or Minimum (lb/in.)	Time After Detonation (msec)	From Internal Pressure (in.-lb/in.)	Maximum and/or Minimum (in.-lb/in.)	Time After Detonation (msec)
CP-1	+2,500	-2,200	20.2	+3.0	-9.0 +31.0	20.5 23.6
CP-2	+2,540	+240	24.7	-13.0	-51.0	36.8
CN-1	0	-1,510 -3,100	20.2 23.1	0	+54.5 +56.5	20.7 23.4

CP-1; with 150 psi internal pressure, no backpacking
CP-2; with 150 psi internal pressure, with backpacking
CN-1; no internal pressure, no backpacking

After determining the peak values of the thrust for the 36-inch diameter models, the effective pressure, p_e, of the soil on the model can be calculated approximately as follows:

$$T + p_i R - p_e R = 0 \tag{12}$$

or

$$p_e = \frac{T + p_i R}{R} \tag{13}$$

where T = maximum thrust, lb/in.

p_i = internal pressure, psi

R = radius of tank, inches

p_e = effective pressure of soil on tank, psi

For internal pressurization of 150 psi and a radius of 18 inches, the effective pressures were calculated and are summarized in Table 6.

As the pressure pulse travels through the soil its peak magnitude continually decreases. The attenuation factors can be obtained from free-field velocity gage data from the following one-dimensional wave equation (Reference 15)

$$\alpha_z = \frac{V_p \rho C_L}{p_o} \tag{14}$$

where α_z = pressure attenuation factor

V_p = peak vertical velocity at selected depth

ρ = mass density of soil

$C_L = \sqrt{M_c/\rho}$ = propagation velocity of peak soil stress

M_c = secant modulus of confined compression

p_o = surface overpressure

Free-field soil velocity data were recorded at 3- and 6-ft depths and used in Equation 14 to yield two attenuation factors. These were used in Newmark's attenuation equation (Equation 1) to yield two values of L_w, an empirical parameter depending on weapon yield, soil properties, and overpressure range (Reference 15). The two values of L_w were averaged as in Reference 2 and an average value of the attenuation factor was obtained to be 0.348.

Utilizing Equation 2 and the procedure presented in Reference 6, the arching factor was calculated for **CN-1** (no internal pressurization and no backpacking) as 0.26. The effective pressure, p_e, on the capsule can be calculated as

$$p_e = (1 - A)\,\alpha_z\, p_o \qquad (15)$$

$$p_e = 175 \text{ psi}$$

where A = arching factor

α_z = pressure attenuation factor

p_o = surface pressure

This agrees closely with the calculated value of 172 psi from strain gage data.

The arching factor for **CP-1** and **CP-2** was calculated from Equation 15 by using the calculated values of effective pressure presented in Table 6. Solving for the arching factor, **A**, in Equation 15:

$$A = 1 - \frac{p_e}{\alpha_z\, p_o} \qquad (16)$$

The arching factor for **CP-1** was calculated to be -0.148. For **CP-2**, the arching factor was calculated to be 0.717 during the crushing of the backpacking phase and 0.422 after the backpacking material was strain hardened.

Utilizing the material properties information of the backfill and the in-situ soil obtained for NCEL by the Waterways Experiment Station (Reference 13), together with the material properties of the backpacking and the steel cylinder, a non-linear large deformation computer run was made for a long cylinder with no backpacking and no internal pressure (**CN-1**). When circumferential thrust at the springing was compared with experimental data, the values obtained from the computer runs were over twice the experimental values (Table 7). This is because of the assumption of plane strain, whereas the cylindrical section of the actual model test data results are influenced by the stiffening effect of the end caps. Reference 5 takes account of the stiffening effect by combining the results of the solutions from the plane strain and the sphere. An elastic, three-dimensional computer program is also available at the Laboratory to study horizontally buried cylinders subjected to static and dynamic loads (Reference 16). Because the cost for a static run can easily exceed a thousand dollars and because funds were limited, the three-dimensional runs were not made for this task; however, these runs will be made, and the results will be included in a future laboratory report.

Table 6. Summary of Effective Interface Pressure of Soil on Models

Model No.	Thrust (lb/in.)	Effective Pressure (psi)	Time After Detonation (msec)	Arching	Remarks
CP-1	-2,200	272	20.2	-0.15	First peak value
CP-2	+1,500	67	21.0	+0.72	Initiation of crushing of backpacking
	+240	137	24.6	+0.42	Maximum value after strain hardening of backpacking was reached
CN-1	-3,100	172	23.0	+0.26	Second peak value

Table 7. Comparison of Experimental Data With Computer Code (Model CN-1)

Measurements, Units	Experiment		Computer	
	Value	Time After Blast Arrival, msec	Value	Time After Blast Arrival, msec
Vertical diametral displacement, in.	-0.430	10.7	-0.878	15
Average circumferential strain at springing line, psi	-23,250	4.2	-57,000	6
Maximum extreme fiber circumferential strain at springing line, psi	-42,190	4.2	n.a.	n.a.
Vertical acceleration at springing of cylinder, g's	-400 -1,100 +430	3.2 3.7 4.2	-360	4
Vertical velocity of crown of cylinder, in./sec	-140	5.7	230	6

Twelve-Inch-Diameter Model

The static test data obtained from the internal pressurization of the 12-inch-diameter model compared very well with the theoretical strains. The values for 100 psi are presented in Table 4.

The 12-inch-diameter model was designed to fail under a blast load of 250 psi (Reference 5); it was fabricated similar to the horizontal model tested at the Waterways Experiment Station (WES) in Vicksburg, Mississippi. For the horizontal models tested at WES, static buckling failure occurred when the surface load was 500 psi and the internal pressure was reduced from 100 psi to 13 psi. Buckling failure did not occur at a peak dynamic overpressure of 250 psi and an internal pressure of 100 psi; however, some of the strains were

above the yield strain of the material. One reason for this test of the 12-inch-diameter model in the Event DIAL PACK was to see whether it could survive a predicted overpressure of 600 psi without complete collapse and loss of internal pressure.

For model **CP-3** (12-inch diameter), information from strain gages 3 and 4 (Figure C-35) indicated that the model buckled while the induced stresses were below the 0.2% offset yield stress of 37,000 psi. Buckling occurred in the cylinder just below the crown line, at the intersection of the cylinder and hemisphere near the springing, at the bottom of the cylindrical section, and in the hemisphere between the springing and the crown (Figure 25).

Backpacking did not provide as much protection for model **CP-3** as it did for **CP-2** because of the overthrusting action of the top layer of soil; the backpacking was permanently displaced horizontally about 5 inches further from ground zero than the model. Although the tank buckled at several locations, the internal pressure of 100 psi was essentially maintained with a loss of only about 2 psi. The flexible tubing used did not require any additional protection from differential displacement; the loops made adjacent to the tank provided enough slack to prevent fracturing of the connections. Internal pressurization prevented complete collapse of the model.

GENERAL SUMMARY

The Project LN311 experiment consisted of tests on four buried cylinders with hemispherical end caps. The models were loaded in the predicted 600-psi range at 180 feet from ground zero in the 500-ton TNT shot of Event DIAL PACK. Different schemes of internal pressurization and backpacking were used.

Comparison of maximum responses summarized in Tables 2 and 3 show that the performance of the model with internal pressurization and backpacking (**CP-2**) is superior to that of the other two (**CP-1** and **CN-1**) because of the low values of deflection, thrust and acceleration. The initial maximum deflection was considerably less for model **CP-2** than for the other two capsules. However, after the first peak deflection trace was recorded, the gage was damaged. The maximum acceleration for model **CP-2** is one-fourth of **CN-1** and two-fifths of **CP-1**. There were no significant differences in the vertical or horizontal velocities among the three models since the ground motion dominated the values.

If internal pressurization is high, a model similar to **CP-2** may fail by meridional buckling. This could occur because the backpacking creates a soft area above the crown of the model, thereby enabling the crown to rise and the meridional strain at the springing to rebound into a high compressive value.

Upon inspection of the models after they were removed from the excavation, no visible deformation could be seen; this was verified by the small permanent deformations summarized in Table 3.

For model **CP-3**, buckling occurred at about 19.0 msec after detonation. This can be clearly seen in all seven strain gage traces (Figures C-34 through C-37).

FINDINGS AND CONCLUSIONS

Analysis of 46 channels of instrumentation acquired indicates that:

1. Of the three 36-inch-diameter models tested, the model with internal pressurization and backpacking received the least load.

2. Peak acceleration was reduced by a factor of four when backpacking and internal pressurization were used.

3. The internally pressurized model without backpacking received more load than the unpressurized model without backpacking. This shows that internal pressurization increases the stiffness of the walls. However, because of the internal pressure, the container walls received less net stress.

4. The largest dynamic (net) strains recorded were -1,360 μin./in. for the 36-inch-diameter capsules and +2,200 μin./in. for the 12-inch-diameter capsule.

5. Arching theory for calculating the total effective pressure was verified by actual pressure measurements on the crown of the model.

6. Internally pressurized tanks can be designed to remain functional even after large overloads cause the tanks to buckle.

7. Looping the flexible pressure hoses adjacent to the models before backfilling provided sufficient slack to avoid rupturing of the lines; post-shot measurements showed that all the models retained most of their original internal pressure.

8. Fuel tanks can be designed economically by using the NCEL optimization equations and be fabricated to survive under surface dynamic loads. Proper proportioning of the backpacking thickness and utilization of internal pressurization can enhance survival of fuel tanks subjected to blast overpressures and reduce the cost of the tanks.

9. Conservative checks of experimental data were made with the two-dimensional non-linear, large deformation computer program; more refined analysis can be made with the currently available three-dimensional computer program.

ACKNOWLEDGMENTS

The authors appreciate the guidance and the many constructive suggestions made by Mr. J. R. Allgood of NCEL throughout the project. Special acknowledgment is extended to Mr. Vincent J. Gerwe, Structural Engineering Technician, who did much of the planning of the field work. Mr. John E. Crawford provided the computer graphic plotting support. Excellent instrumentation support was provided by Messrs. I. M. Derr and D. H. Johnson of the NCEL Instrumentation Division. Much of the field work was also done by Messrs. F. L. Yost

and F. H. Billingsley of NCEL. The timely and efficient support provided by Mr. Richard H. Seabold, Program 3 Director, and by the Canadian Defence Research Establishment Suffield, Ralston, Alberta, Canada, is particularly noted.

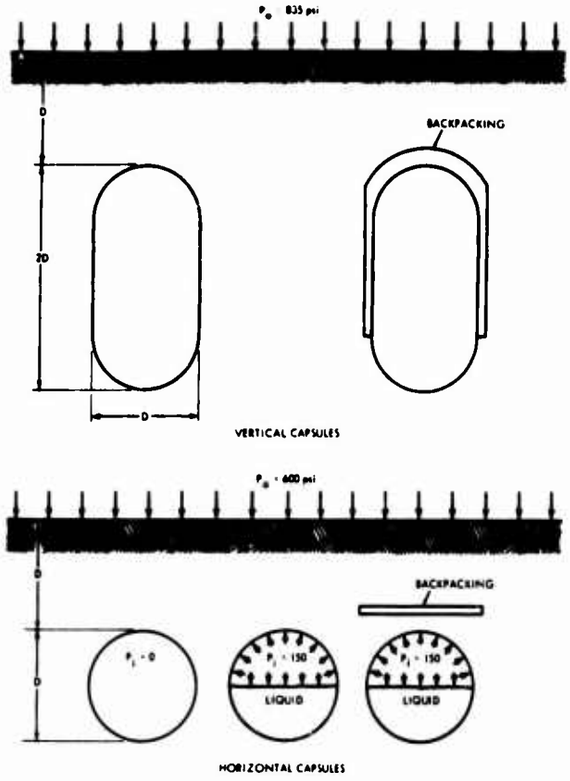

Figure 1. Configurations of models for vertically and horizontally oriented capsules.

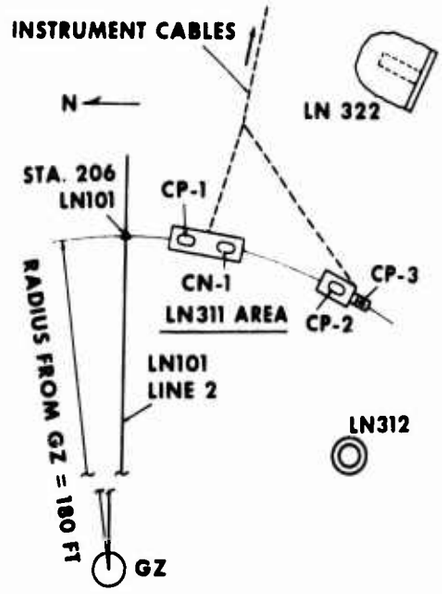

Figure 2. Project LN'11 test site layout.

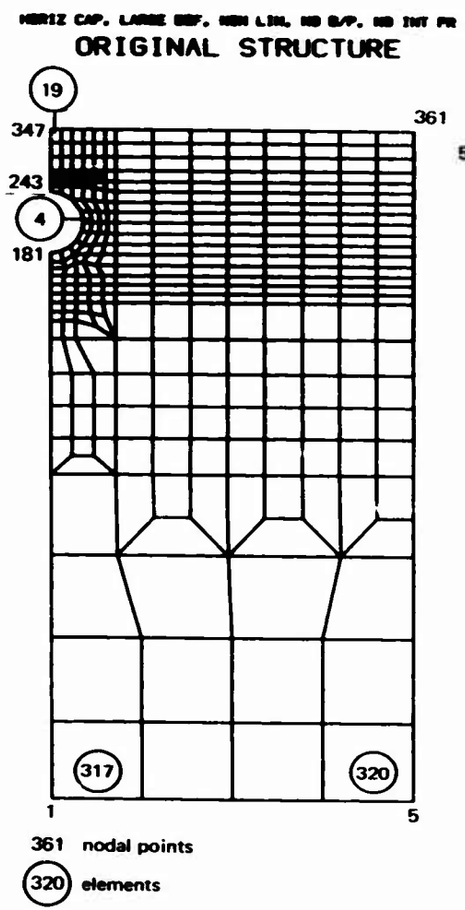

Figure 3. Finite element mesh of buried horizontal cylinder.

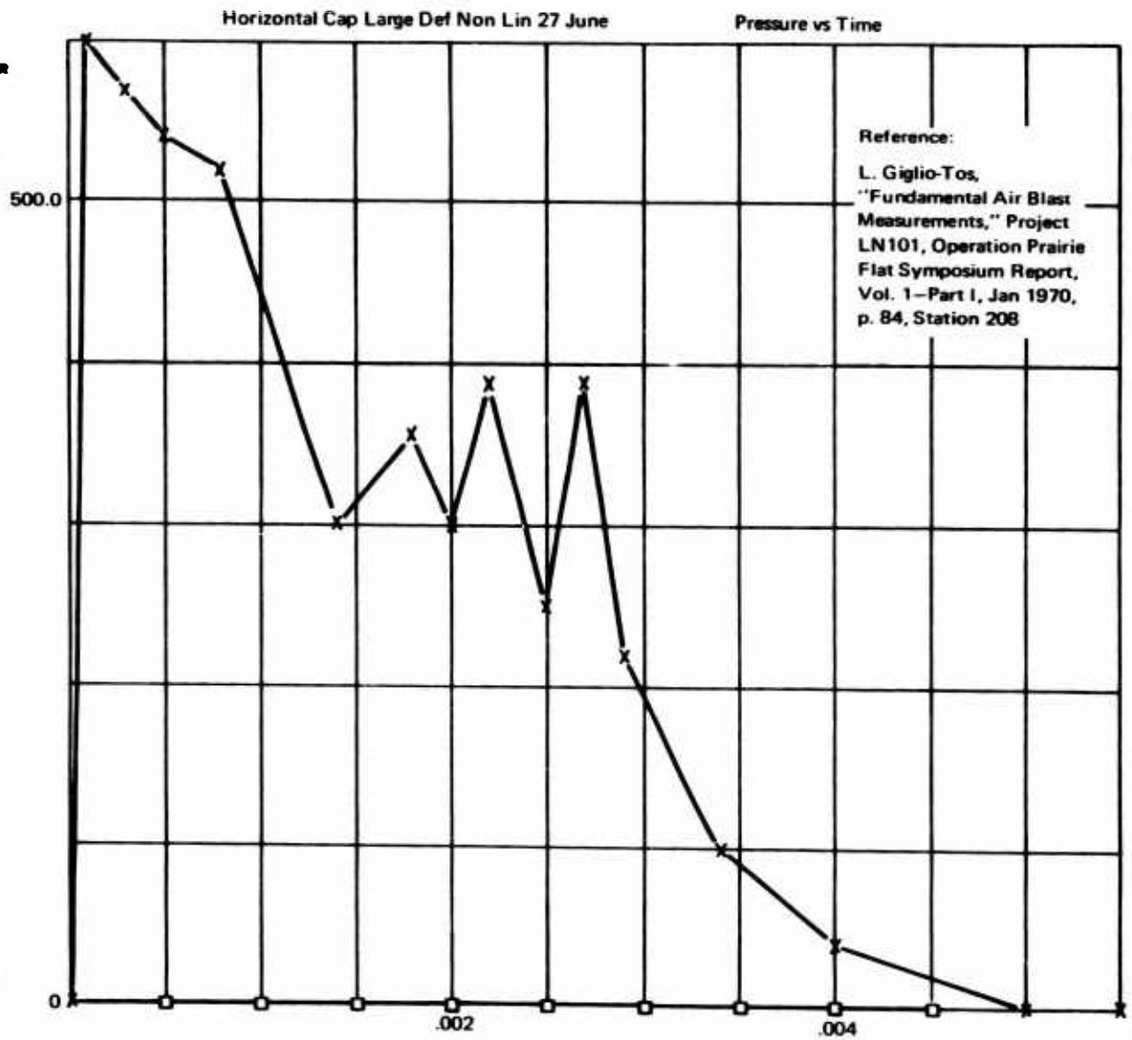

Figure 4. Overpressure-time curve for computer input.

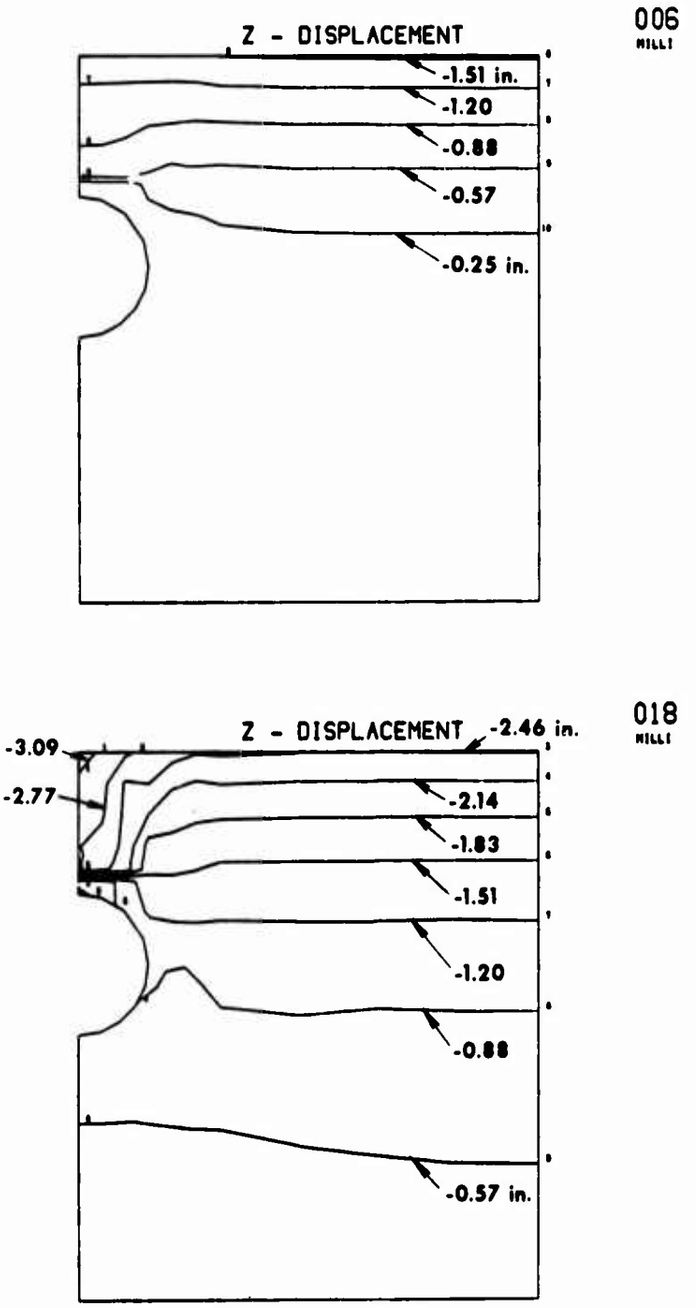

Figure 5. Vertical displacement patterns at 6 and 18 msec after load application.

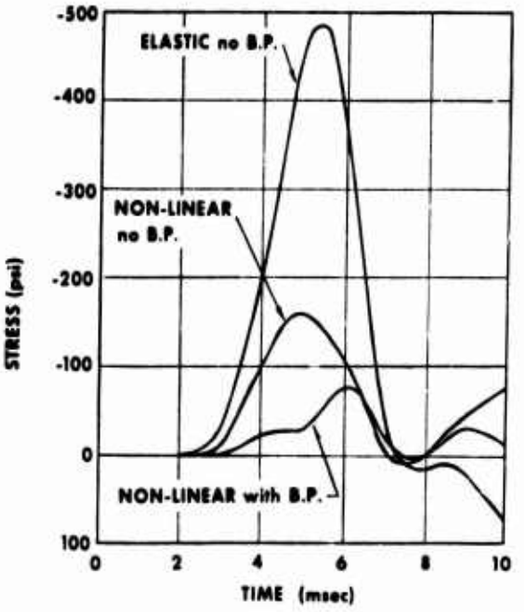

Figure 6. Vertical stress in soil above the cylinder crown (element 51).

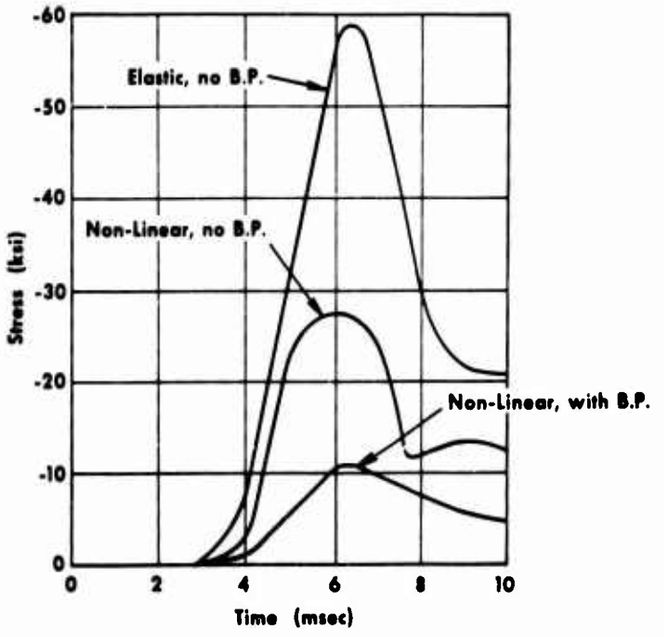

Figure 7. Minimum stress at springing of buried cylinder (element 4).

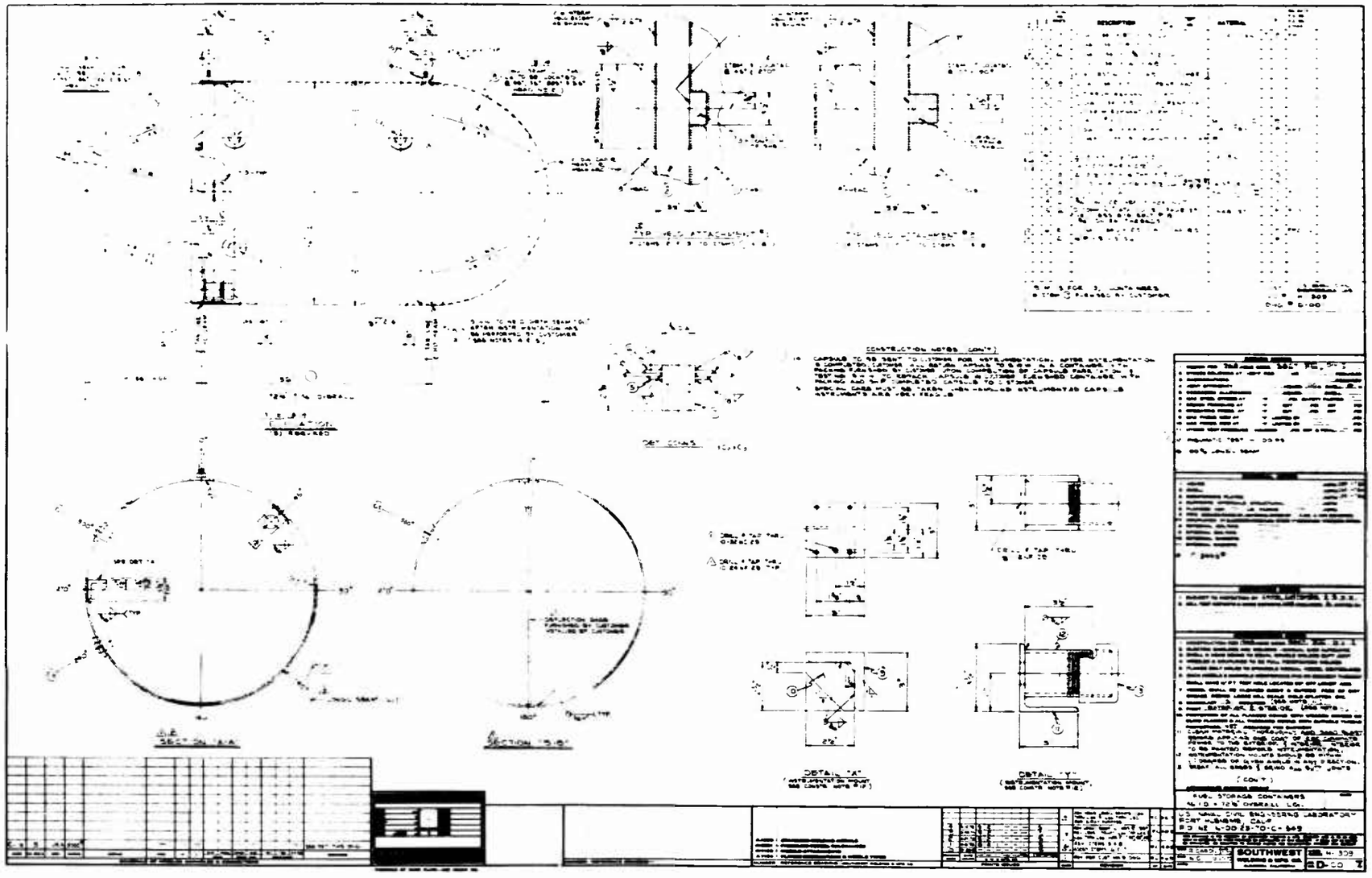

Figure 8. Fabrication drawing of 36-in. diameter model fuel storage container.

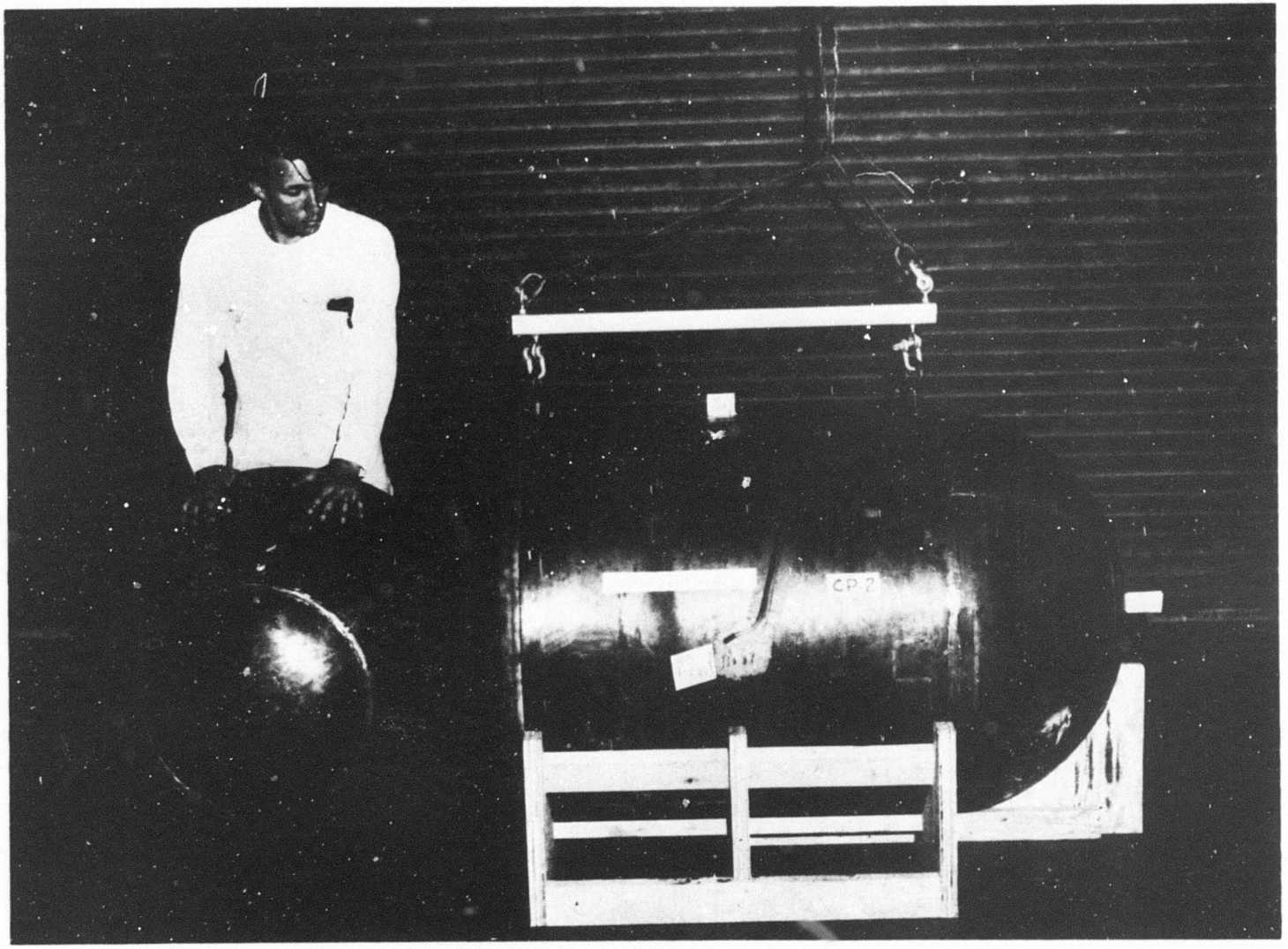

Figure 9. Overall view of 36-in. diameter model fuel storage container.

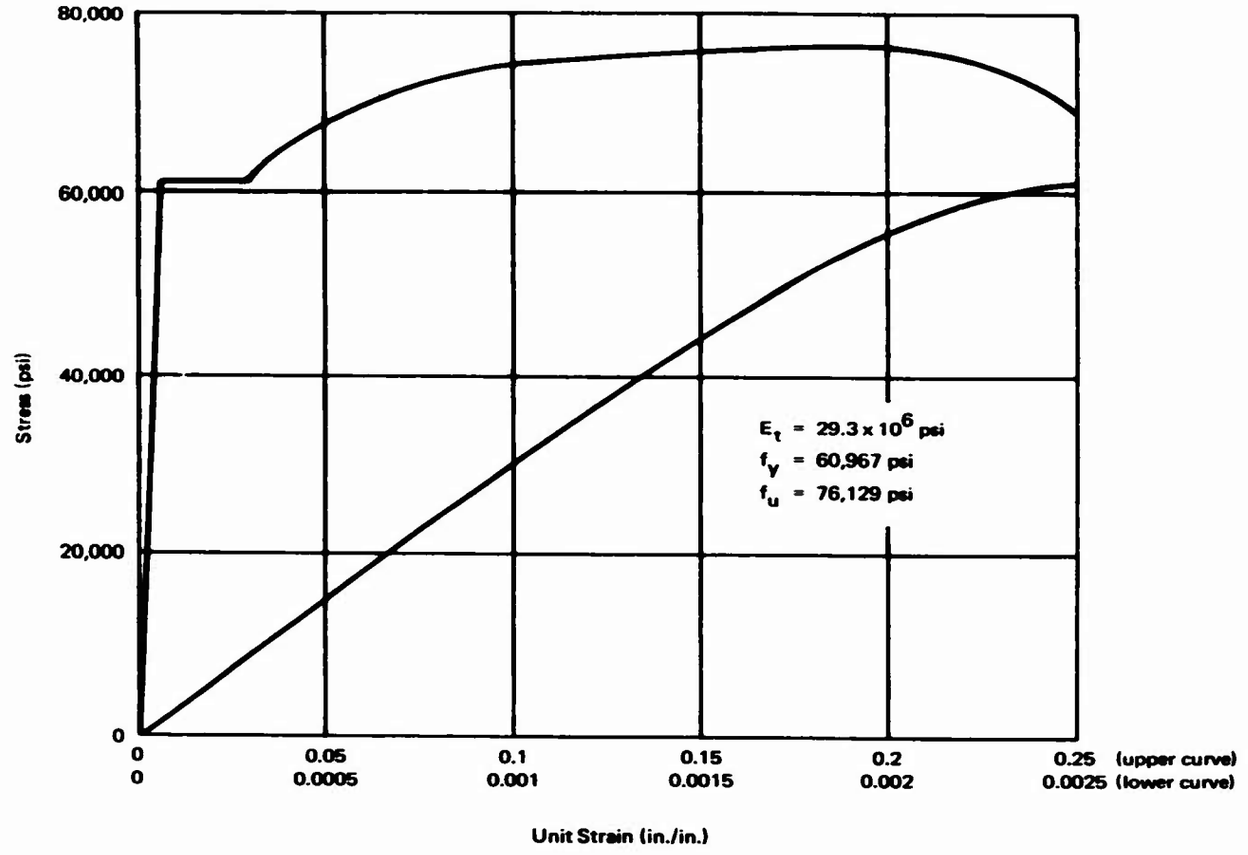

Figure 10. Stress-strain curve for 10-gage USS Cor-Ten steel.

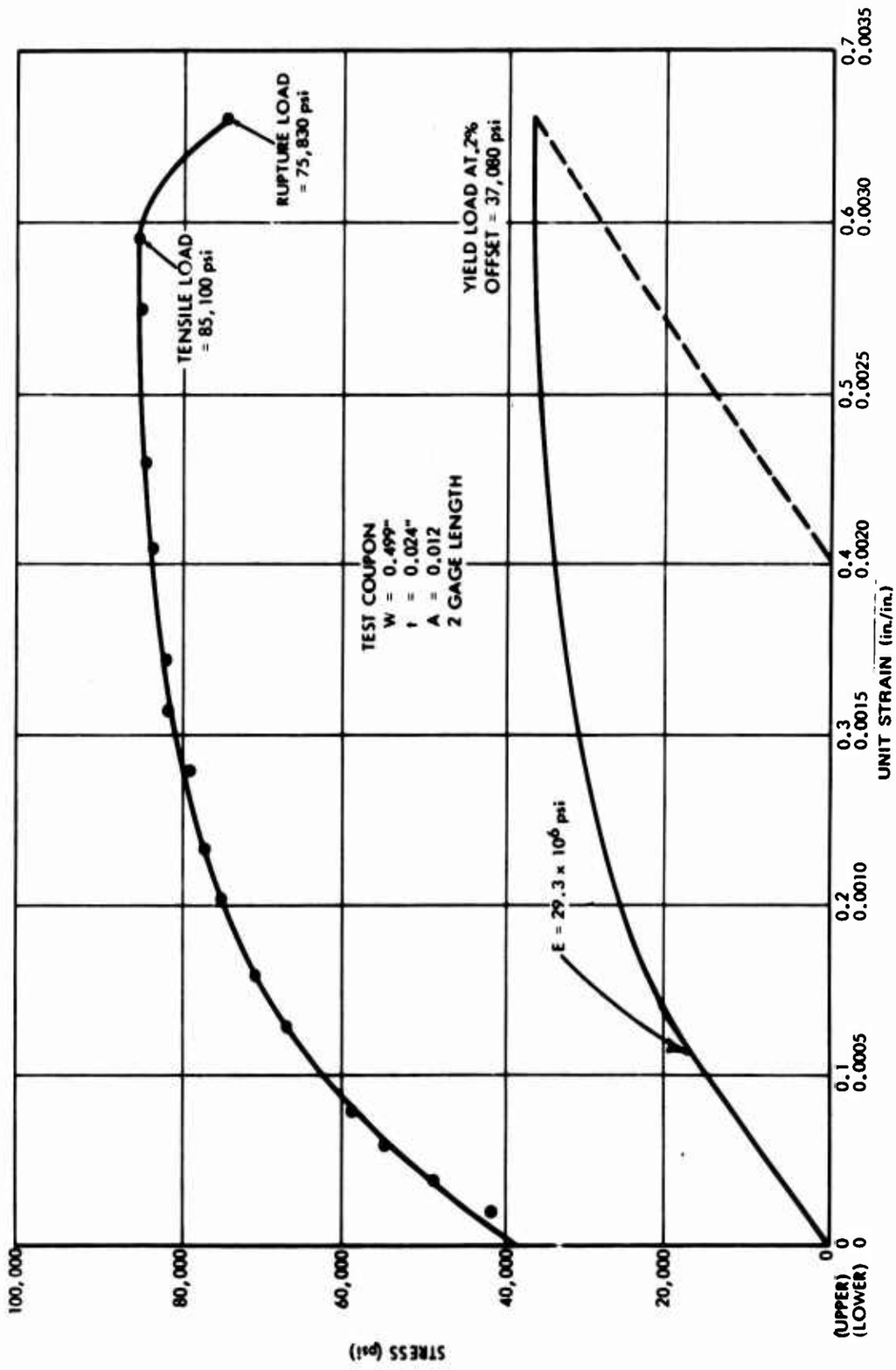

Figure 11. Stress-strain curve for T-304 steel.

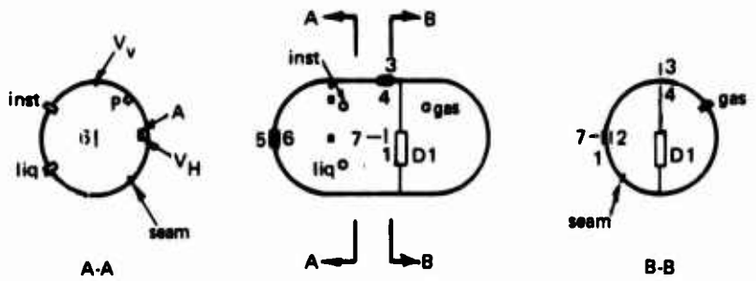

Instrumentation For 3-Ft-Diam
Model Tanks

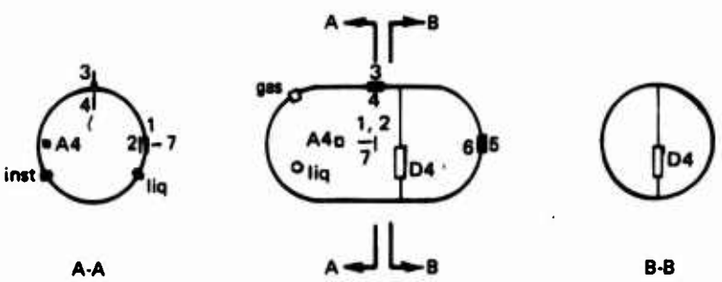

Instrumentation For 12-In.-Diam
Model Tanks

Legend:

A – Accelerometer
D – Deflection
P – Pressure
V – Velocity
Numbers Only – Strains

Wall Connections

Gas – Nitrogen
Inst – Instrumentation
Liq – Silicone Fluid

Figure 12. Instrumentation layout for buried fuel model tanks.

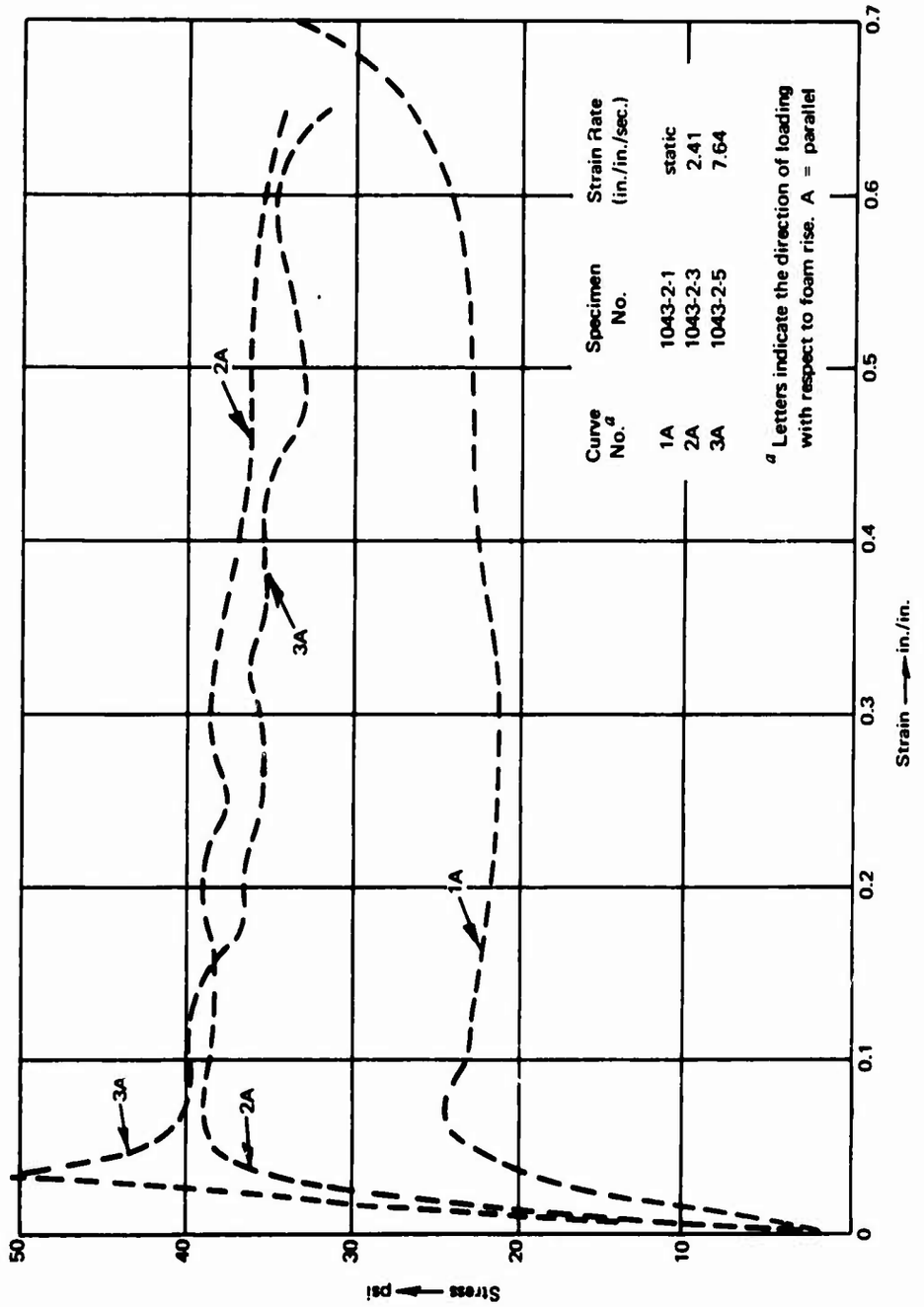

Figure 13. Test results of polyurethane specimen group 1043-2.

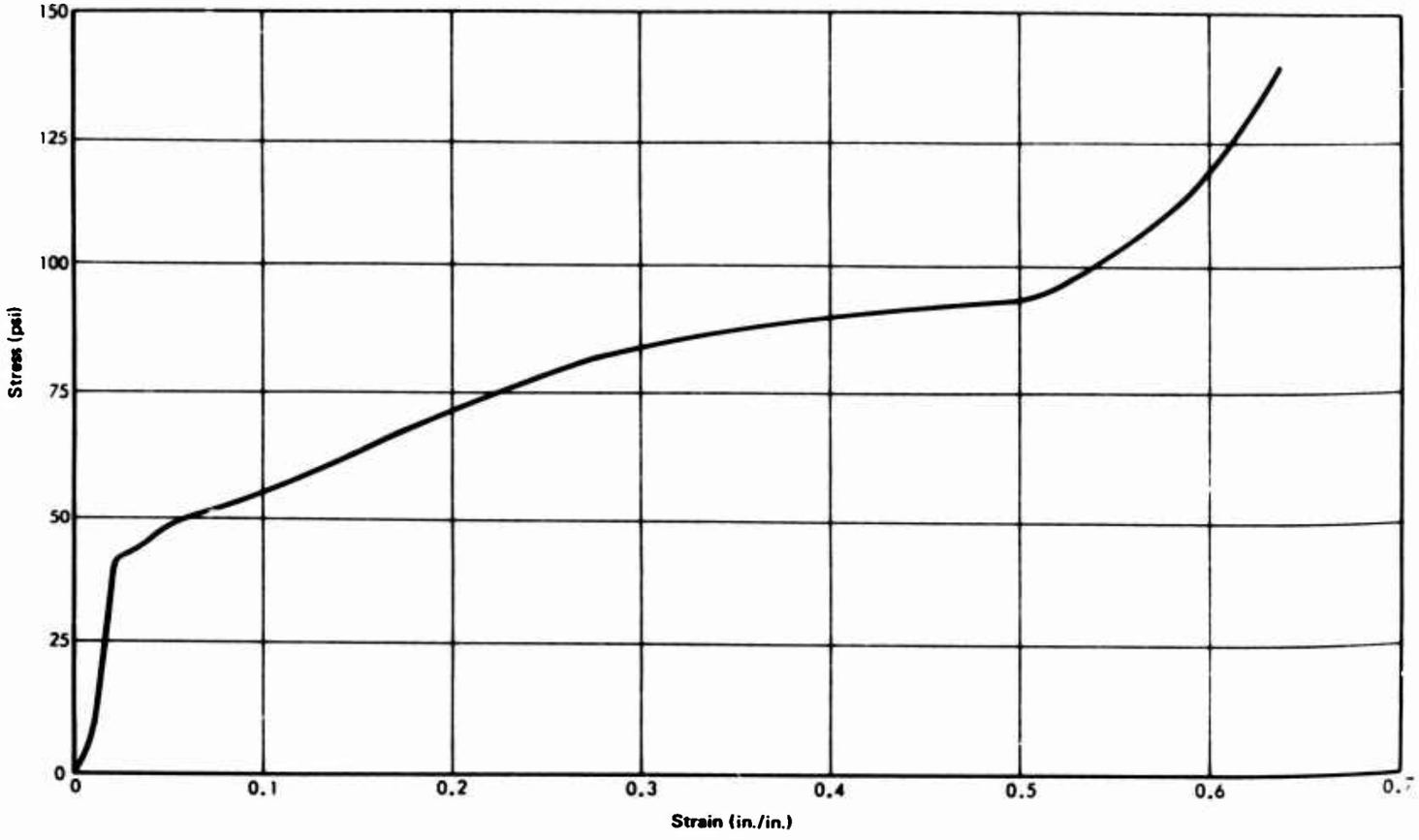

Figure 14. Stress-strain curve for SM styrofoam test cube (2 x 2 x 2 in.).

Figure 15. Raining of Cook's Bayou sand over CP-3.

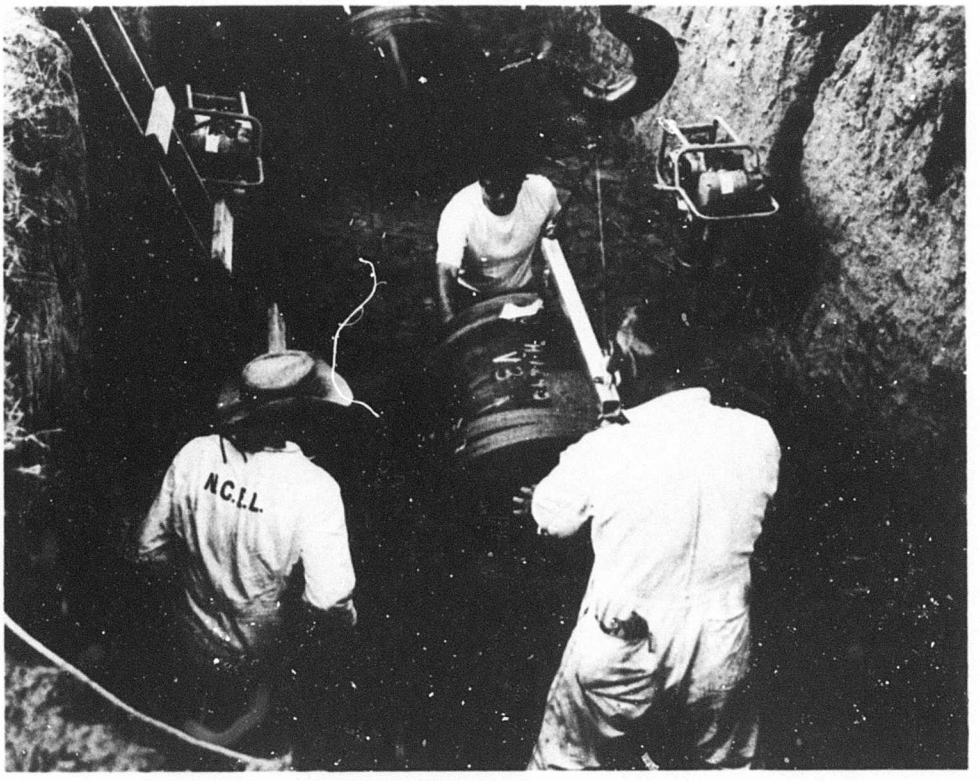

Figure 16. Lowering of model CN-1 on soil bed with crane.

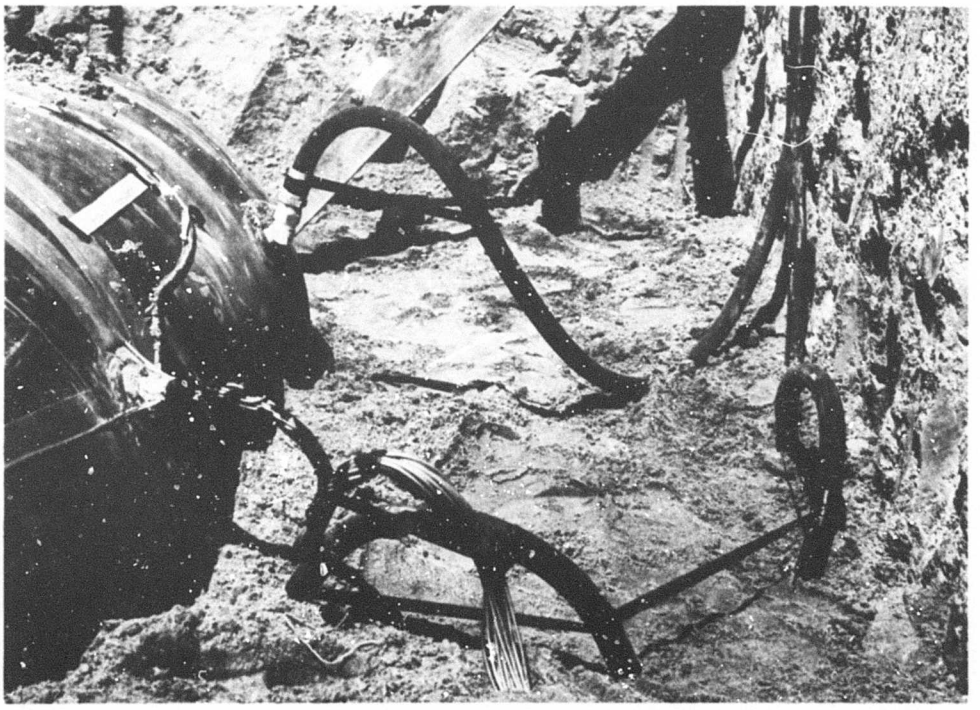

Figure 17. Looping of instrumentation and pressure lines to prevent damage from ground motion.

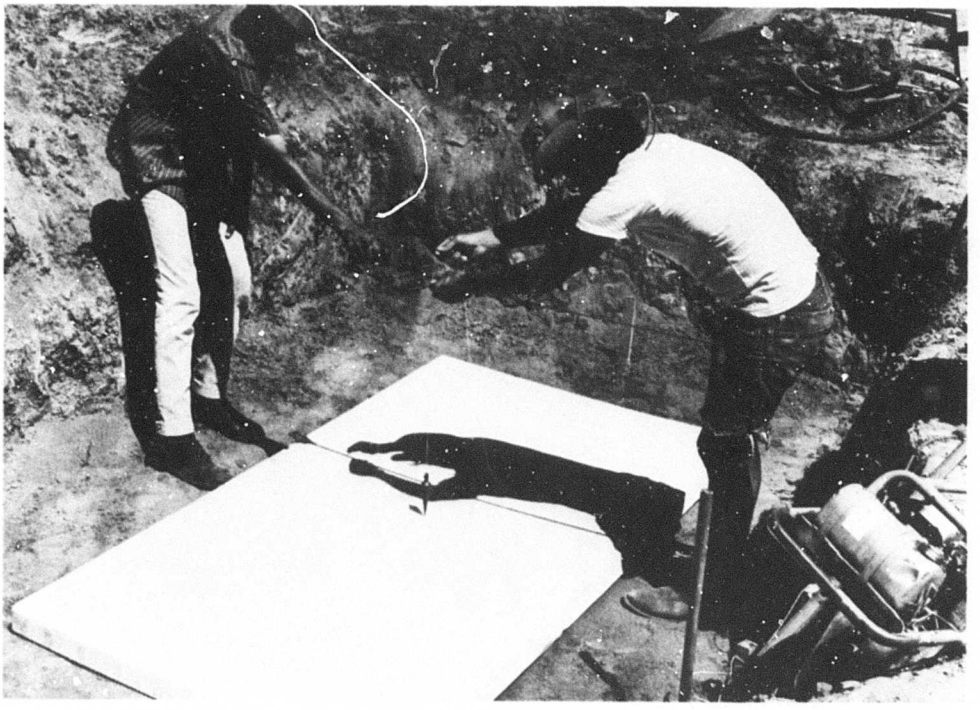

Figure 18. Placing of 3-in. thick rigid urethane foam over model CP-2.
(neg no. DPK 962-70 LN311 Dupe Uncl)

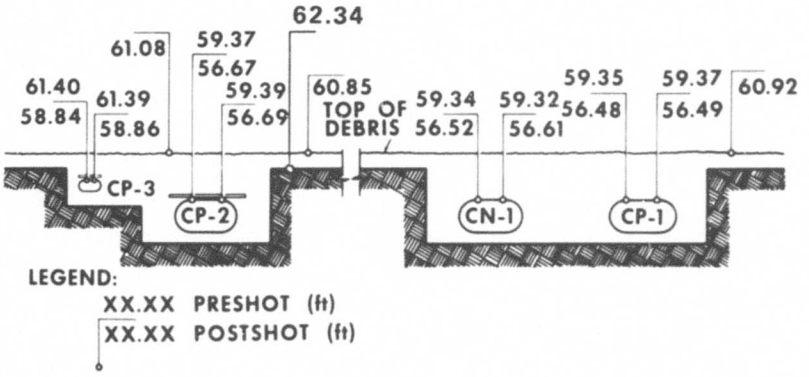

Figure 19. Pre- and post-shot elevation of top of ground and models.

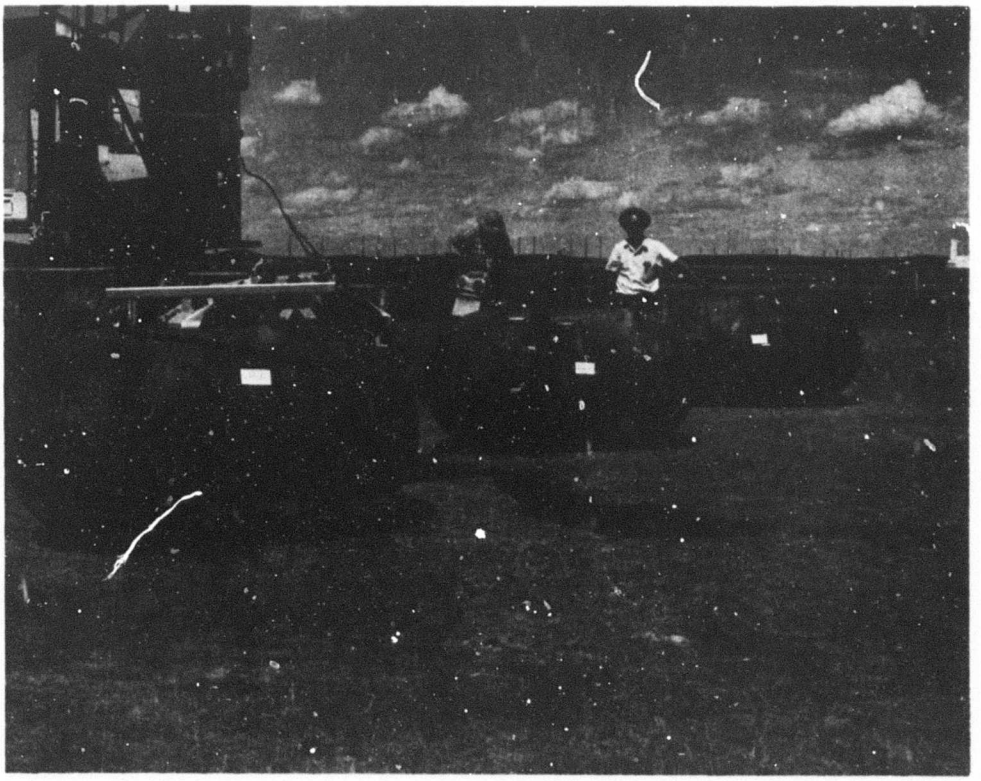

Figure 20. View of models CP-1, CN-1 and CP-2 after test.

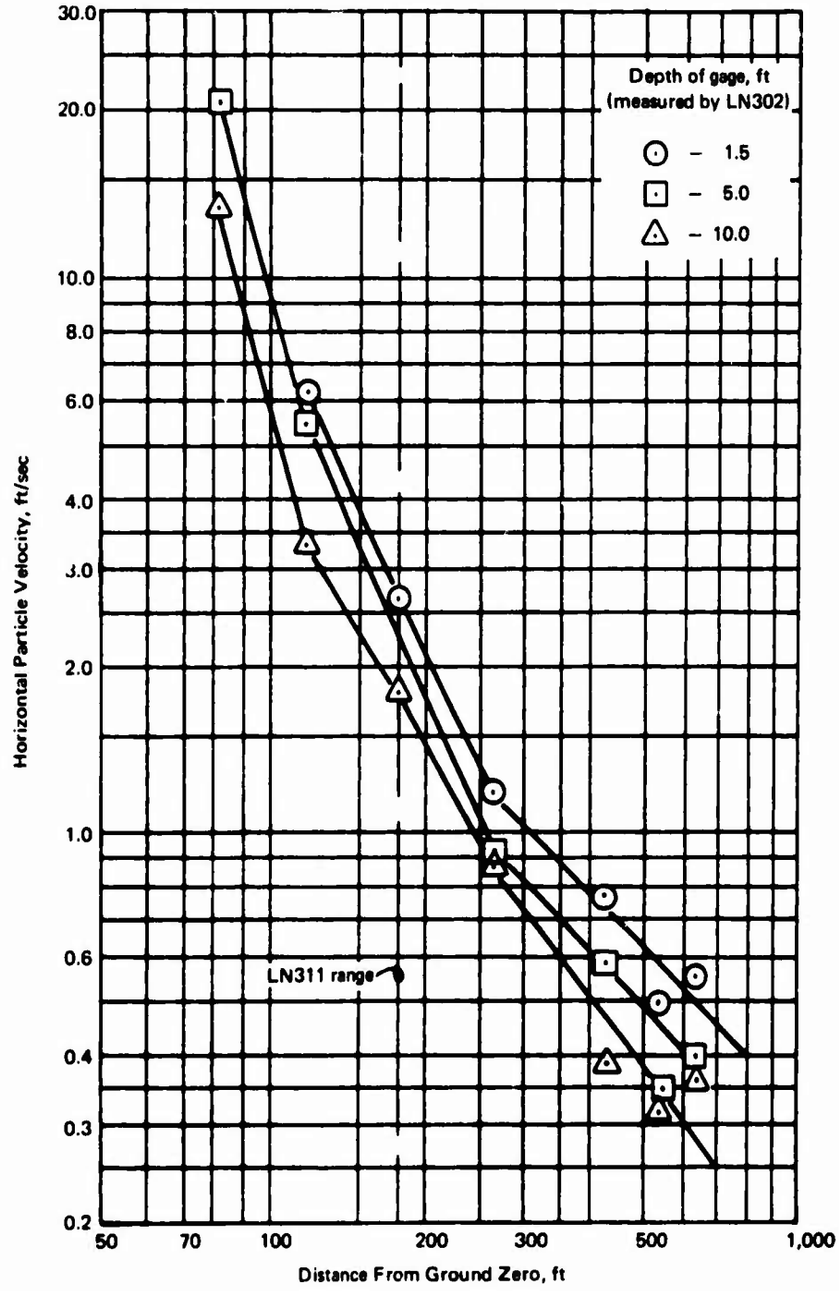

Figure 21. Horizontal particle velocity versus distance.

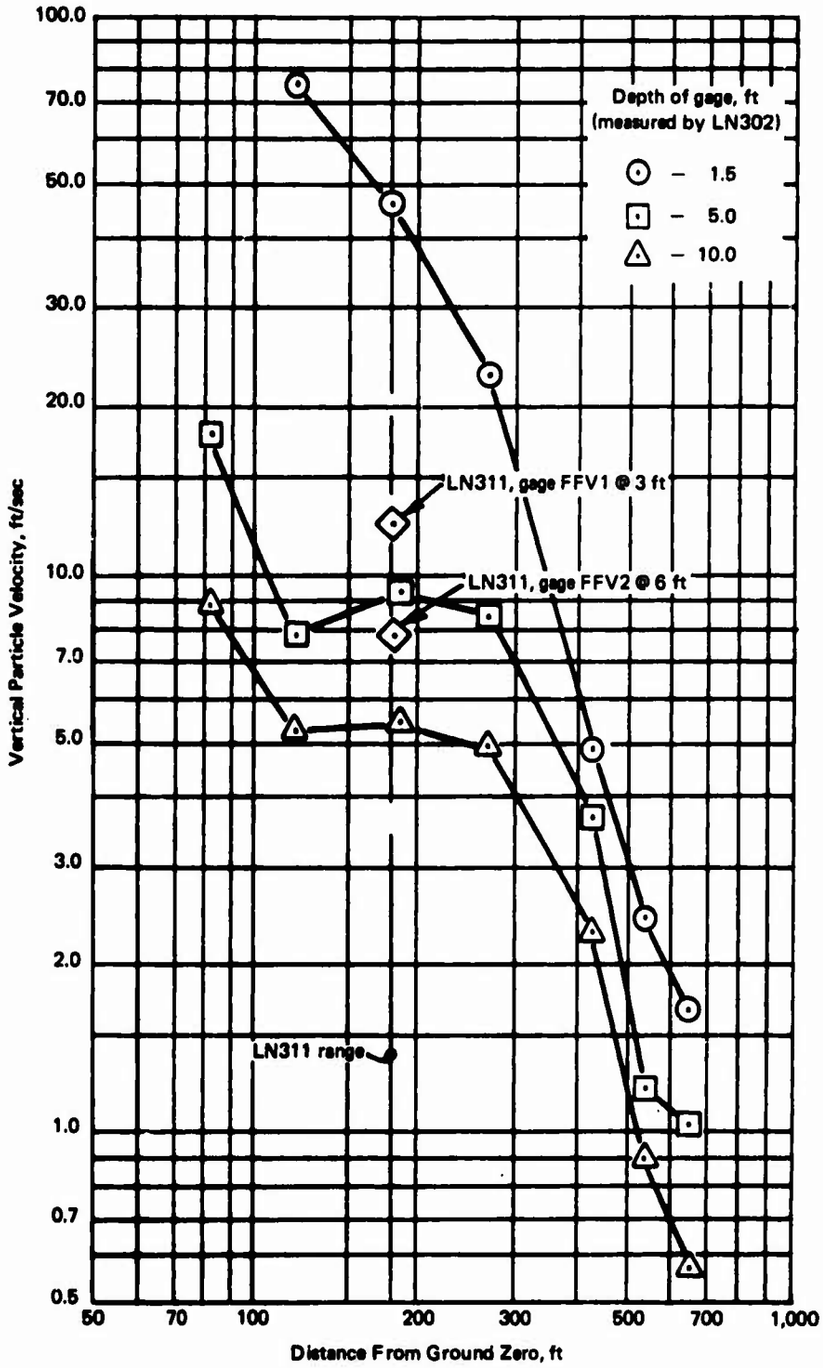

Figure 22. Vertical particle velocity versus distance.

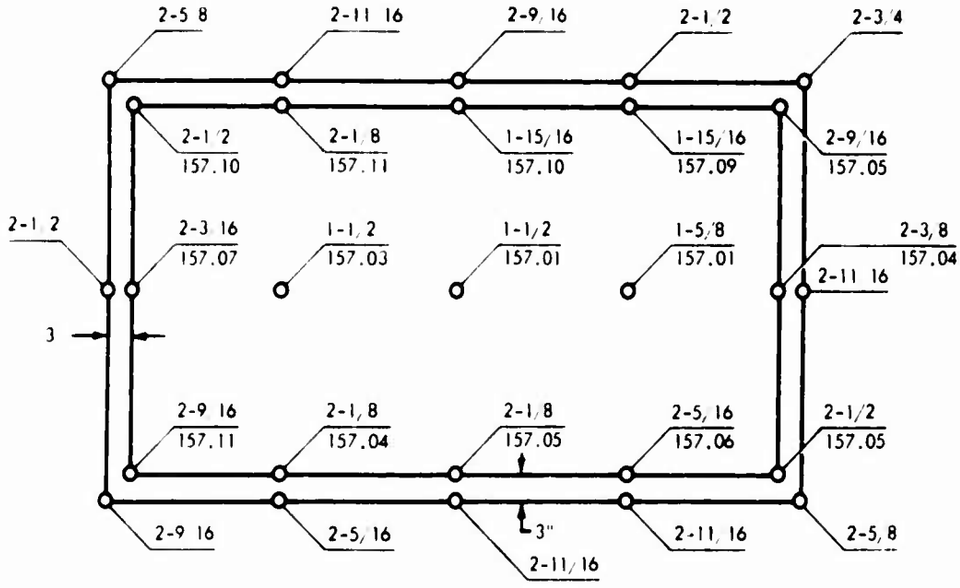

PLAN VIEW

ELEVATIONS AND THICKNESS OF URETHANE BACKPACKING FOR MODEL CP-2

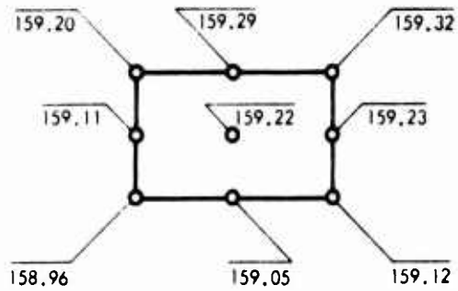

PLAN VIEW

ELEVATIONS OF STYROFOAM BACKPACKING FOR MODEL CP-3

LEGEND

XXX THICKNESS (in)
XX.XX ELEVATION (ft)

Figure 23. Postshot elevations and thicknesses of backpacking for Models CP-2 and CP-3.

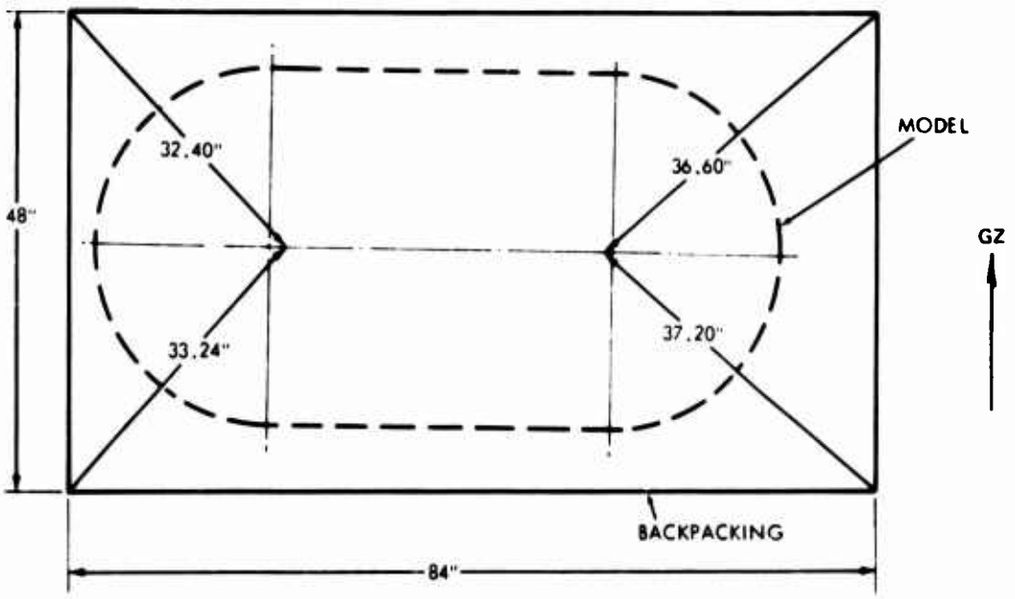

PLAN VIEW

RELATIVE POSITIONS OF 3-IN BACKPACKING
AND MODEL CP-2 AFTER TEST

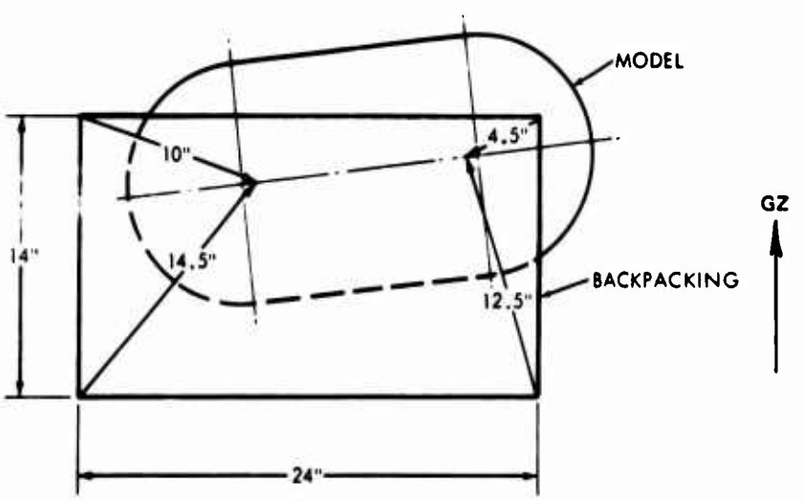

PLAN VIEW

RELATIVE POSITIONS OF 1-IN BACKPACKING
AND MODEL CP-3 AFTER TEST

Figure 24. Relative positions of backpacking and models after test.

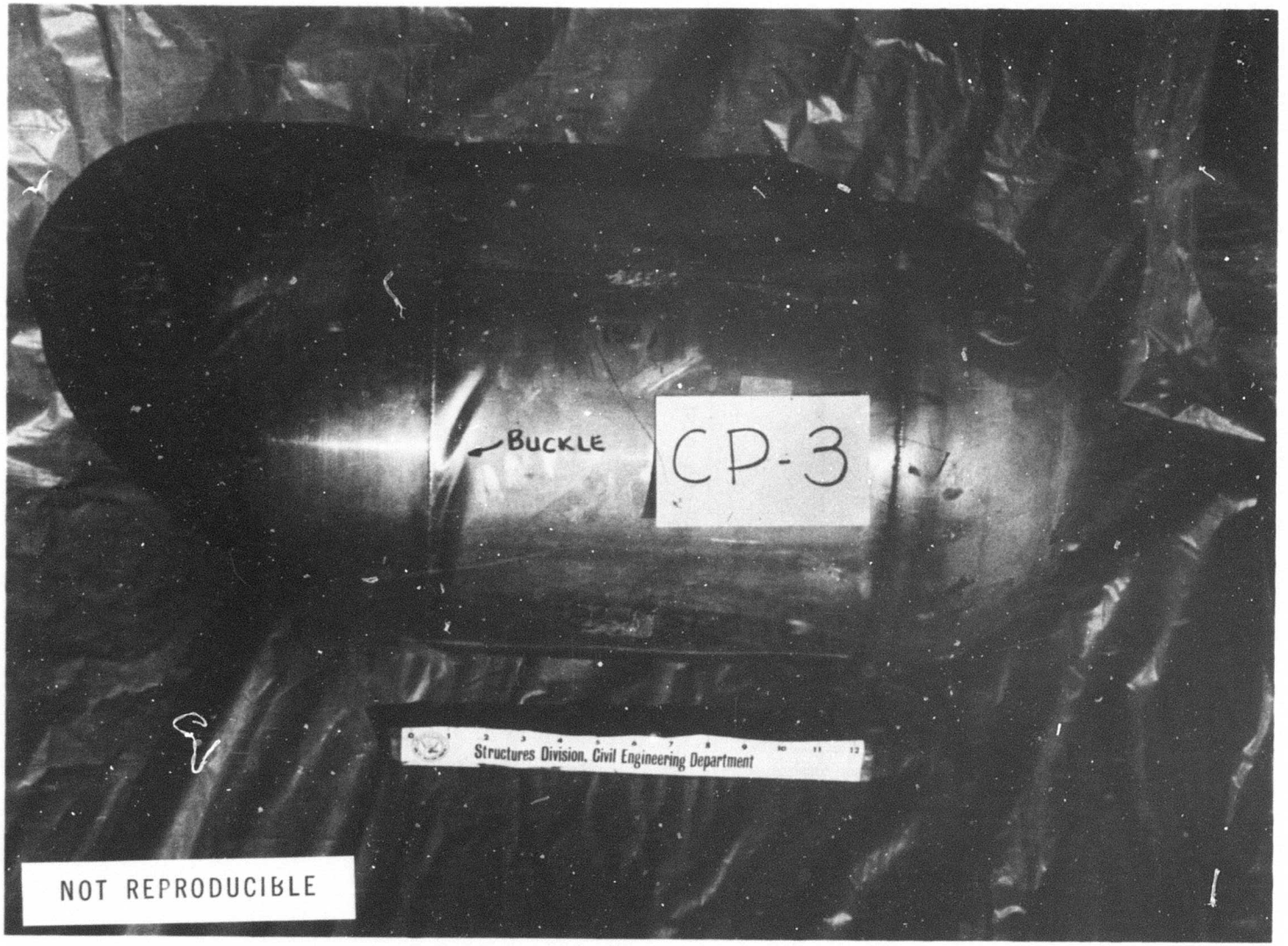

Figure 25. View of model CP-3 after test.

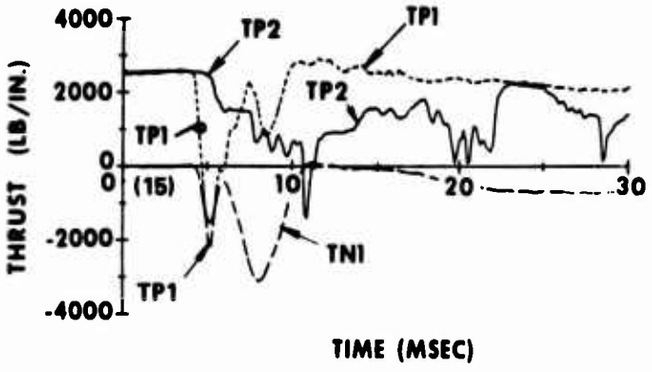

Figure 26. Vertical thrust at springing of models CP-1, CP-2 and CN-1.

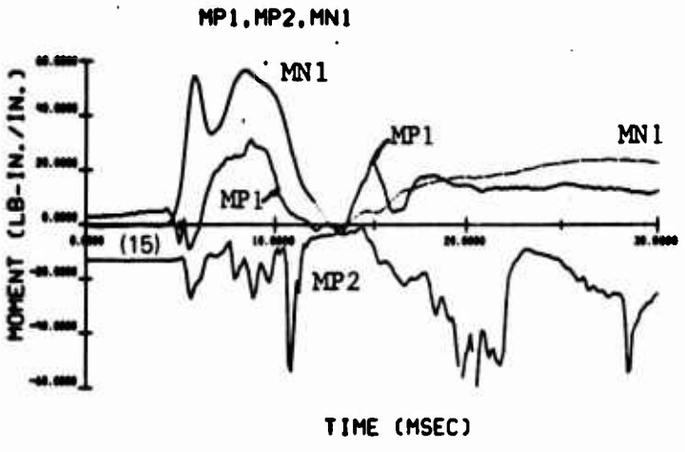

Figure 27. Circumferential moments at springing of models, CP-1, CP-2 and CN-1.

Appendix A

INSTRUMENTATION

by

Dale H. Johnson

INTRODUCTION

The Instrumentation Division of the Naval Civil Engineering Laboratory provided and operated the instrumentation system for seven NCEL projects including LN311.

The signal conditioning, amplifying and recording system was housed in a wooden bunker located 2,700 feet from ground zero. Project LN311 included 8 velocity gages, 4 pressure gages, 4 accelerometers, 4 deflection gages and 28 strain gages for a total of 48 channels. A description of the transducers, recording equipment, calibration procedures, and installation procedures are presented in this appendix. A sketch of the transducer locations on the structure is given in Figure 8.

EQUIPMENT DESCRIPTION

Transducers

Velocity Gages. Sparton Southwest Model 601H velocity gages were used to measure structure velocity in the horizontal and vertical directions. Velocity gages are basically an integrating accelerometer with a pendulous mass suspended in a highly viscous fluid. The gage is designed so that the accelerating force is automatically integrated as the mass is damped by the viscous characteristics of the fluid and also by restriction of the fluid flow within the mass-fluid housing. Displacement of the mass is sensed by a variable reluctance transformer, which produces an output proportional to velocity.

The range and sensitivity of the gage can be adjusted by changing the mass of the pendulum or the viscosity of the silicone oil damping fluid. For measuring free-field velocity the gages were mounted in an aluminum canister 8 inches long by 5-1/2 inches in diameter which has a mass similar to that of the soil it displaces so that it would, under dynamic loading, react similarly to the soil around it.

Pressure Gages. Bytrex Model HFG-SE gages were used. These transducers were specifically designed for use in the measurement of blast phenomena and are insensitive to acceleration, of rugged mechanical construction, and include a shield to reduce the effects of thermal and nuclear radiation and to protect the diaphragm from flying debris. They incorporate semiconductor sensing elements which produce a high electrical output thereby reducing adverse effects from spurious signals generated from blast effects.

A Sensotec Model SA-SA M-7F 0-750 psia gage was used to measure soil pressure reacting against the top surface of one of the cylinders. It is 0.270 inches in diameter and 0.035 inches thick and is designed to measure soil pressure without the errors caused by arching and edge effect.

Accelerometers. Endevco Model 2261 and 2264M1 piezo-resistive accelerometers were used. The Model 2261 is a four-active-arm transducer with a range of ±2,500 g's, a mounted resonant frequency of 30 kHz, are 15/16 inches high by 0.610 inch diameter and weigh 1.25 ounces. The Model 2264M1 is a two-active-arm transducer with a range of ±4,500 g's, a mounted resonant frequency of 20 kHz, with dimensions of 0.40 by 0.40 by 0.18 inches and weighs 1 gram. Two 500 ohm resistors must be used with this transducer to produce a complete bridge.

These transducers were chosen for their low mass and high frequency response characteristics.

Deflection Gages. Bourns Model 156.4 inch align-O-pot and Model 108, 1.31 inch linear motion potentiometers were used to measure the deflection of the top of each cylinder with reference to the bottom of each cylinder. The transducers have a resistance of 10k ohms and were connected across two adjacent arms of a 1,250 ohm wheatstone bridge. Resolution of these potentiometers is 0.0024 inches and they can sustain a shock of 100 g's without electrical discontinuity. The transducer body was attached to one portion of a telescoping rigid aluminum pipe while the shaft was attached to the other section of the pipe. The pipe was firmly attached to the wall of the cylinder that had been strengthened in that location; no apparent incongruity of the cylinders flexibility due to this mechanical strengthening was noticed.

Strain Gages. BLH Type FAE-50-1256 and EA-06-250BG-120 strain gages were used. These gages have a resistance of 120 ohms, a gage factor of 2, and acted as a single active arm of a 4-arm wheatstone bridge. The gages were attached to the inner and outer surface of the cylinders using Eastman 910 cement and were waterproofed with William T. Bean Gage Coat #1 followed by Gage Coat #2 on the inside of the cylinder, gages on the outside were protected with Petrosene wax.

Recording Equipment

Signal Conditioners. Magnetic Instruments Company Model 363-2 coupling units are designed for use with CEC System D amplifiers and provide for local and remote calibration, additional capacitive and resistive balance, signal attenuation, and reversal of signal polarity. The units provide for solderless mounting of phase altering and shunt calibration elements. Bridge excitation is supplied by System D.

B&F Model 1-700 signal conditioners provide for 0-15VDC gage excitation, gage balance and local and remote shunt calibration. A plug-in module has solder-lugs for calibration and balance limiting resistors. The power supply for the Model 1-700 can be operated in either a constant voltage or constant current mode. For this test they were operated in a constant voltage mode.

Amplifiers. Consolidated Electrodynamics Corporation Model 1-113B Amplifiers (CEC System D) were used for operation of all velocity gages. The Model 2-105A power supply provides a 3 kHz, 10 volt rms excitation voltage for 12 gages as well as the operating voltage for 12 Model 1-113B data amplifiers. The balancing system for compensation of resistive and reactive unbalance in the gage and its cable is included in the amplifier. Amplifiers were modified to properly drive the tape recorder electronics. These modifications were (1) the addition of 1,000 ohm resistors in series with each demodulator diode, (2) the removal of the neon overload lamp and (3) the addition of a 6 kHz filter between the output of each amplifier and the tape recorder VCO. The higher harmonics of the 3 kHz excitation voltage are filtered out by the galvanometer in the normal system but they are of sufficient amplitude to cause a problem if not removed by the additional filter when recording on tape.

Consolidated Electrodynamics Corporation Model 1-165 amplifiers were used for the remainder of the channels. This is a DC differential amplifier that is designed to accept signals to 20 kHz and has gains of 10 to 1,000 in 7 steps plus a vernier.

Tape Recorders. Sangamo Model 4784, 32 track tape recorders were used to record the data. The recorders were operated at 60 ips using FM record amplifiers with a center frequency of 108 kHz. A 1-volt-rms input produced a ±40% deviation. Frequency response of the recording system was 0-20 kHz. Tape heads were of standard IRIG format.

Peripheral Equipment

Detonation Zero. The detonation zero pulse was provided by DRES and was recorded directly as received onto track number 32 of each tape recorder. This pulse is of 2 volt amplitude and 20 microsecond duration.

Timing. Two timing channels were used on each tape recorder. Standard IRIG-B from a Systron-Donner Model 8150 time code generator provided correlation between tape recorders and programming for the computer on data reduction. An NCEL designed timer was used to provide timing for use when data was recovered onto oscillograph paper. The NCEL generator provided pulses of 1 msec to 1 second with each decade at a different DC level.

Oscillographs. Field recovery of data was done by playing the tapes back through Dana 3850 V2 amplifiers into CEC 7-361 galvanometers. Recording was done in a CEC 5-119 oscillograph and then processed in a CEC processor thereby giving high quality permanent records in a very short time. The oscillograph records were used to facilitate writing the field report. Upon return to the Laboratory a complete analysis of each channel of data was made on a Control Data Corporation 6600 computer and this information was used in the final report.

CALIBRATION PROCEDURES

Velocity Gages

A standard fall-through method of calibration was used to calibrate the velocity gages. For this method of calibration a magnet was placed on the velocity gage to lift the mass upward; when the magnet was removed the mass was released and the force of gravity acting upon it produced a deflection corresponding to an acceleration of 32.2 ft/sec.^{2} In the case of gages used in the vertical mode an additional force equal to the force of gravity was placed upon the mass by the restoring spring thereby making the total force upon the mass equal to 2 g's, producing a deflection corresponding to an acceleration of 64.4 ft/sec^2 or a velocity of 64.4 ft/sec at the end of 1 second.

A CEC 5-134 direct write oscillograph was used to record the slope of time vs acceleration to determine the sensitivity of the gage. A shunt resistor was chosen that would give a chart deflection that was comparable to that of the predicted velocity. Temperatures were noted for each gage at the time of calibration and also while mounted just previous to the test and a correction factor was given to each gage to compensate for the change in gage sensitivity.

Pressure Gages

The pressure gages were calibrated "in-place" in the field by applying the predicted value of pressure to them. An air-tight fixture was placed over the gage diaphragm and pressurized using a King Nutronics Corporation Model 3540 pneumatic calibrator. When the desired value was reached, the FM record oscillator frequency deviation was noted and a shunt calibration resistor was chosen that produced a similar change in oscillator frequency. The exact value of pressure that the substitution resistor simulated was determined by the ratio of the two frequency deviations. The soil pressure gage was affixed to the inside of a special pressure housing and then calibrated in a like manner.

Accelerometers

Accelerometers were calibrated at the Laboratory on a Shaevitz rotary accelerator and a shunt resistance value was noted. In the field this value was placed across the transducer and the frequency deviation on the FM record oscillator was noted. A shunt calibration resistor was then chosen and its frequency deviation compared to the laboratory calibrated value to determine the equivalent acceleration in g's. FM frequency change was noted while the accelerometer was placed base down and base up to determine acceleration direction.

Deflection Gages

The linear motion potentiometers were calibrated by placing them into a jig and deflecting the shaft using a depth micrometer. The change of the FM record oscillator frequency was noted for the desired deflection and a shunt calibration resistor chosen. The ratio of the oscillator frequency change between the calibration resistor calibration and of the deflection was determined and used in calculating the calibration factor.

Strain Gages

Strain gages were calibrated by calculating the value of a shunt resistor that would simulate the predicted strain level by using the formula $R_c = R/GNS - R$. This value of resistance was put directly across the active strain gage and denoted the desired strain in compression. A calibration resistor was then chosen and placed into the signal conditioner and the ratio of the two oscillator frequency deviations was used to determine the exact value of strain that the calibration resistor simulated.

GROUNDING

A common ground rod was installed by DRES to serve as a ground for the power mains as well as for the signal conditioners, amplifiers and recorders. Each transducer cable was grounded by connecting its metallic sheath and drain wire through the connector to the ground of the signal conditioner. The transducer end of each cable remained ungrounded to eliminate ground loops. Tests of grounding effectiveness were made by inducing electromagnetic interference into the system and monitoring the tape recorder reproducing amplifiers on an oscilloscope to observe any pulses that were recorded by the system.

SLAVING OF SYSTEM D POWER SUPPLIES

CEC System D equipment utilizes a 3-kHz carrier. To avoid interference between oscillator frequencies when using two or more of these systems simultaneously, the oscillators are normally slaved together and only one oscillator is turned on and allowed to drive the others. The procedure that NCEL utilized for slaving was to install 0.05 μfd condensors in each slave interconnecting cable and operate with all oscillators on. In the event one oscillator is turned off or malfunctions, the other oscillators will drive it at a reduced output.

Appendix B

SOILS TESTS DATA BY THE WATERWAYS EXPERIMENT STATION

INTRODUCTION

The results presented in this appendix are separated into three categories. The first is test results on undisturbed clay samples from the LN311 test site. The second is test results of remolded sand used for backfill taken from nearby the test site. The third is test results on Cook's Bayou sand.

TESTS ON UNDISTURBED CLAY

The following samples were hand-trimmed from the natural material at the LN311 location into 2-1/2 inch high by 5-inch-diameter uniaxial strain (UX) test rings and shipped via air freight to WES for testing:

No.	Location	Depth	Disposition
6-2-N	North Pit	6 in.	Disturbed, not used
6-3-N	North Pit	6 in.	Disturbed, not used
7-2-N	North Pit	7 ft	Dynamic UX test
7-3-N	North Pit	7 ft	Static UX and classification tests
6-2-S	South Pit	6 in.	Disturbed, not used
6-3-S	South Pit	6 in.	Static UX and classification tests
7-2-S	South Pit	7 ft	Dynamic UX test
7-3-S	South Pit	7 ft	Disturbed, not used

The near-surface Watching Hill soils have a very delicate, friable structure and are extremely difficult to preserve in an undisturbed condition. Inspection of the samples after arrival at WES resulted in only four samples (7-2-N, 7-3-N, 6-3-S, and 7-2-S) being judged as suitable for property testing.

The material from both pits is a light brown silty clay (CL) with a trace of fine sand. The index properties, grain-size distributions and specific gravities obtained from samples 7-3-N and 6-3-S are given in Figures B-1 and B-2, respectively. The specific gravity values of 2.75 and 2.69 bound a value of 2.73 that is thought to be representative based on previous investigations at the site; the latter value was used in the phase composition calculations for each of the four UX tests conducted.

Stress-time and strain-time results from the two dynamic tests are given in Figures B-3 and B-4 along with their corresponding vertical stress versus vertical strain relations. Vertical stress versus vertical strain results for the two static tests are given in Figures B-5 and B-6. Horizontal stress measurements were erratic, perhaps due to sample disturbance, and have not been included.

TESTS ON REMOLDED SAND

Three bags of sand from the stockpile used as a source of backfill for the LN311 structure test pits were shipped to WES for uniaxial strain testing. After the sand was air dried and thoroughly mixed, classifications, grain-size distributions and specific gravities were obtained for two selected samples; results are given in Figures B-7 and B-8. All test specimens were 2-1/2 inch high by 5-inch-diameter and were remolded as closely as practicable to target values for water content and dry density of 6.1 percent and 110.7 pcf, respectively, as specified by NCEL.

Samples RD1 through RD4 were compacted in three equal lifts to the specified dry density with a drop-hammer and tested dynamically. Stress-time and strain-time results from these tests are given in Figures B-9 through B-12 along with their corresponding vertical stress versus vertical strain relations. Two similarly prepared samples, RS1 and RS2, were statically loaded to approximately 600 psi and unloaded; vertical stress versus vertical strain results for these tests are given in Figures B-13 and B-14. Sample No. RS3 was statically loaded to 300 psi, unloaded and then reloaded to approximately 600 psi and subsequently unloaded; horizontal stress measurements were made throughout the test. Results are given in Figure B-15. The initial σ_v versus σ_h data are questionable, and are thought to be influenced by initial stresses induced in the test ring by the dynamic compaction method employed. A different compaction technique that should have minimized introduction of initial stresses was used with sample No. RS4, Figure B-16; the σ_v versus σ_h data for this test are considered quite reasonable.

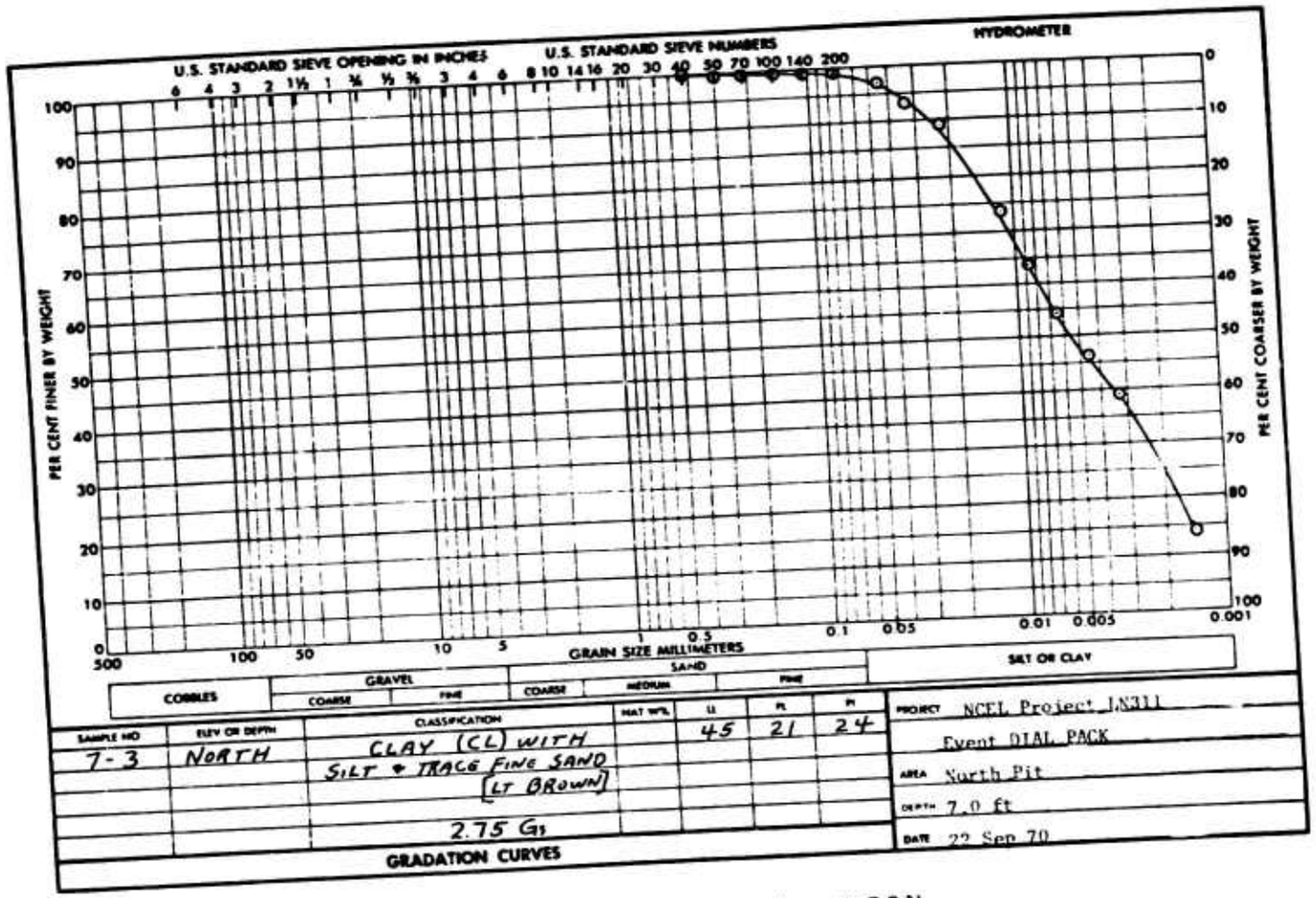

Figure B1. Material properties for soil sample 7-3-N.

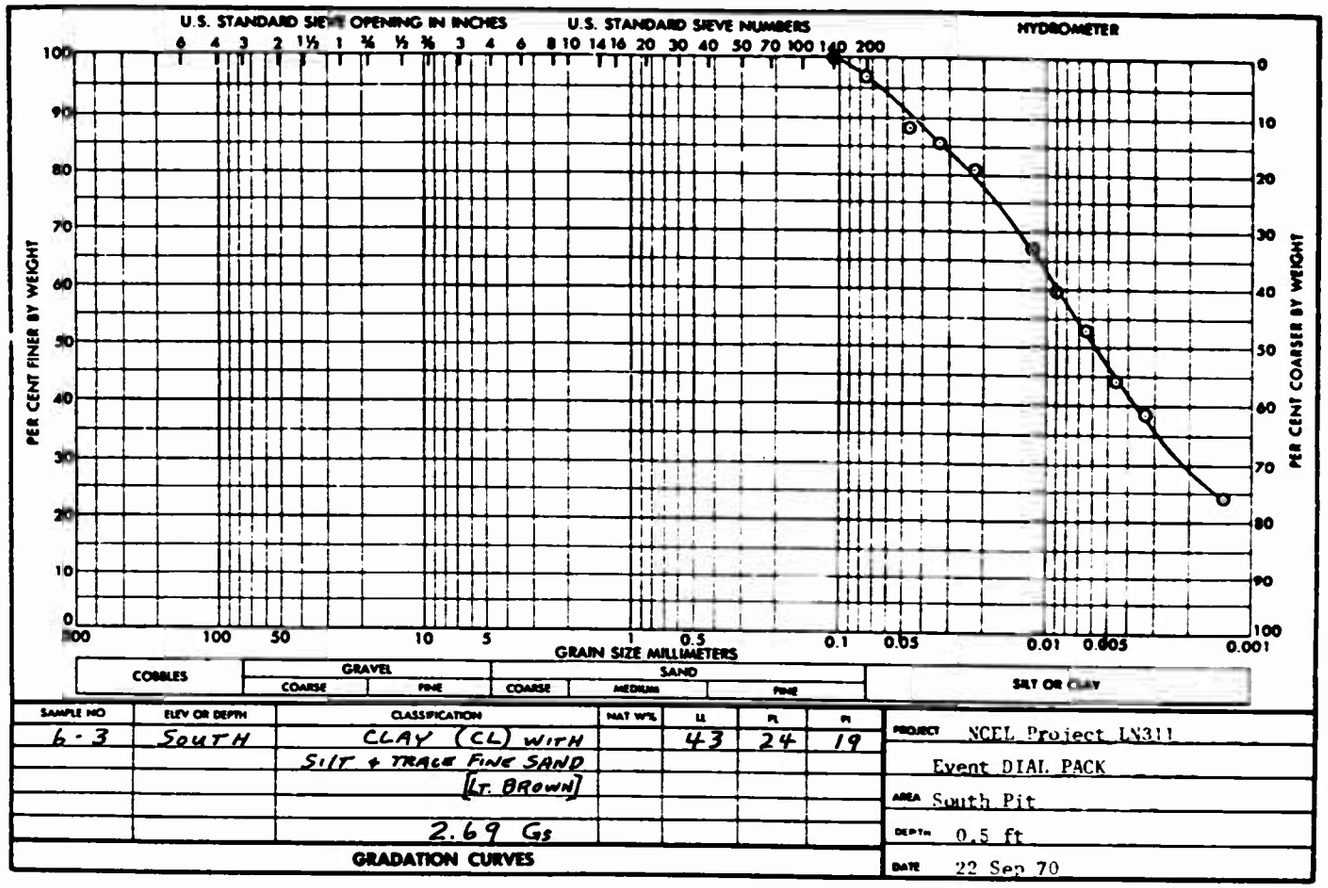

Figure B-2. Material properties for soil sample 6-3-8.

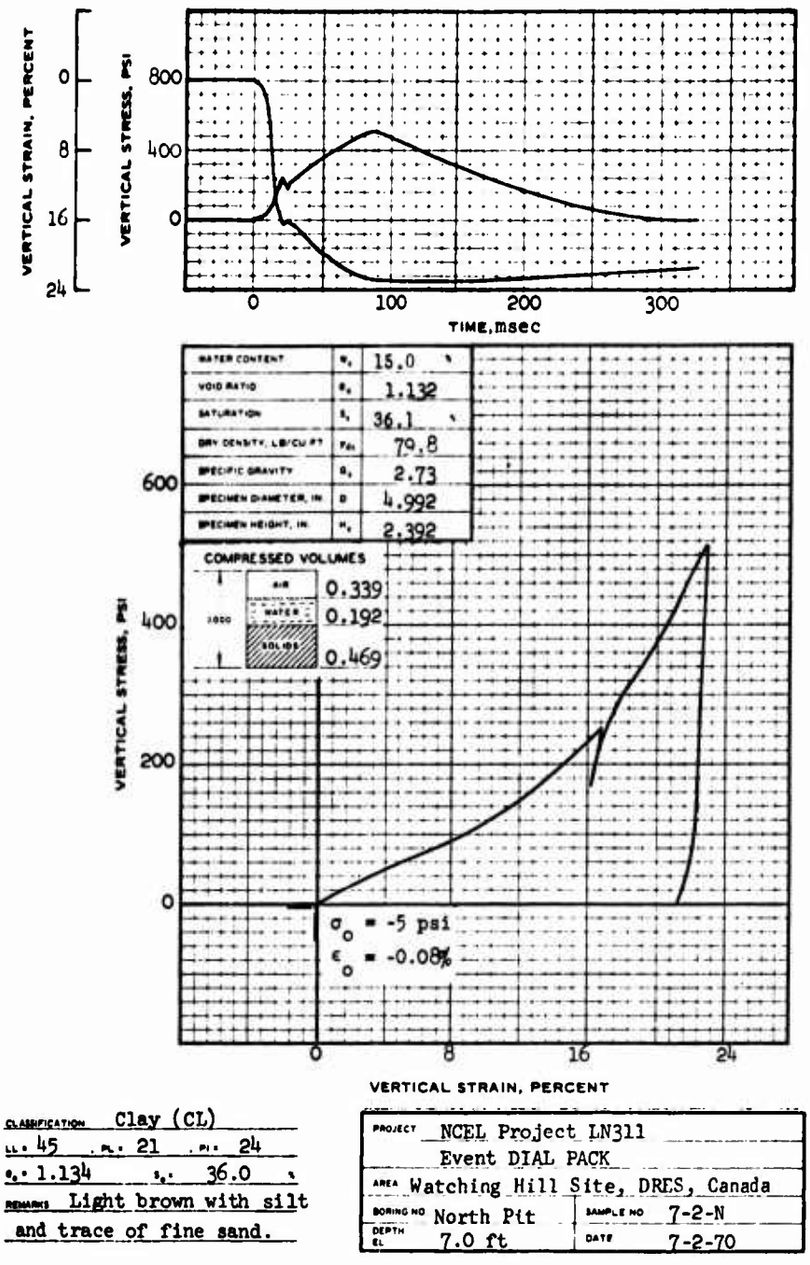

CLASSIFICATION Clay (CL)

LL= 45 , PL= 21 , PI= 24

e_o= 1.134 s_o= 36.0 %

REMARKS Light brown with silt and trace of fine sand.

PROJECT	NCEL Project LN311 Event DIAL PACK		
AREA	Watching Hill Site, DRES, Canada		
BORING NO	North Pit	SAMPLE NO	7-2-N
DEPTH EL	7.0 ft	DATE	7-2-70

UNIAXIAL STRAIN TEST RESULTS

Figure B-3. Undisturbed dynamic test no. DPK (LN311) 7-2-N.

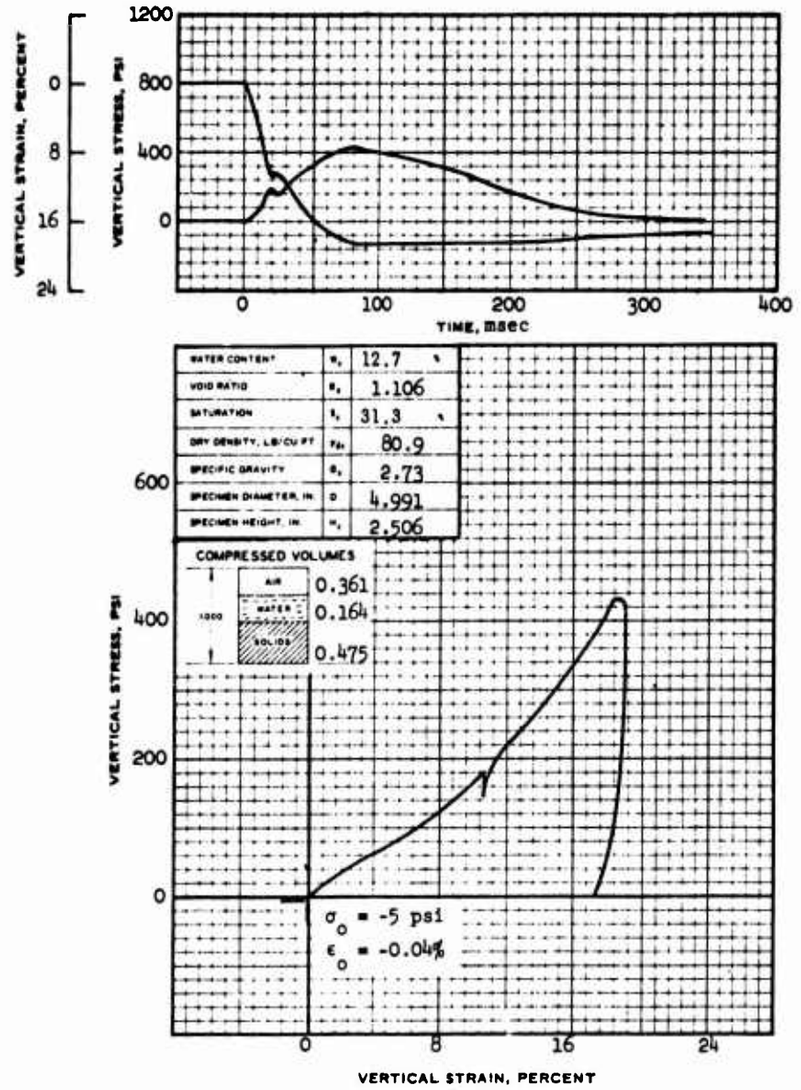

CLASSIFICATION Clay (CL)

LL = 45 , PL = 21 , PI = 24

γ_d = 1.107 S_r = 31.3 %

REMARKS Light brown with silt and trace of fine sand.

PROJECT NCEL Project LN311 Event DIAL PACK	
AREA Watching Hill Site, DRES, Canada	
BORING NO South Pit	SAMPLE NO. 7-2-S
DEPTH EL 7.0 ft	DATE 7-2-70

UNIAXIAL STRAIN TEST RESULTS

Figure B-4. Undisturbed dynamic test no. DPK (LN311) 7-2-S.

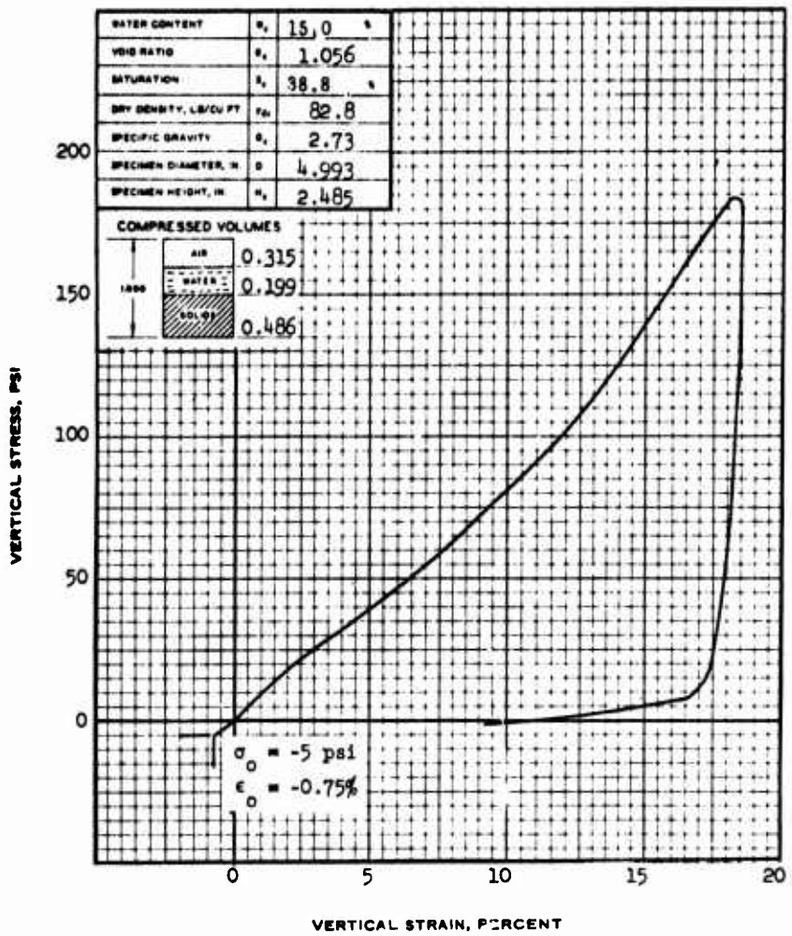

CLASSIFICATION Clay (CL)
LL = 45 , PL = 21 , PI = 24
γ_o = 1.071 S_o = 38.2 %
REMARKS Light brown with silt and trace of fine sand.

PROJECT NCEL Project LN311 Event DIAL PACK	
AREA Watching Hill Site, DRES, Canada	
BORING NO. North Pit	SAMPLE NO 7-3-N
DEPTH EL 7.0 ft	DATE 8-27-70

UNIAXIAL STRAIN TEST RESULTS

Figure B-5. Undisturbed static test no. DPK (LN311) 7-3-N.

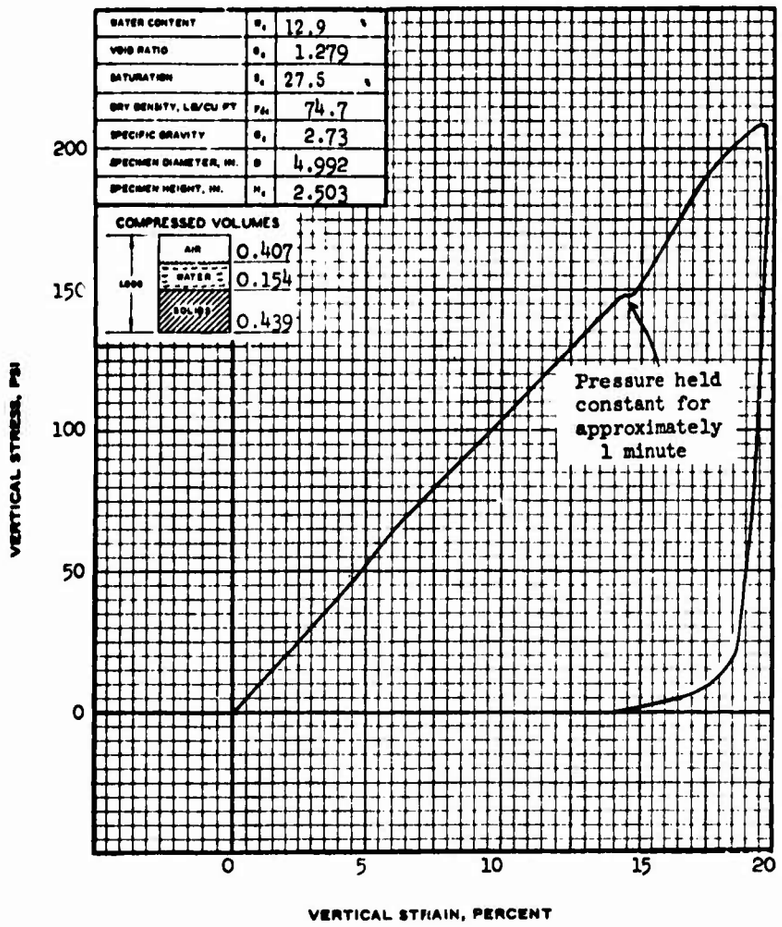

CLASSIFICATION Clay (CL)
LL= 43 , PL= 21 , PI= 19
γ_d= 1.279 w_o= 27.5 %
REMARKS: Light brown with silt and trace of fine sand.

PROJECT	NCEL Project LN311 Event DIAL PACK
AREA	Watching Hill Site, DRES, Canada
BORING NO. South Pit	SAMPLE NO 6-3-S
DEPTH EL 0.5 ft	DATE 8-27-70

UNIAXIAL STRAIN TEST RESULTS

Figure B-6. Undisturbed static test no. DPK (LN311) 6-3-S.

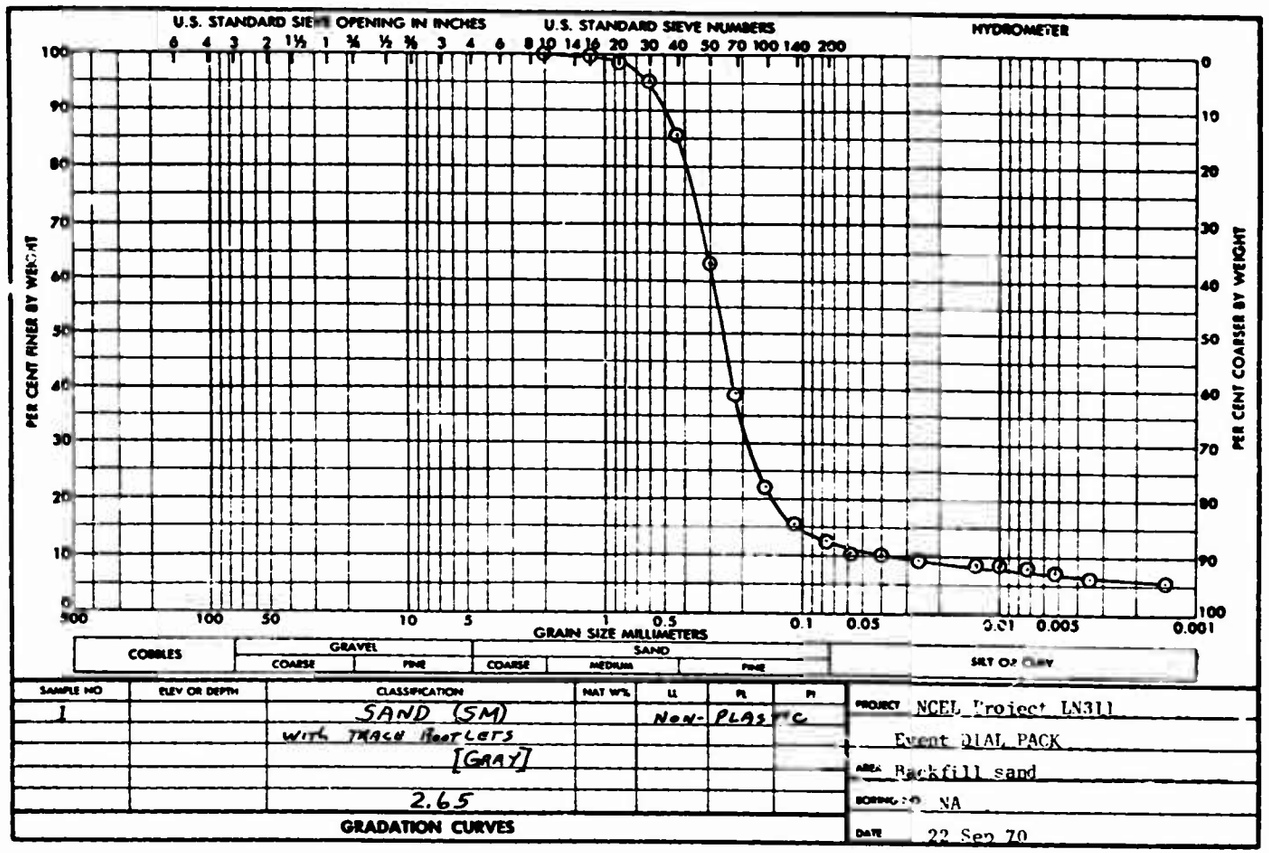

Figure B-7. Material properties for soil sample 1.

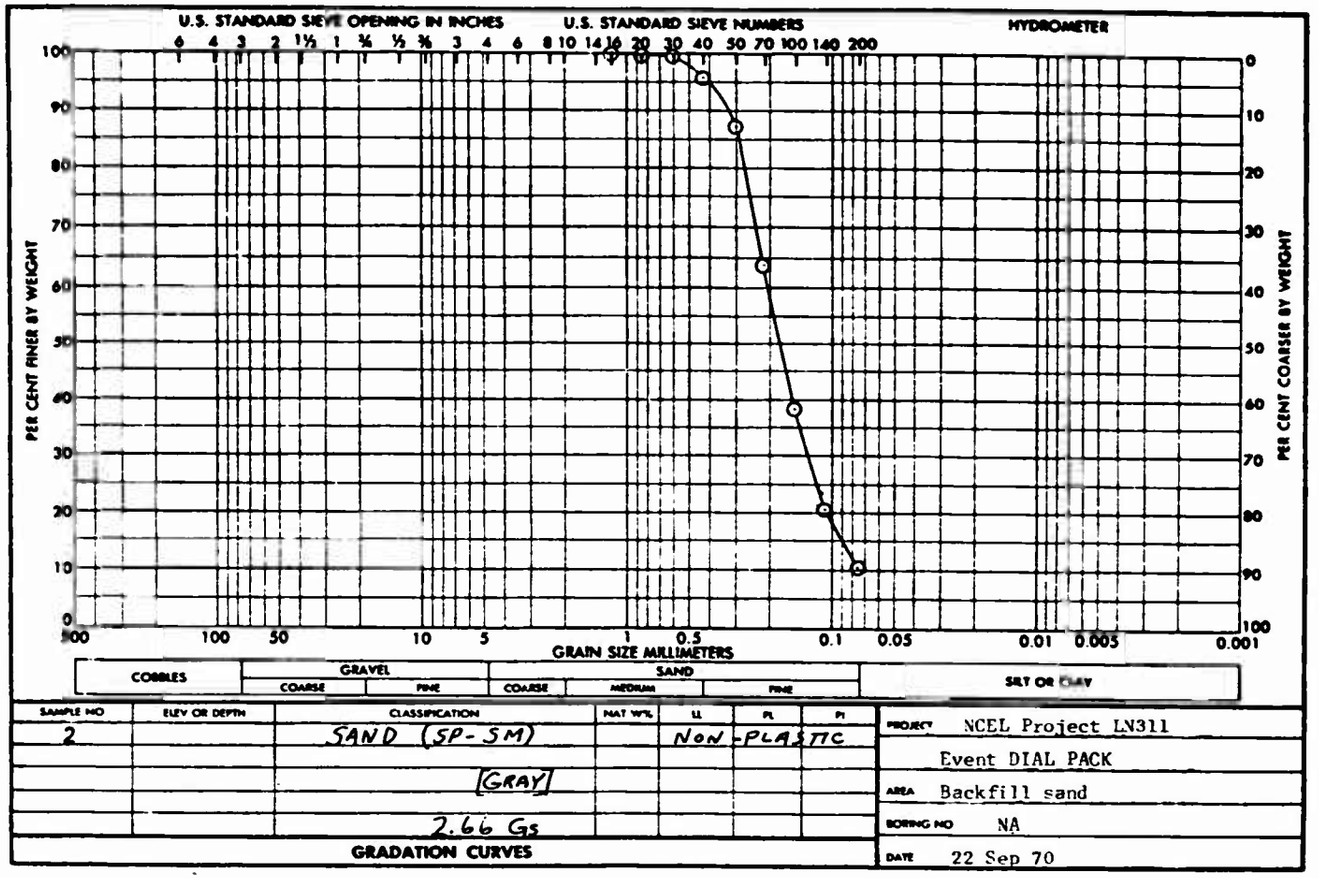

Figure B-8. Material properties for soil sample 2.

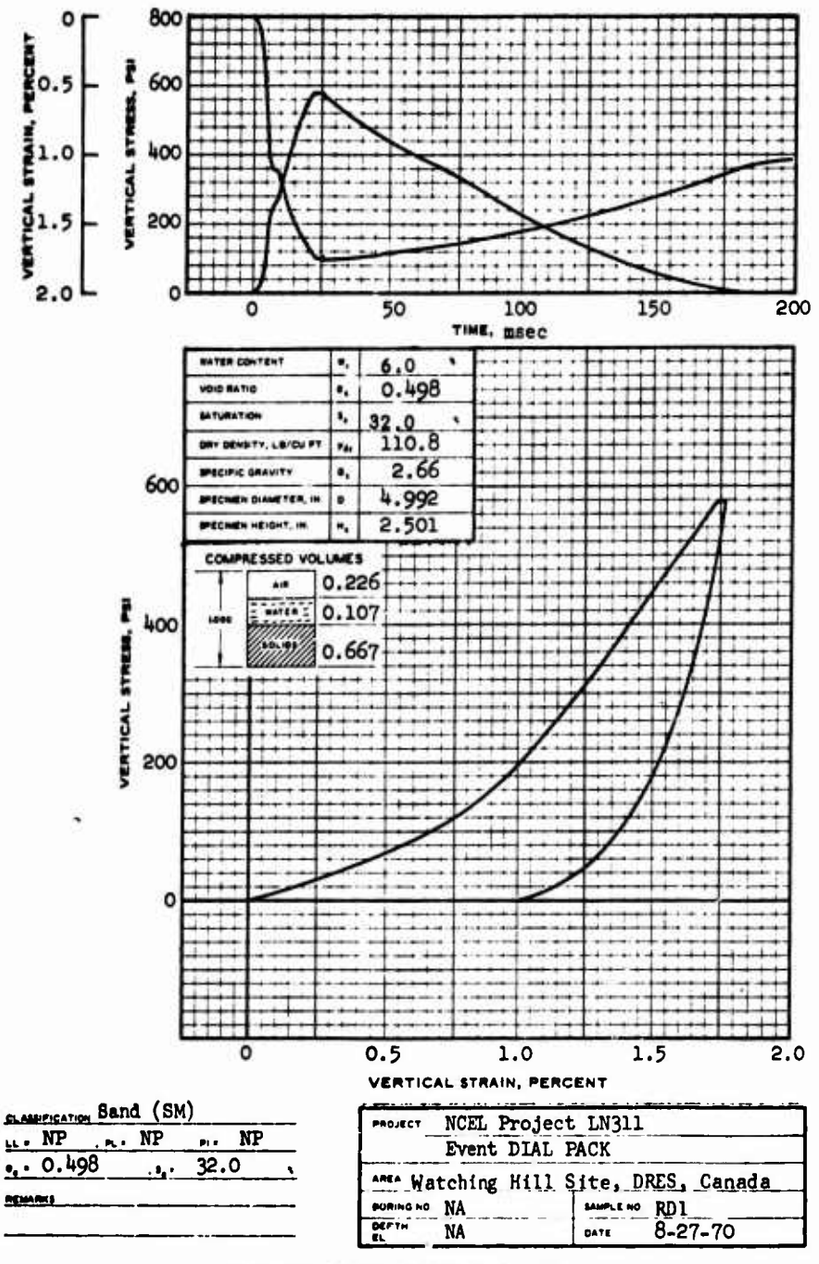

CLASSIFICATION Sand (SM)

LL = NP PL = NP PI = NP

e_0 = 0.498 S_0 = 32.0 %

REMARKS

PROJECT	NCEL Project LN311 Event DIAL PACK
AREA	Watching Hill Site, DRES, Canada
BORING NO	NA
SAMPLE NO	RD1
DEPTH EL	NA
DATE	8-27-70

UNIAXIAL STRAIN TEST RESULTS

Figure B-9. Remolded dynamic test no. DPK (LN311) RD1.

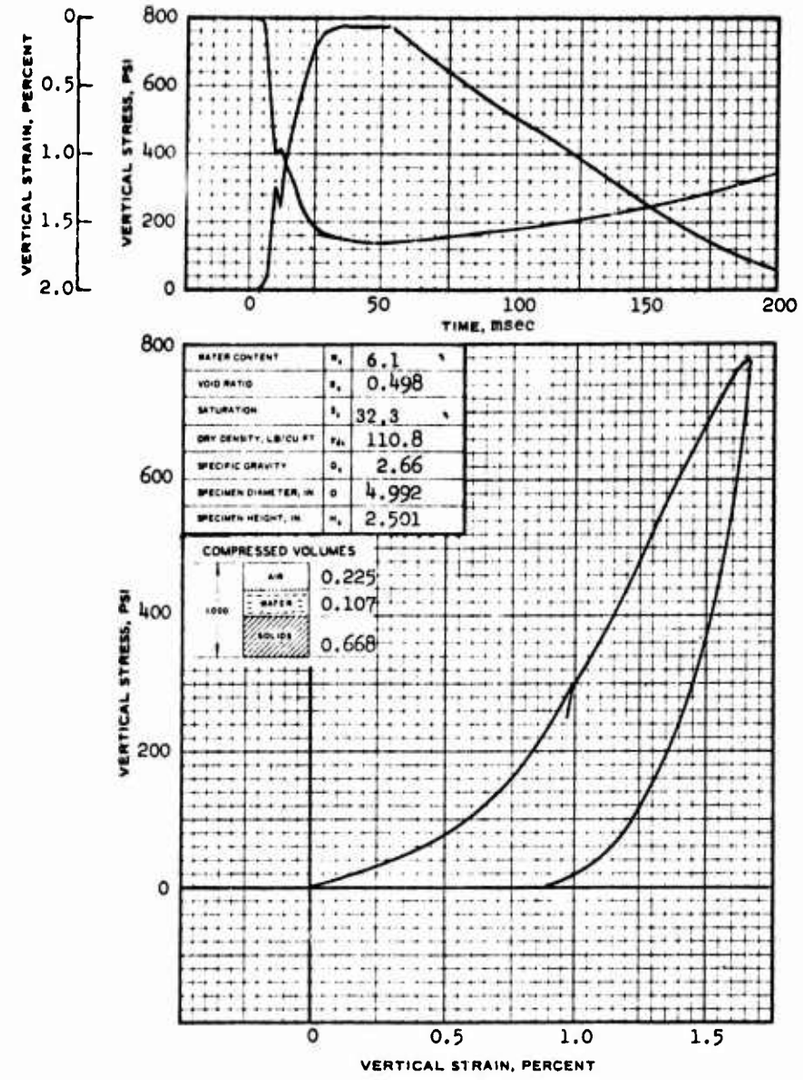

CLASSIFICATION Sand (SM)

LL = NP PL = NP PI = NP

e_o = 0.498 S_r = 32.3 %

REMARKS

PROJECT	NCEL Project LN311 Event DIAL PACK		
AREA	Watching Hill Site, DRES, Canada		
BORING NO	NA	SAMPLE NO	RD2
DEPTH EL	NA	DATE	8-31-70

UNIAXIAL STRAIN TEST RESULTS

Figure B-10. Remolded dynamic test no. DPK (LN311) RD2.

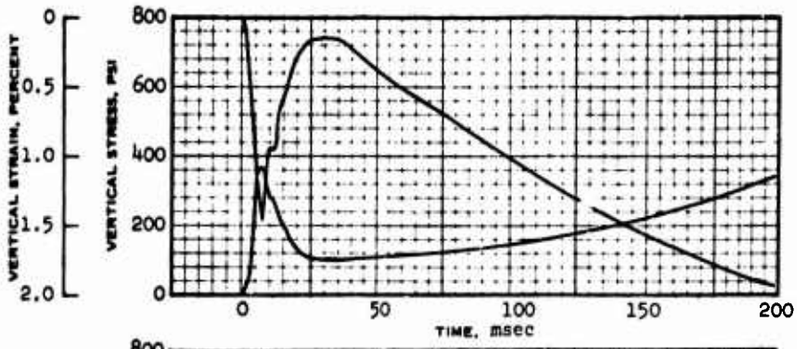

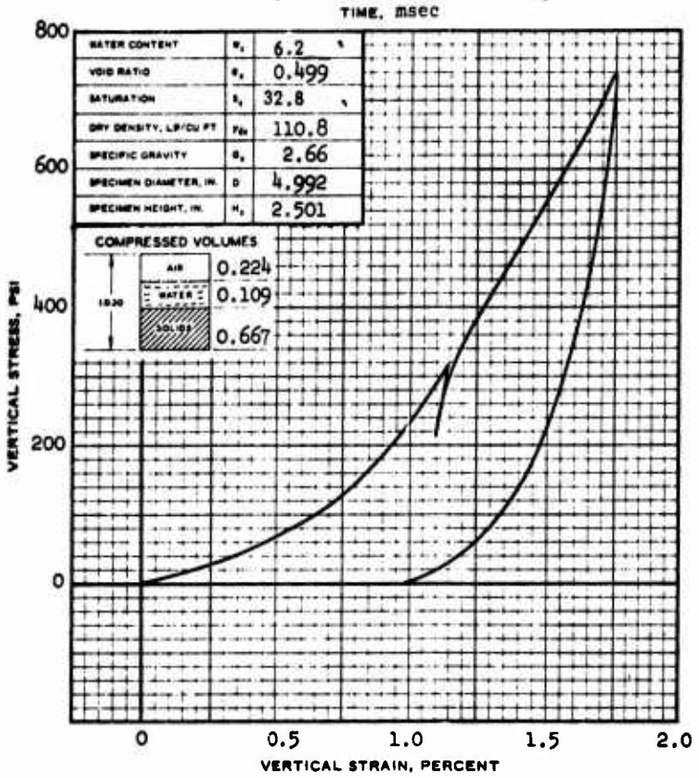

WATER CONTENT	w_c	6.2 %
VOID RATIO	e_c	0.499
SATURATION	S_c	32.8 %
DRY DENSITY, LB/CU FT	γ_{dc}	110.8
SPECIFIC GRAVITY	G_s	2.66
SPECIMEN DIAMETER, IN.	D	4.992
SPECIMEN HEIGHT, IN.	H_c	2.501

COMPRESSED VOLUMES

AIR	0.224
WATER	0.109
SOLIDS	0.667

CLASSIFICATION Sand (SM)

LL = NP , PL = NP , PI = NP

e_c = 0.499 , S_c = 32.8 %

REMARKS

PROJECT	NCEL Project LN311 Event DIAL PACK		
AREA	Watching Hill Site, DRES, Canada		
BORING NO	NA	SAMPLE NO	RD3
DEPTH EL	NA	DATE	8-31-70

UNIAXIAL STRAIN TEST RESULTS

Figure B-11. Remolded dynamic test no. DPK (LN311) RD3.

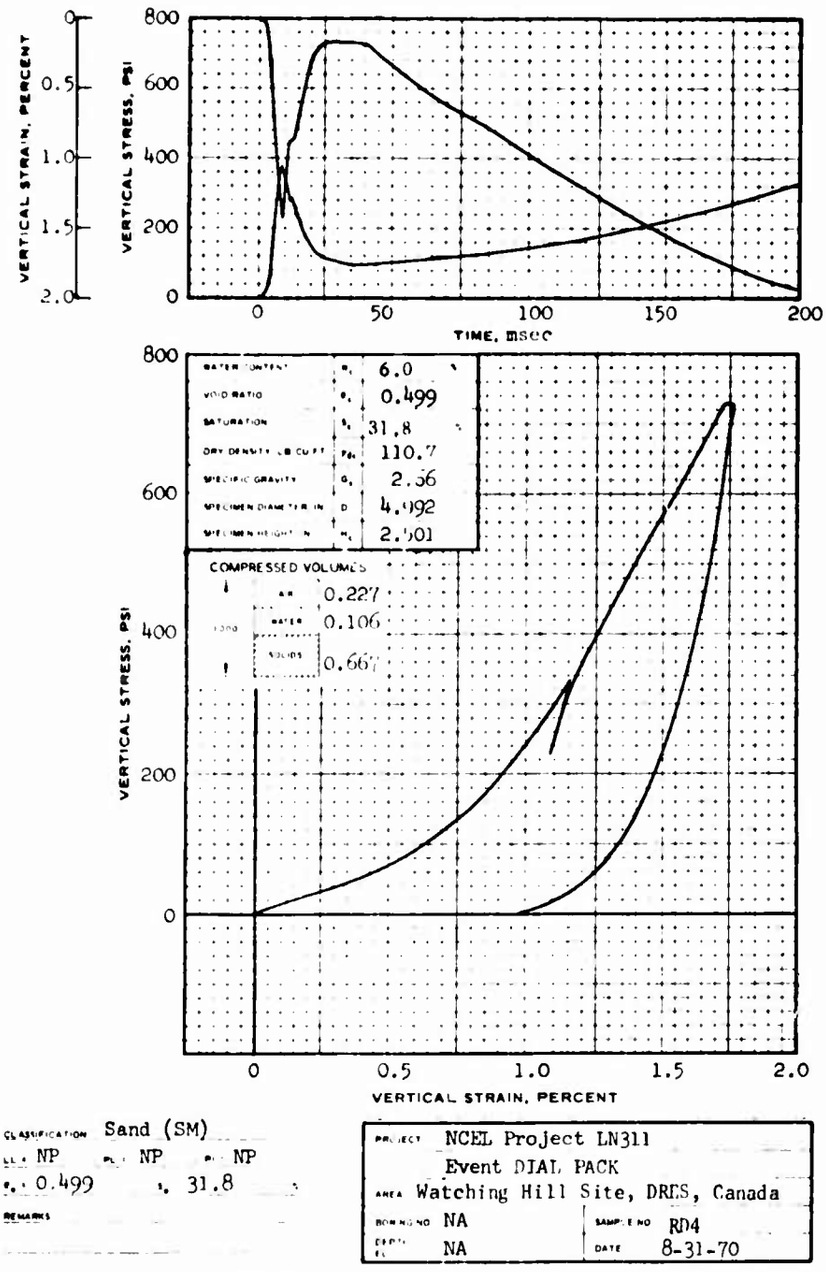

Figure B-12. Remolded dynamic test no. DPK (LN311) RD4.

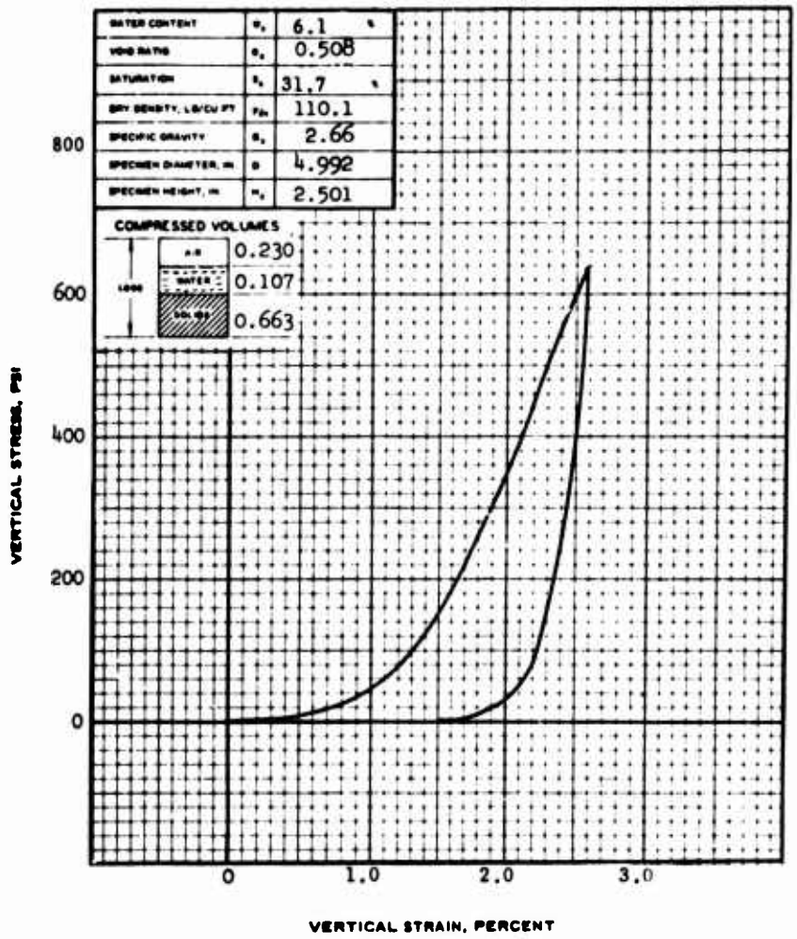

CLASSIFICATION Sand (SM)

LL = NP , PL = NP , PI = NP

e_0 = 0.508 S_0 = 31.7 %

REMARKS

PROJECT NCEL Project LN311	
Event DIAL PACK	
AREA Watching Hill Site, DRES, Canada	
BORING NO NA	SAMPLE NO RS1
DEPTH EL NA	DATE 8-27-70

UNIAXIAL STRAIN TEST RESULTS

Figure B-13. Remolded static test no. DPK (LN311) RS1.

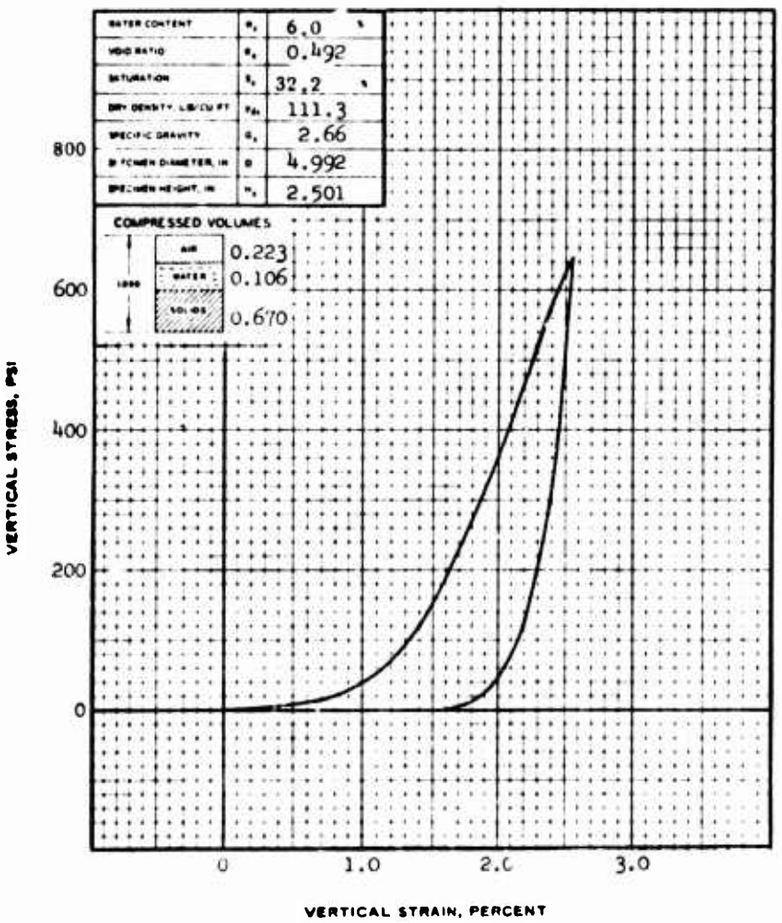

CLASSIFICATION Sand (SM)

LL = NP PL = NP PI = NP

e_o = 0.492 S_o = 32.2 %

REMARKS

PROJECT	NCEL Project LN311 Event DIAL PACK		
AREA	Watching Hill Site, DRES, Canada		
BORING NO	NA	SAMPLE NO	RS2
DEPTH EL	NA	DATE	9-14-70

UNIAXIAL STRAIN TEST RESULTS

Figure B-14. Remolded static test no. DPK (LN311) RS2.

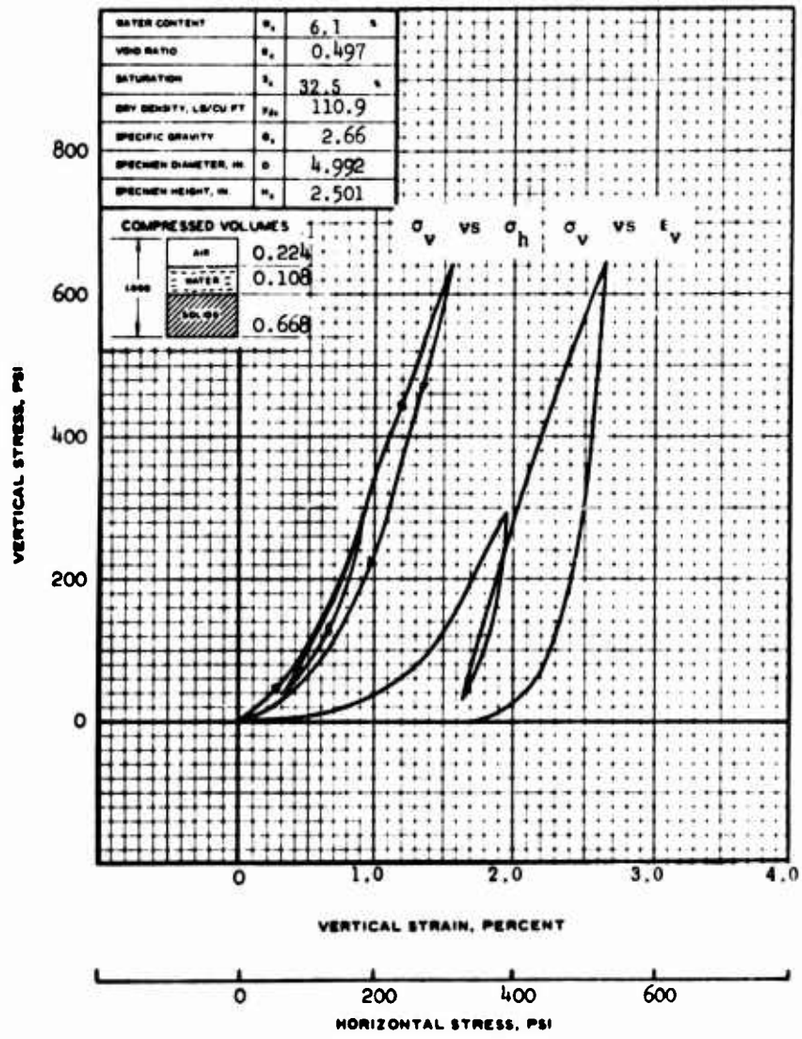

CLASSIFICATION Sand (SM)

LL = NP , PL = NP , PI = NP

γ_s = 0.497 S_r = 32.5 %

REMARKS

PROJECT	NCEL Project LN311 Event DIAL PACK		
AREA	Watching Hill Site, DRES, Canada		
BORING NO	NA	SAMPLE NO	RS3
DEPTH GL	NA	DATE	8-27-70

UNIAXIAL STRAIN TEST RESULTS

Figure B-15. Remolded static test no. DPK (LN311) RS3.

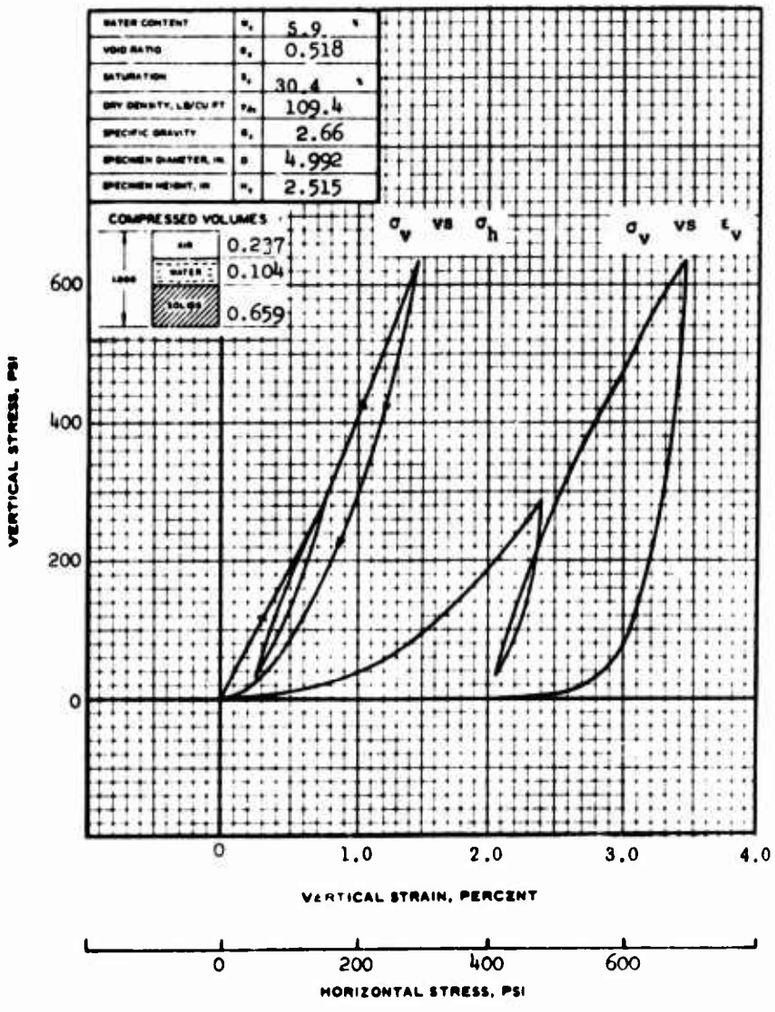

CLASSIFICATION Sand (SM)

LL = NP PL = NP PI = NP

γ_o = 0.518 S_o = 30.4 %

REMARKS

PROJECT	NCEL Project LN311 Event IAL PACK		
AREA	Watching ill Site, DRES, Canada		
BORING NO	NA	SAMPLE NO	RS4
DEPTH FT	NA	DATE	9-14-70

UNIAXIAL STRAIN TEST RESULTS

Figure B-16. Remolded static test no. DPK (LN311) RS4.

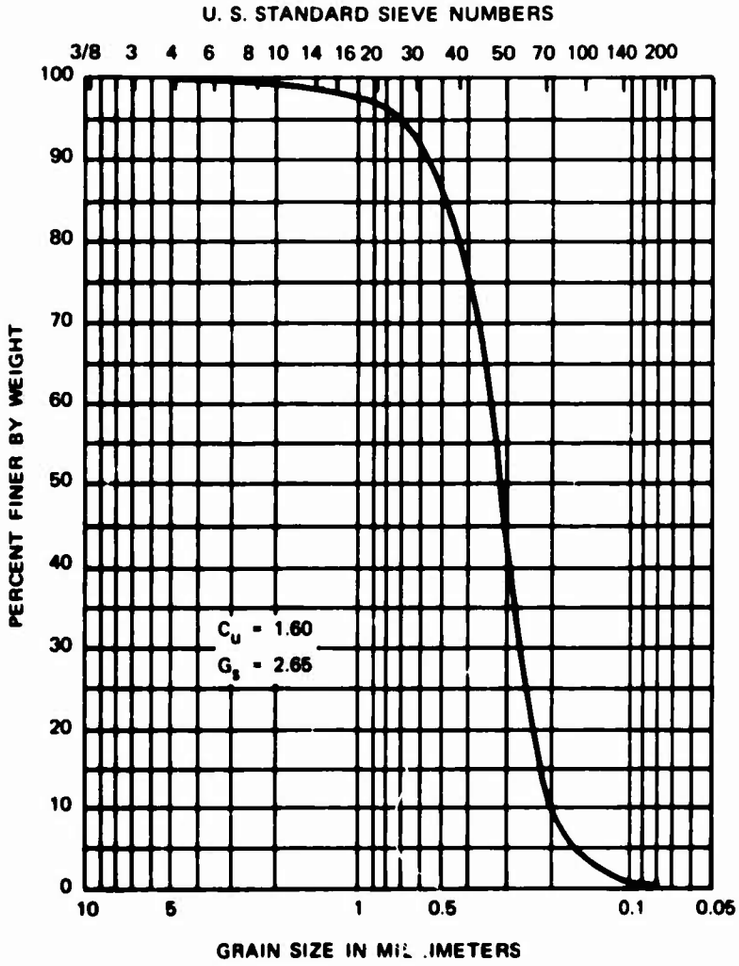

Figure B-17. Gradation curve for Cook's Bayou sand.

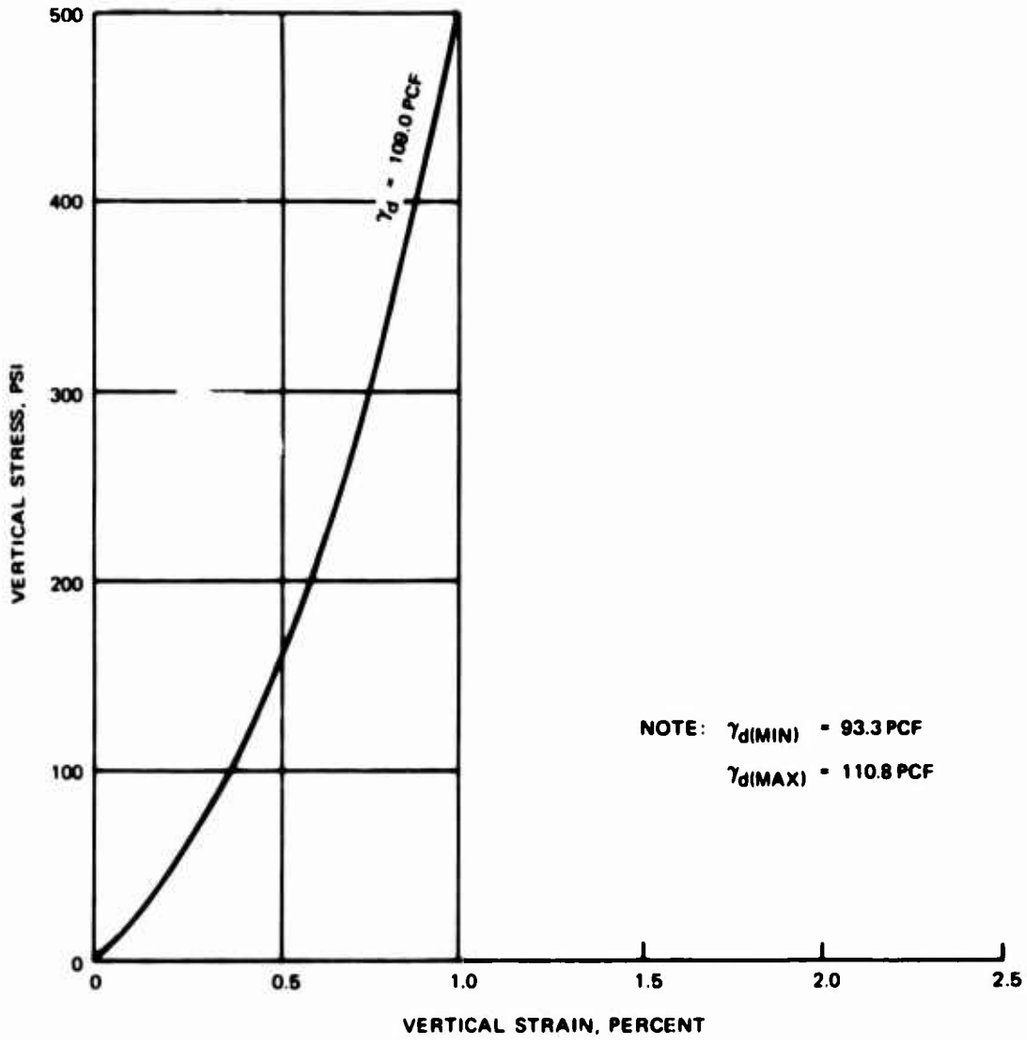

Figure B-18. Results of static one-dimensional compression tests on Cook's Bayou sand.

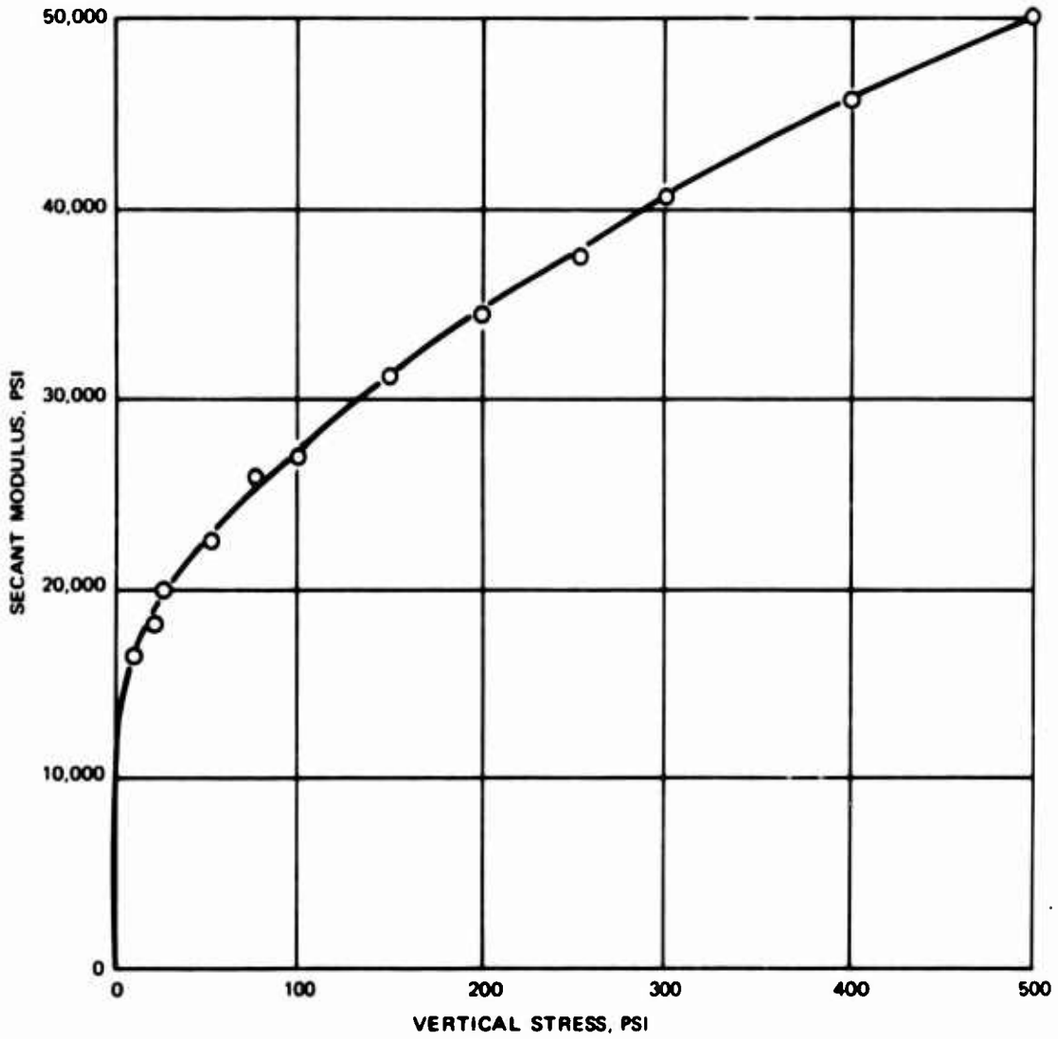

Figure B-19. Relation between secant modulus and vertical stress for Cook's Bayou sand.

Appendix C

GRAPHICAL PLOTS OF DIGITIZED DATA

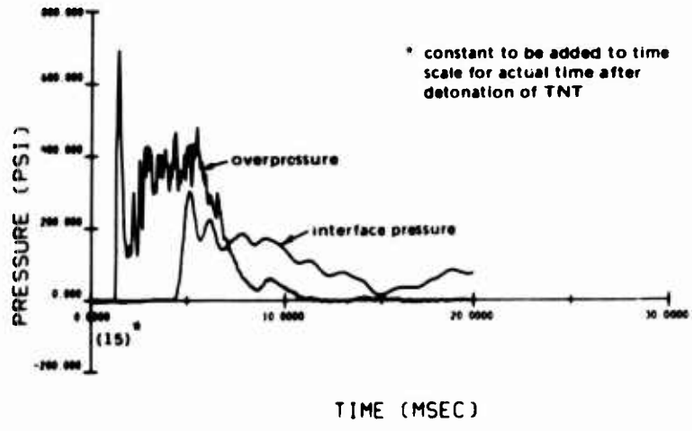

Figure C-1. Surface overpressure and interface pressure for model CP-1.

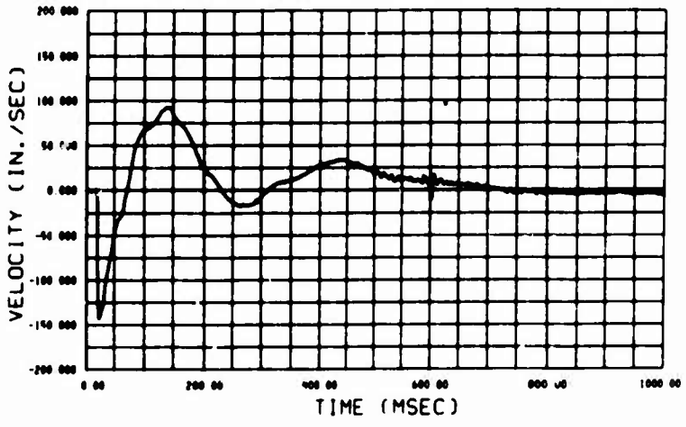

Figure C-2. Free-field vertical velocity at 3-ft depth.

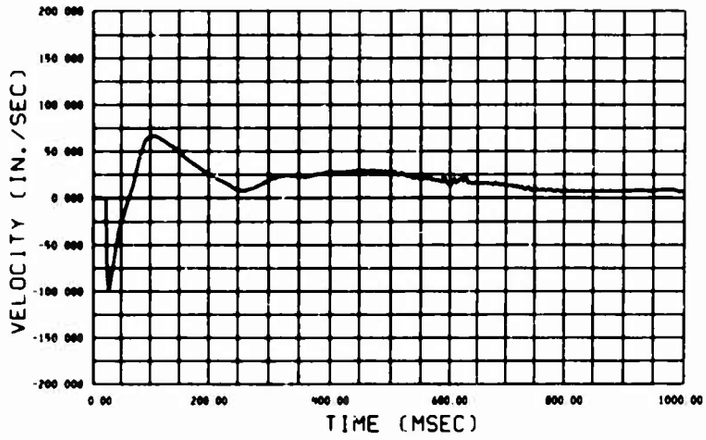

Figure C-3. Free-field vertical velocity at 6-ft depth.

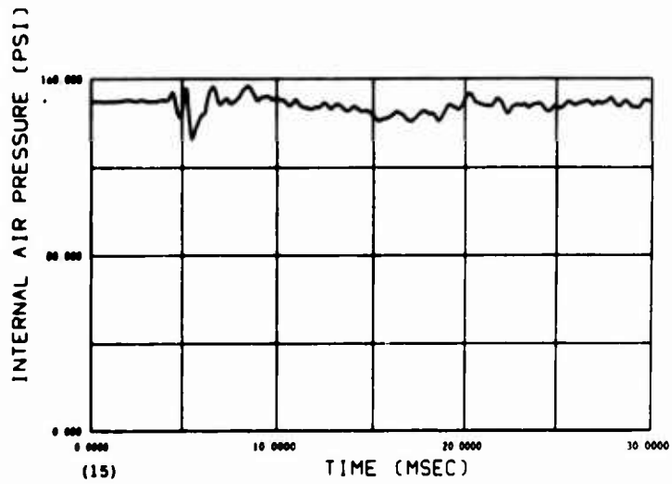

Figure C-4. Variation in internal pressure of gage P2, model CP-1.

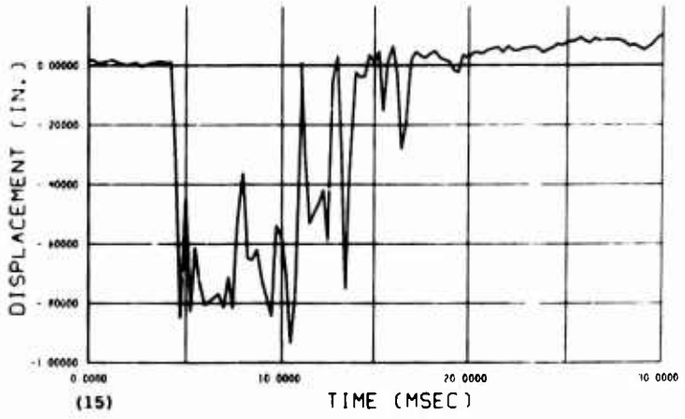

Figure C-5. Diametral deformation from gage D1, model CP-1.

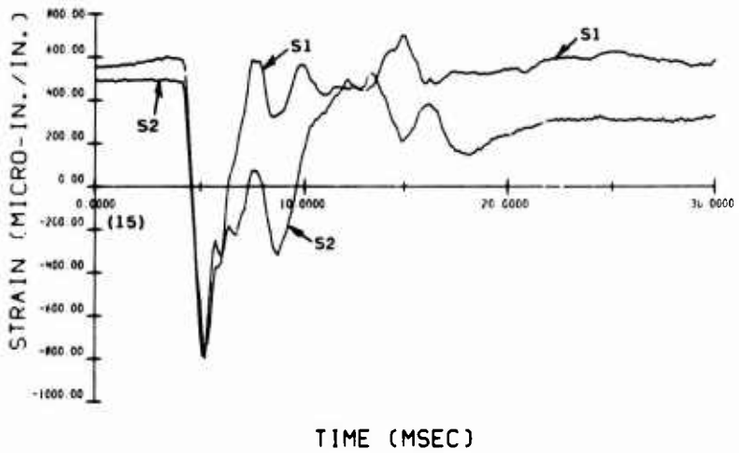

Figure C-6. Strain versus time from gages S1 and S2, model CP-1.

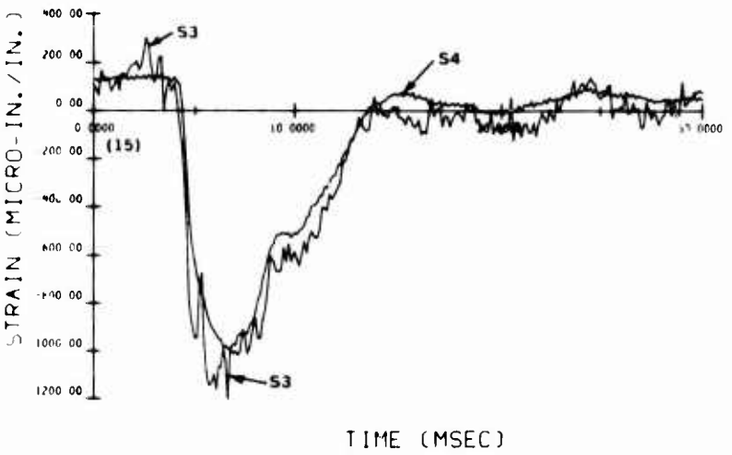

Figure C-7. Strain versus time from gages S3 and S4, model CP-1.

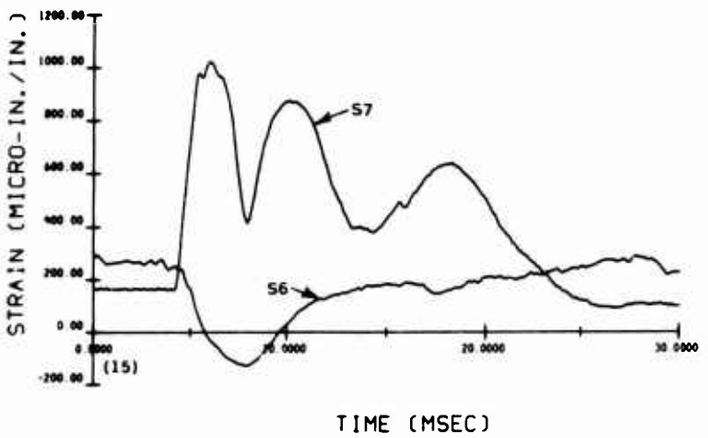

Figure C-8. Strain versus time from gages S6 and S7, model CP-1.

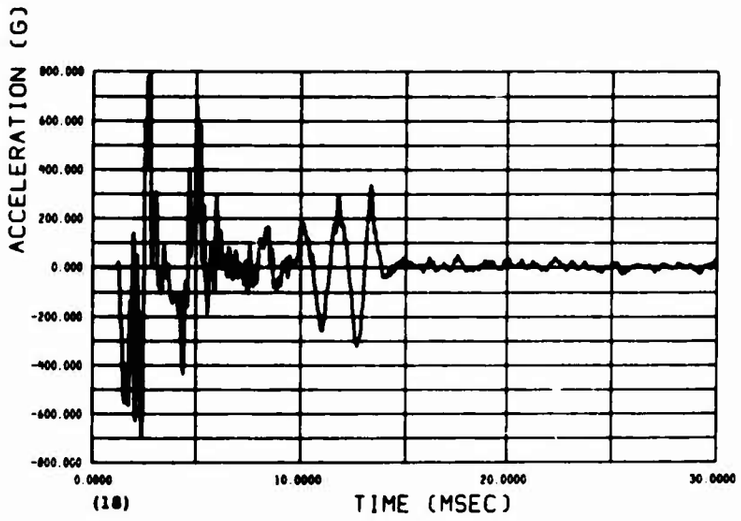

Figure C-9. Vertical acceleration from accelerometer AV1, model CP-1.

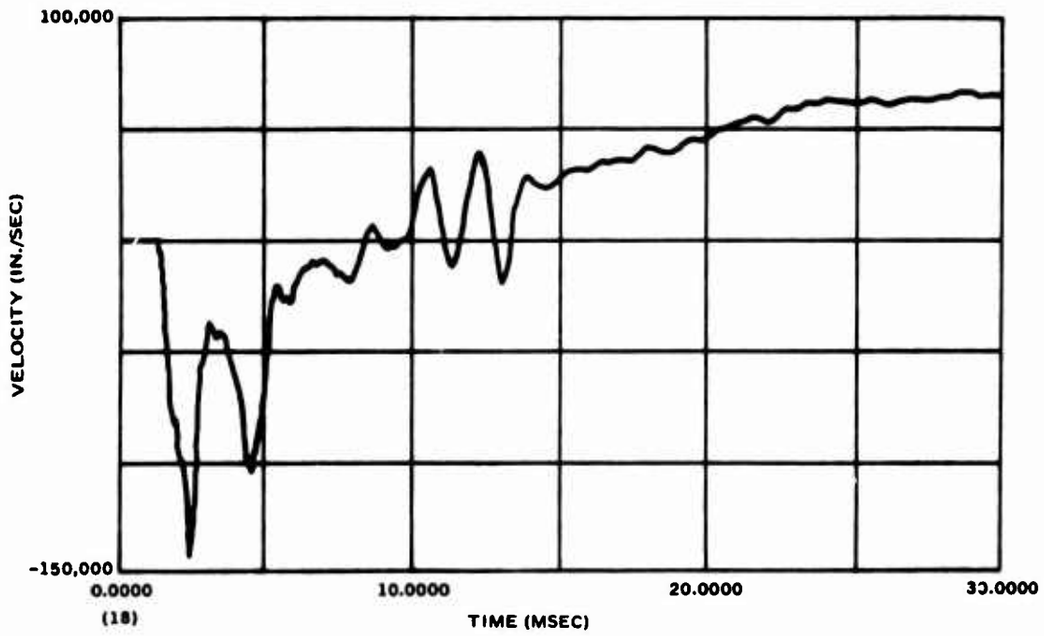

Figure C-10. Vertical velocity from integration of acceleration data, AV1, model CP-1.

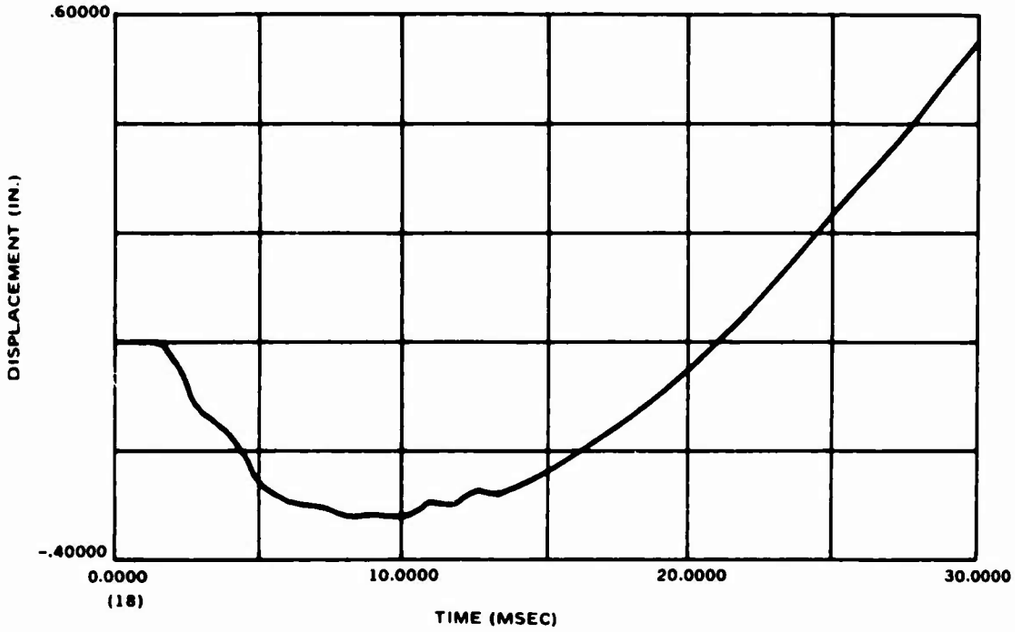

Figure C-11. Vertical displacement from double integration of acceleration data, AV1, model CP-1.

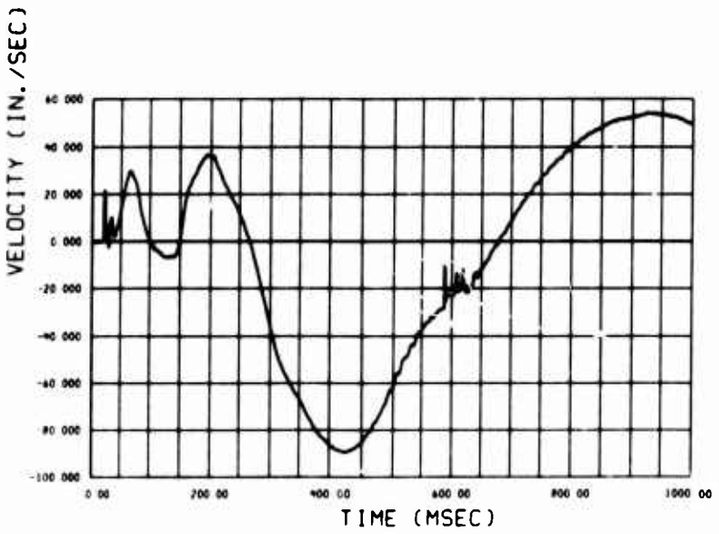

Figure C-12. Horizontal velocity from gage VH1, model CP-1.

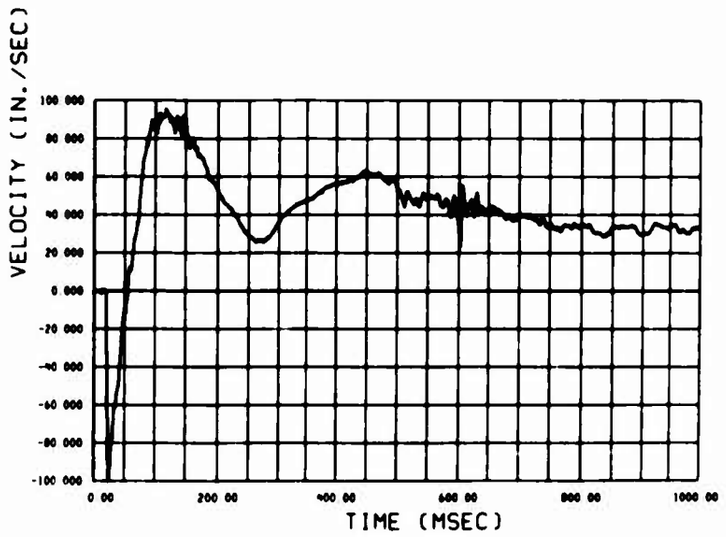

Figure C-13. Vertical velocity from gage VV2, model CP-1.

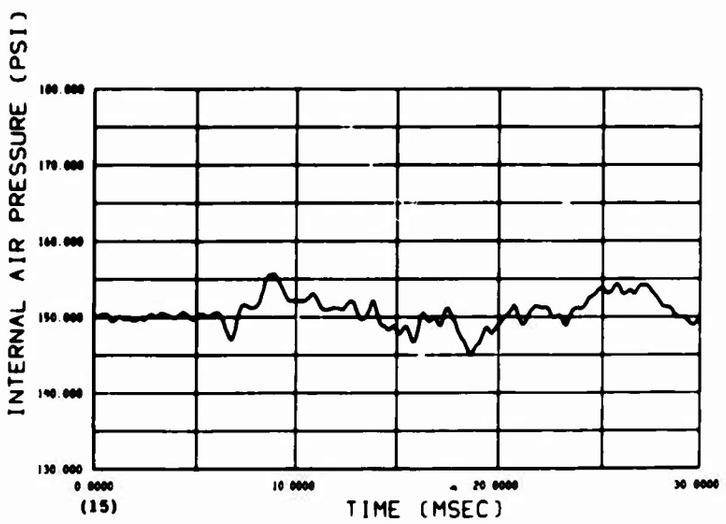

Figure C-14. Variation in internal pressure, P3, model CP-2.

Figure C-15. Diametral deformation from gage D2, model CP-2.

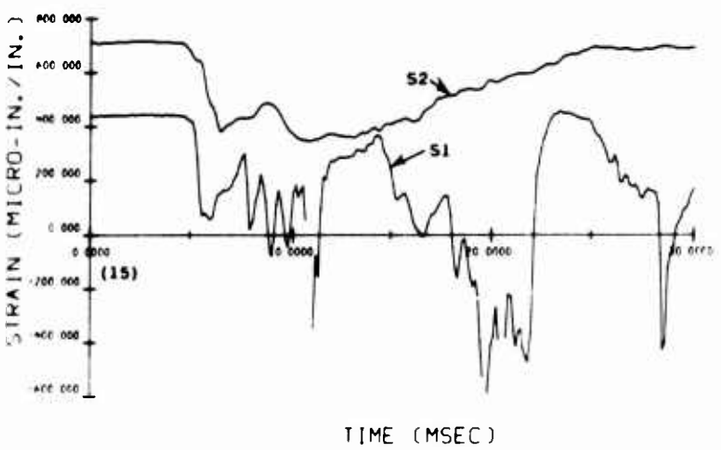

Figure C-16. Strain versus time from gages S1 and S2, model CP-2.

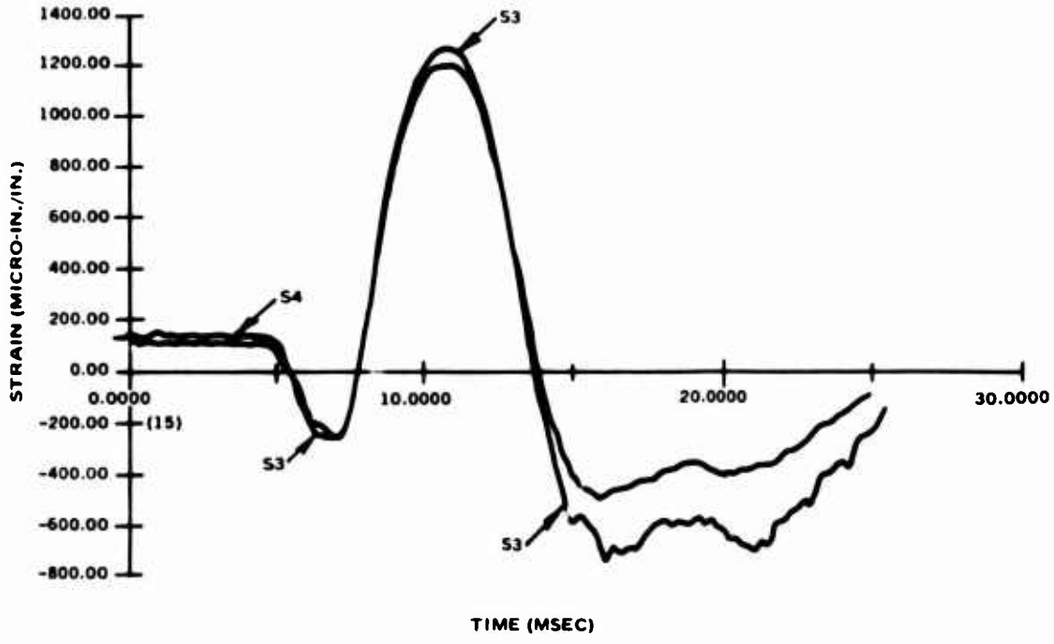

Figure C-17. Strain versus time from gages S3 and S4, model CP-2.

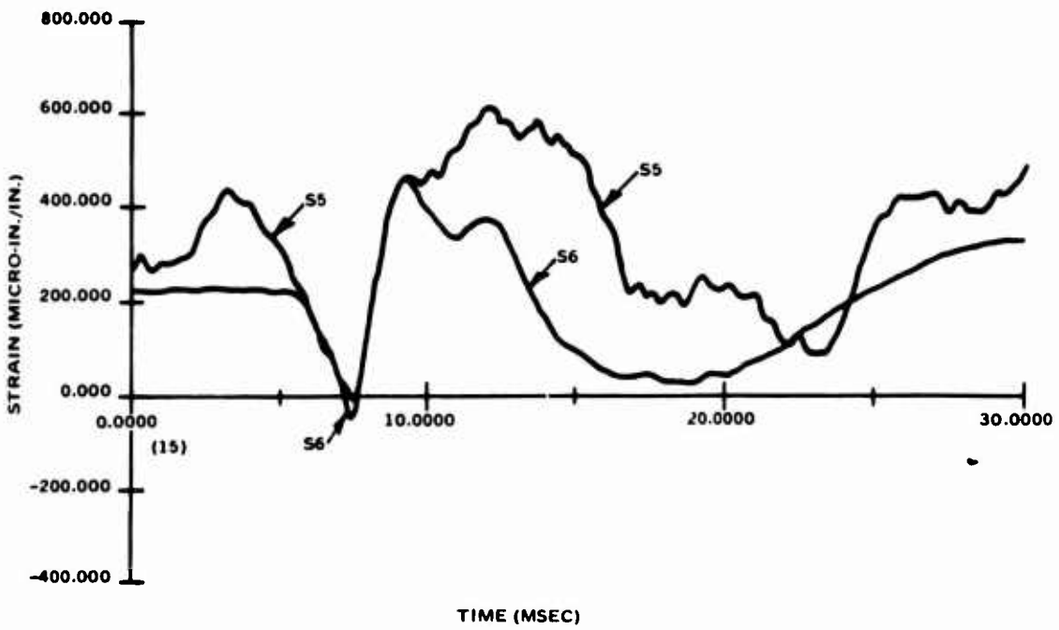

Figure C-18. Strain versus time from gages S5 and S6, model CP-2.

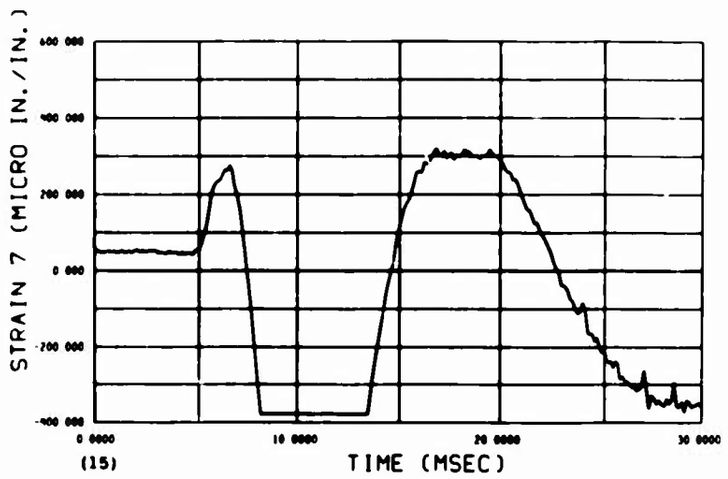

Figure C-19. Strain versus time from gage S7, model CP-2.

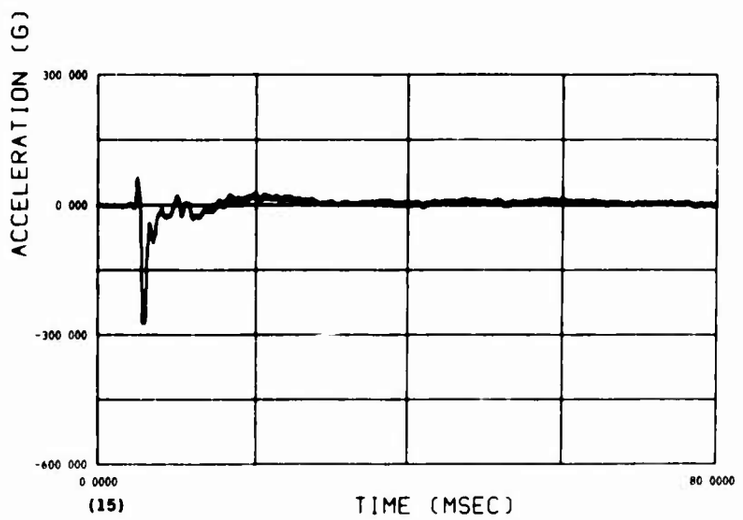

Figure C-20. Vertical acceleration from accelerometer AV2, model CP-2.

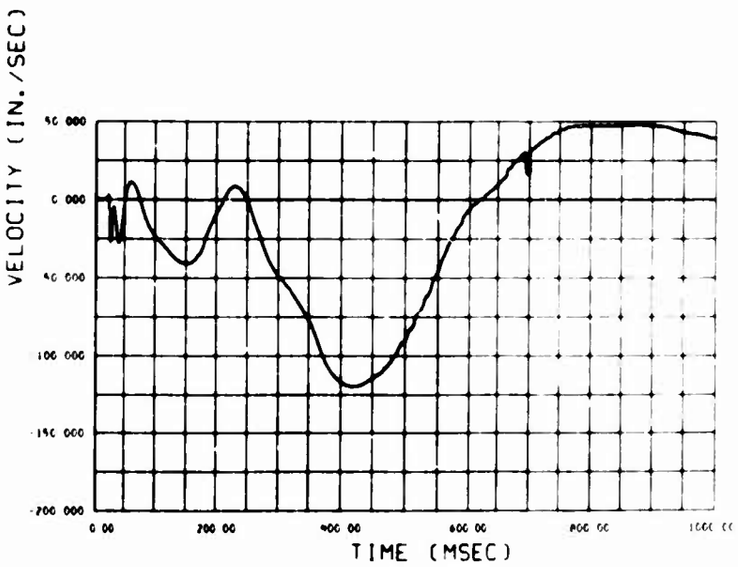

Figure C-21. Horizontal velocity from gage VH3, model CP-2.

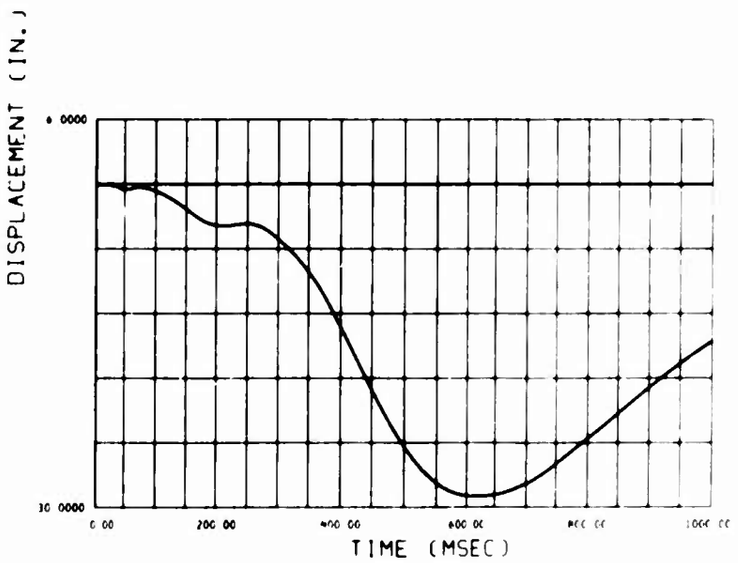

Figure C-22. Horizontal displacement from integration of velocity data, gage VH3, model CP-2.

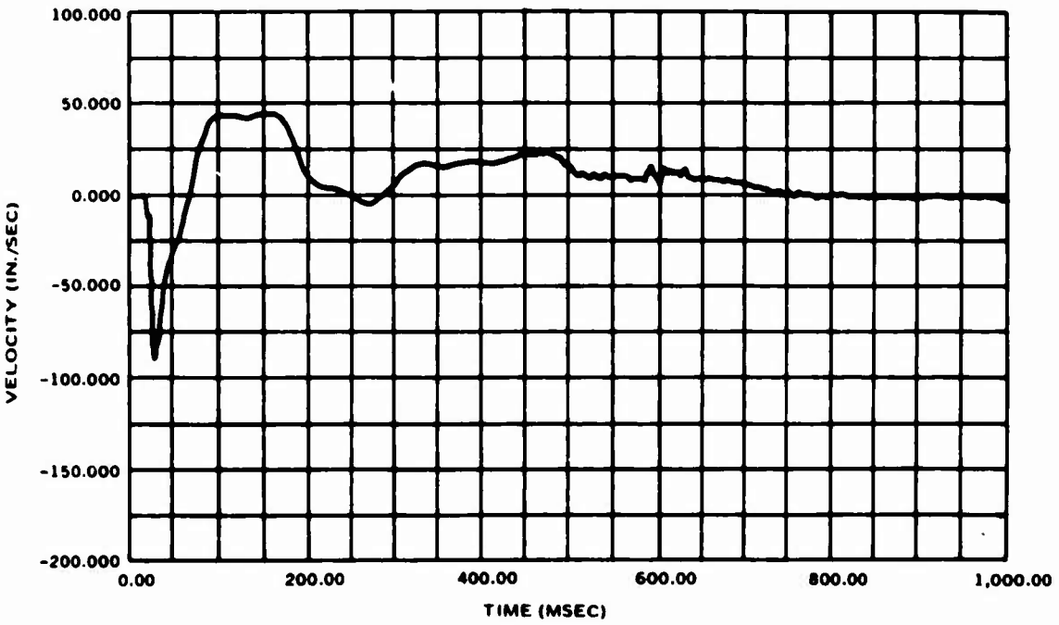

Figure C-23. Vertical velocity from gage VV4, model CP-2.

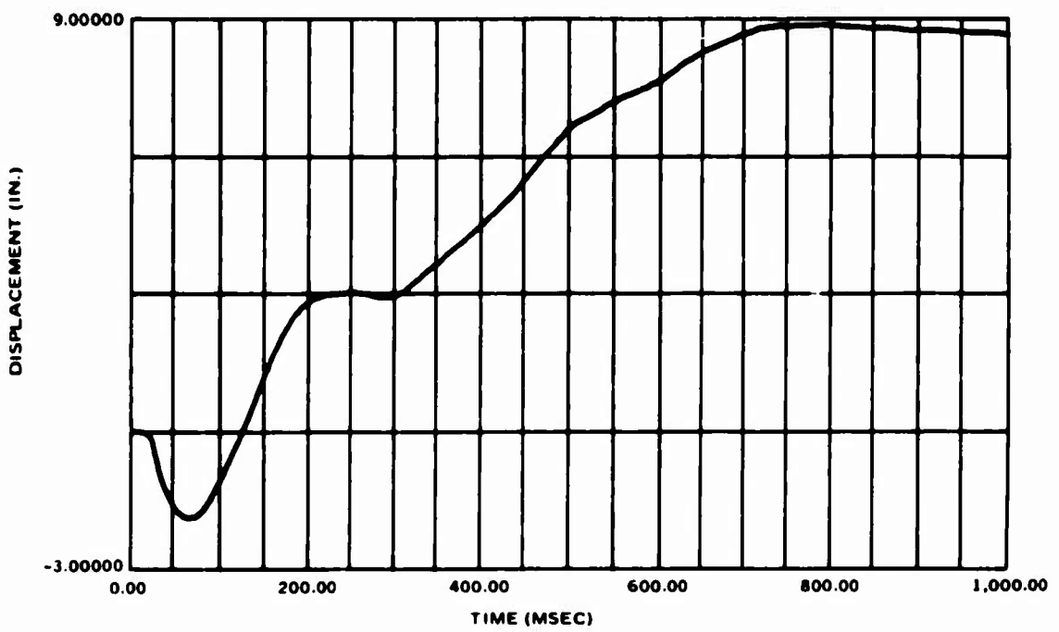

Figure C-24. Vertical displacement from integration of velocity data, VV4, model CP-2.

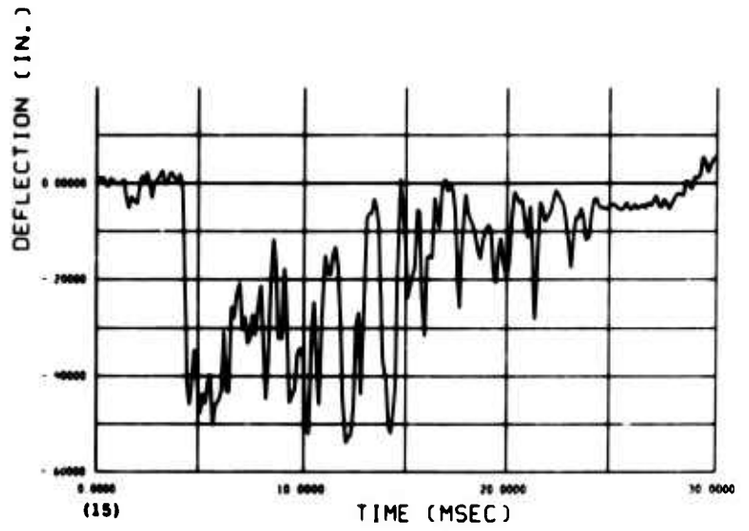

Figure C-25. Diametral deformation from gage D3, model CN-1.

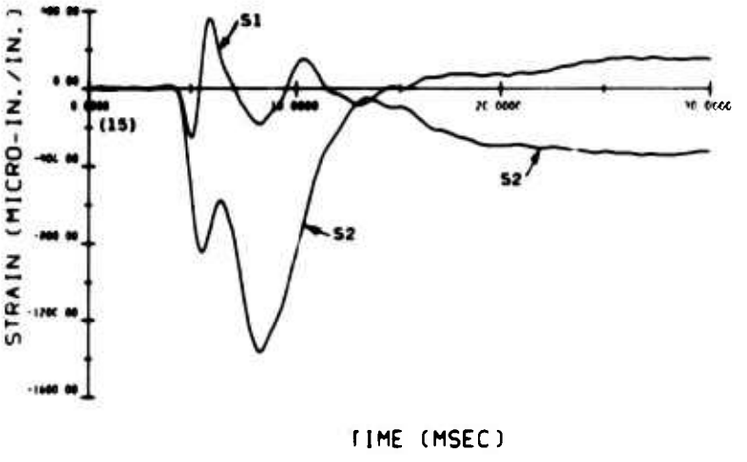

Figure C-26. Strain versus time from gages S1 and S2, model CN-1.

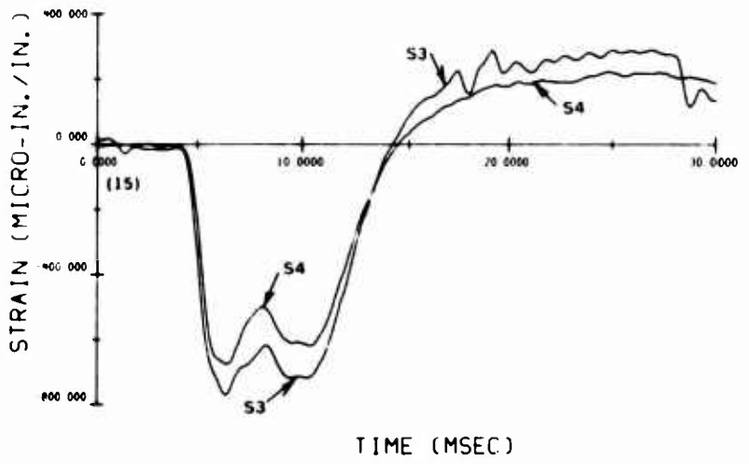

Figure C-27. Strain versus time from gages S3 and S4, model CN-1.

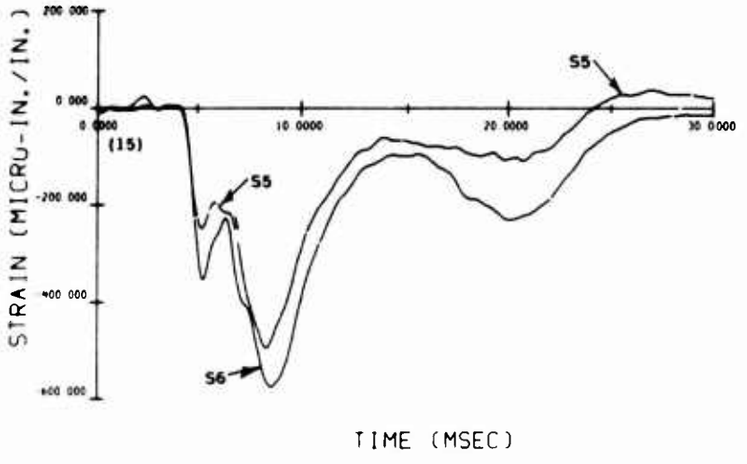

Figure C-28. Strain versus time from gages S5 and S6, model CN-1.

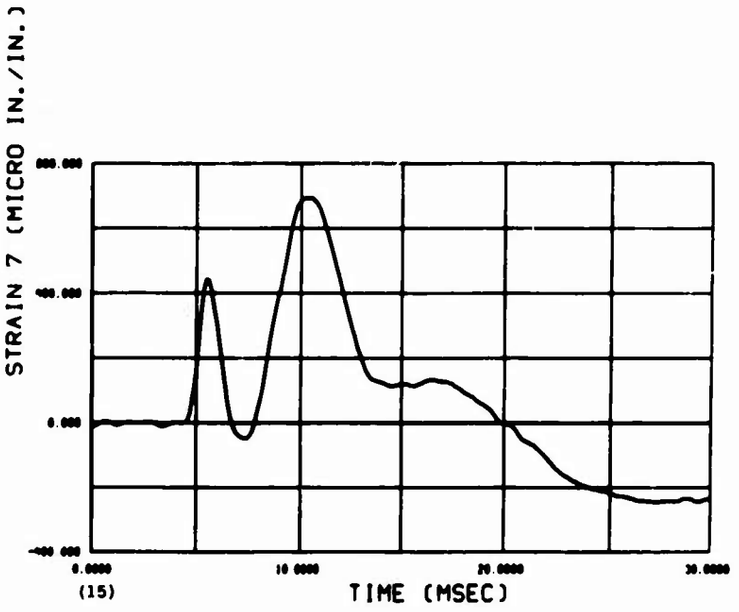

Figure C-29. Strain versus time from gage S7, model CN-1.

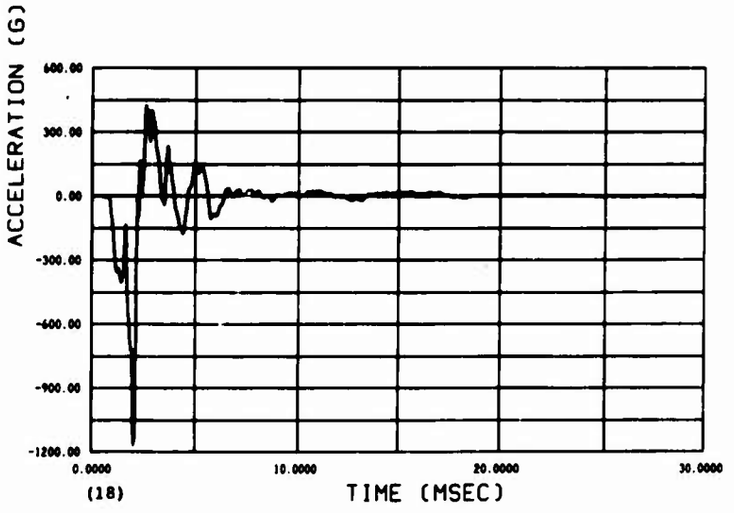

Figure C-30. Vertical acceleration from accelerometer AV3, model CN-1.

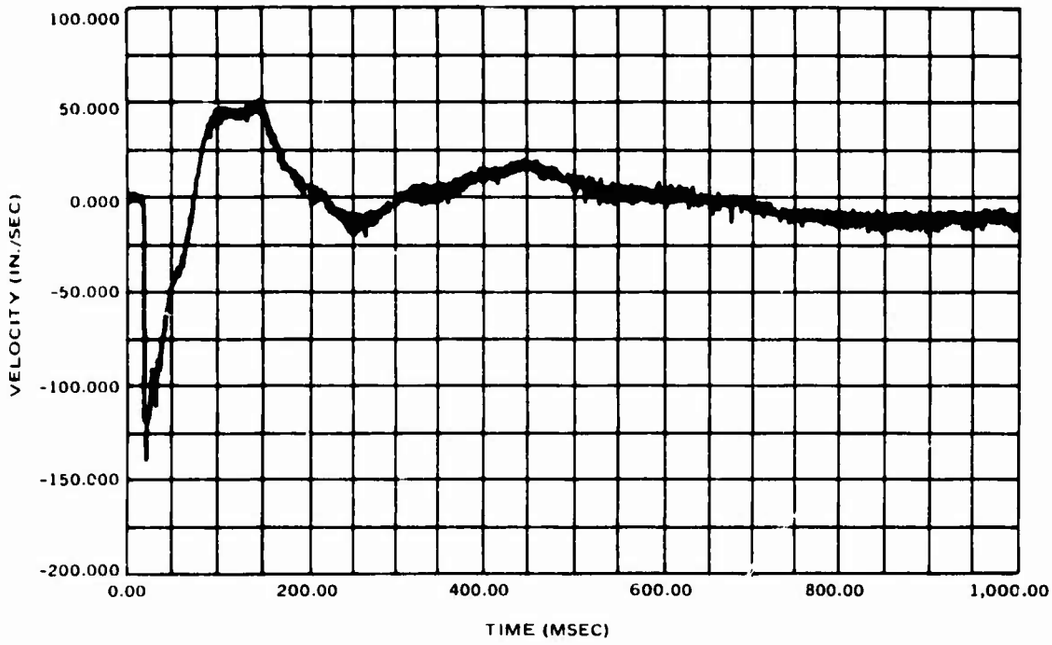

Figure C-31. Vertical velocity from gage VV6, model CN-1.

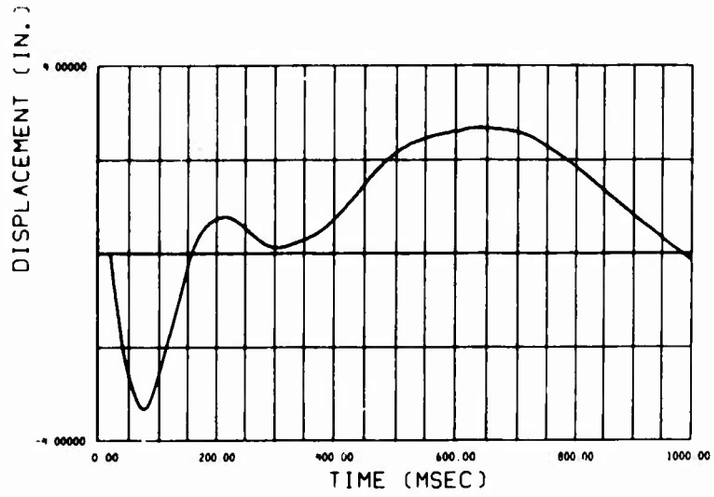

Figure C-32. Vertical displacement from integration of velocity data, VV6, model CN-1.

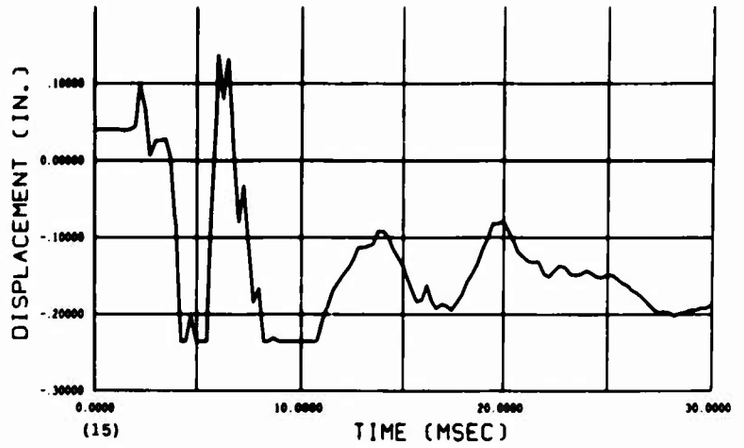

Figure C-33. Vertical diametral deformation from gage D4, model CP-3.

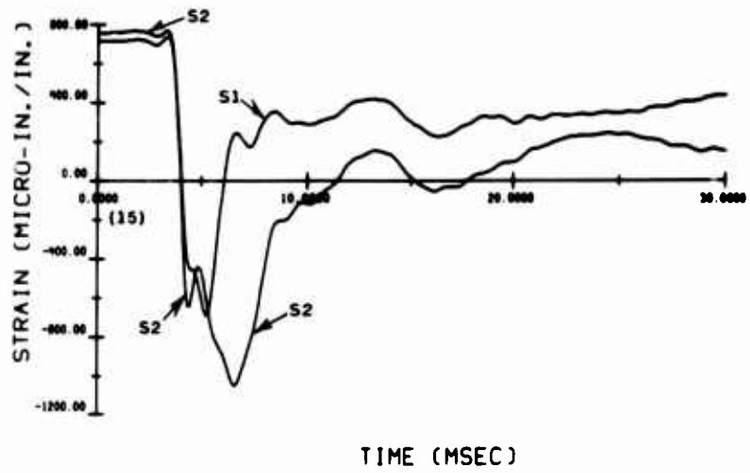

Figure C-34. Strain versus time from gages S1 and S2, model CP-3.

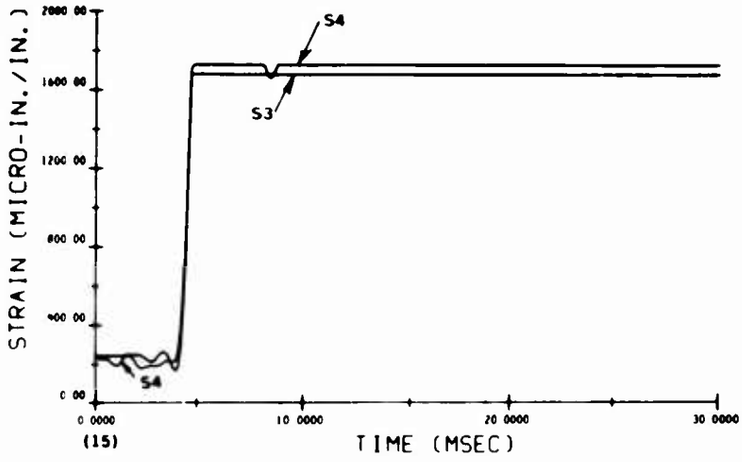

Figure C-35. Strain versus time from gages S3 and S4, model CP-3.

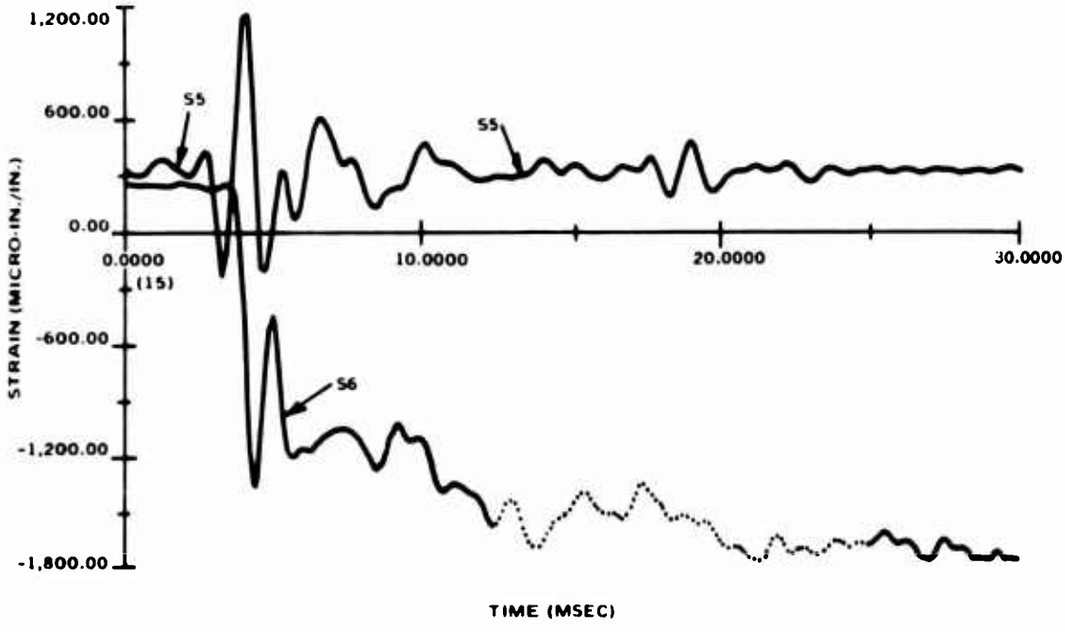

Figure C-36. Strain versus time from gages S5 and S6, model CP-3.

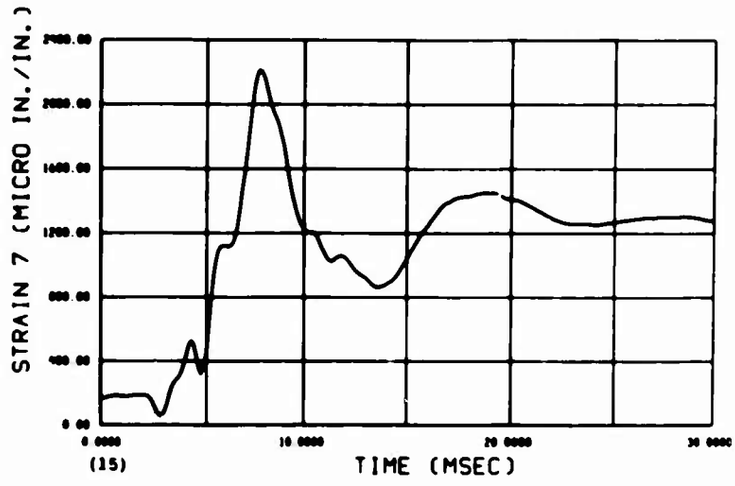

Figure C-37. Strain versus time from gage S7, model CP-3.

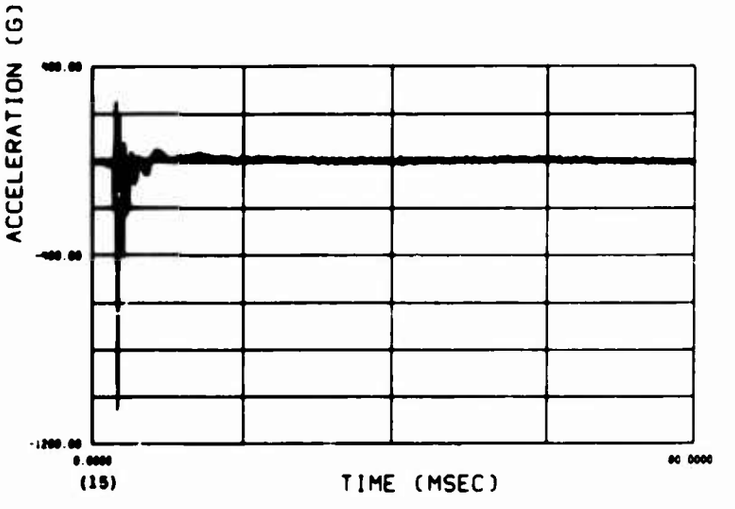

Figure C-38. Vertical acceleration from accelerometer AV4, model CP-3.

REFERENCES

1. Air Force Weapons Laboratory, Technical Report No. AFWL-TR-68-40, Effect of Backpacking on structure-medium interaction by D. A. Linger, Kirtland Air Force Base, New Mexico, July 1968.

2. Naval Civil Engineering Laboratory, Technical Report R-668: Response of buried capsules in the high-overpressure region, by R. J. Odello and J. R. Allgood. Port Hueneme, California, August 1970 (AD 705990)

3. J. R. Allgood. "Structures in soil under high loads," paper presented at ASCE Structural Engineering Conference, Portland, Oregon, April 6-10, 1970. (Also published in ASCE Proceedings, Journal of the Soil Mechanics and Foundations Division, Vol. 97, No. SM3, March 1971).

4. Naval Civil Engineering Laboratory. Technical Note N-1004: Preliminary study of the feasibility of underground pressurized containers, by S. B. Dong. Port Hueneme, Calif., Jan. 1969. (AD 684820)

5.——— Technical Report R-728: Static and dynamic tests of model pressurized, underground fuel storage containers, by W. E. Gates and S. K. Takahashi. Port Hueneme, Calif., May 1971

6.——— Contract Report CR 69.024: Design of pressurized fuel storage tanks to resist air overpressures, by W. E. Gates. Van Nuys, Calif., T. Y. Lin and Associates, May 1970. (AD 874828L) (Contract N62399-69-C-0017)

7.———. Contract Report CR 69.019: Dynamic response analysis of two-dimensional structure with internal stresses and non-homogeneous damping, by I. Farhoomand, E. Rukos, and E. L. Wilson, Berkeley, California, University of California, Department of Civil Engineering, Nov. 1969. (Contract N 62399-69-C-0016) (AD 874628L)

8. I. Farhoomand. Nonlinear dynamic stress analysis of two-dimensional solids, Ph.D. thesis, University of California, Berkeley, Calif., June 1970.

9. Naval Civil Engineering Laboratory. Technical Note N-773: Critical pressures for radially supported bylinders, by C. V. Chelapati, Port Hueneme, California, January 1966.

10. L. Giglio-Tos. "Project LN101: Fundamental air blast measurements," in Operation PRAIRIE FLAT symposium report, vol. 1, pt. 1. Defense Atomic Support Agency, Information and Analysis Center, Special Report DASIAC SR-92, Santa Barbara, California., Jan. 1970, p. 84, Station 208. (DASA 2377-1)

11. University of California. Structural Engineering Laboratory. Report on Contract DACW 68-67-C-004. SAP, a general structural analysis program, by E. L. Wilson. Berkeley, Calif., Sept. 1970.

12. Naval Civil Engineering Laboratory. Technical Note N-873, Dynamic compression tests on polyurethane foam, by W. L. Cowell and G. M. Dunn, Port Hueneme, California, October 1966.

13. Army Engineer Waterways Experiment Station. Transmittal of soil property test results for NCEL Project LN311, Event DIAL PACK. Vicksburg, Miss., Oct. 1970. (Enclosures 1 and 2 to WESSD letter of 7 October 1970)

14. Army Engineer Waterways Experiment Station. Technical Report No. 1-821: Behavior of flexible cylinders buried in sand under static and dynamic loading, by G. E. Albritton. Vicksburg, Miss., April 1968. (AD 670015)

15. Air Force Special Weapons Center. Technical Documentary Report NO. AFSWC-TDR-62-138: Air Force design manual: Principles and practices for design of hardened structures, by N. M. Newmark, and J. D. Haltiwanger. Kirtland Air Force Base, N. M., Dec. 1962. (Contract AF 29(601)-2390) (AD 295408)

16. University of California. Structural Engineering Laboratory. Report on Contract N62399-71-C-0003: Modification of SAP code for dynamic loads, by E. L. Wilson. Berkeley, Calif., (being written).

LIST OF SYMBOLS

A	Cross-sectional area, arching factor
A_g	$\frac{\text{(plan perimeter of tank)(depth of cover over crown)}}{\text{(plan area of tank)(mean diameter of tank)}}$
A_o	Experimentally determined constant
C_L	Propagation velocity of peak soil stresses
C_u	Uniformity coefficient
CN-1	Model with no internal pressure and no backpacking (36-in. diam)
CP-1	Model with 150 psi internal pressure but not backpacking (36-in. diam)
CP-2	Model with 150 psi internal pressure and with 3" backpacking (36-in. diam)
CP-3	Model with 100 psi internal pressure and with 1" backpacking (12-in. diam)
D	Diameter of models
DF	Dynamic amplification factor
E	Young's modulus of elasticity
E_s	Modulus of soil
E_t	Modulus of cylinder material
f_m	Meridional stress
f_θ	Circumferential stress
f_u	Ultimate stress of tank material
f_y	Yield stress of tank material
G_s	Specific gravity of sand
GZ	Ground zero
H	Height of inclusion
L	Length
L_w	Depth factor
M_c	Confined compression (secant) m
n	Experimentally determined const
p_{CR}	Critical buckling pressure of tank
p_{DL}	Dead load pressure
p_e	Total effective pressure
p_i	Internal pressure
p_o	Peak surface overpressure
p_v	Uniform pressure in free-field at crown
p_y	Critical yield pressure on tank
R	Radius of model
T	Maximum thrust
T_n	Natural period of model
t	Tank thickness
t_d	Positive phase duration
t_L	Thickness of backpacking
V_p	Peak vertical velocity at selected
W	Width
z	Depth below ground surface
α_z	Pressure attenuation factor

H Height of inclusion

L Length

L_w Depth factor

M_c Confined compression (secant) modulus of soil

n Experimentally determined constant

p_{CR} Critical buckling pressure of tank

p_{DL} Dead load pressure

p_e Total effective pressure

p_i Internal pressure

p_o Peak surface overpressure

p_v Uniform pressure in free-field at elevation of crown

p_y Critical yield pressure on tank

R Radius of model

T Maximum thrust

T_n Natural period of model

t Tank thickness

t_d Positive phase duration

t_L Thickness of backpacking

V_p Peak vertical velocity at selected depth

W Width

z Depth below ground surface

α_z Pressure attenuation factor

γ_d Unit weight of soil

δ Relative deflection between soil and tank

ϵ_{hL} Hardening strain of backpacking

ϵ_m Meridional strain

ϵ_θ Circumferential strain

ϵ_s Average strain in free field over height of inclusion

Φ Equals to $\left(A_g\right)\left(\frac{M_c}{p_v}\right)\left(\delta\right)$

Φ_m Constant (4.0 for maximum arching of sand)

ν Poisson's ratio

ρ Mass density of soil